NASA CR-72626
PWA FR-3461

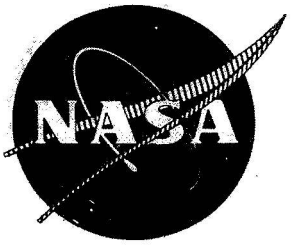

SINGLE STAGE EXPERIMENTAL EVALUATION OF COMPRESSOR BLADING WITH SLOTS AND VORTEX GENERATORS

PART 1 - ANALYSIS AND DESIGN OF STAGES 4 AND 5

by

R. W. Rockenbach, J. A. Brent, and B. A. Jones

Prepared for
National Aeronautics and Space Administration
Contract NAS3-10481

Pratt & Whitney Aircraft DIVISION OF UNITED AIRCRAFT CORPORATION
FLORIDA RESEARCH AND DEVELOPMENT CENTER
BOX 2691, WEST PALM BEACH, FLORIDA 33402

Requests for copies of this report should be referred to:

National Aeronautics and Space Administration
Scientific and Technical Information Facility
P.O. Box 33
College Park, Md. 20740

NASA CR-72626
PWA FR-3461

SINGLE STAGE EXPERIMENTAL EVALUATION OF COMPRESSOR BLADING WITH SLOTS AND VORTEX GENERATORS

PART 1 - ANALYSIS AND DESIGN OF STAGES 4 AND 5

by
R. W. Rockenbach, J. A. Brent, and B. A. Jones

Prepared for
National Aeronautics and Space Administration

20 March 1970

Contract NAS3-10481

Technical Management
NASA Lewis Research Center
Cleveland, Ohio 44135

NASA Program Manager: L. Joseph Herrig
Fluid System Components Division

Pratt & Whitney Aircraft
DIVISION OF UNITED AIRCRAFT CORPORATION
FLORIDA RESEARCH AND DEVELOPMENT CENTER
BOX 2691, WEST PALM BEACH, FLORIDA 33402

ABSTRACT

Two compressor stages, each comprising a rotor and a stator, were designed with differing mean work levels and corresponding radial work gradients. Data from tests of slotted rotor and stator blading obtained under Contract NAS3-7603 were used to form the basis for the selection of loss, deviation, and incidence distributions. The loss data correlation was modified to reflect an assumed reduction in loss due to the addition of blade slots and wall vortex generators.

CONTENTS

ILLUSTRATIONS

ILLUSTRATIONS (Continued)

SINGLE STAGE EXPERIMENTAL EVALUATION OF COMPRESSOR BLADING WITH SLOTS AND VORTEX GENERATORS

PART I - ANALYSIS AND DESIGN OF STAGES 4 AND 5

R. W. Rockenbach, J. A. Brent and B. A. Jones

SUMMARY

Two compressor stages, each comprising a rotor and a stator, were designed with differing mean work levels and corresponding radial work gradients. Data from tests of slotted rotor and stator blading obtained under Contract NAS3-7603 were used to form the basis for the selection of loss coefficient, deviation angle, and incidence angle distributions. The loss data correlation was modified to reflect an assumed reduction in loss due to the addition of blade slots and secondary flow fences or wall vortex generators.

Both stages were designed for a rotor tip velocity of 757 ft/sec (230.73 m/sec), an equivalent flow of 110 lb/sec (49.894 kg/sec) and a rotor inlet hub/tip ratio of approximately 0.8. All rotors and stators were designed with NACA 65-series airfoil sections with A = 1.0 mean-lines. Table 1 shows the differences in the stages 4 and 5 design.

Table 1. Differences in the Design of Stages 4 and 5

Factors	Stage 4	Stage 5
Pressure Ratio	1.325	1.375
Adiabatic Efficiency	84%	82%
Diffusion Factor		
Rotor Hub	0.74	0.82
Stator Hub	0.69	0.81

Stress and vibration analyses were performed for both stages. Blade slots and wall vortex generators were designed and analyzed only for stage 4.

INTRODUCTION

The effectiveness of slotted rotor and stator blading as a means for increasing the allowable loading limit of compressor blade rows was investigated at the Florida Research and Development Center of Pratt & Whitney Aircraft under Contract NAS3-7603 for the National Aeronautics and Space Administration (Reference 1). Results obtained from the single stage tests of three slotted rotor and three slotted stators under that program indicated good performance for the blade row midspan regions but poor performance near the walls (References 3 through 8). The relative effectiveness of the slots at midspan and their ineffectiveness near the wall was attributed to chordal placement of the slots and their inability to reduce the large secondary flows in the wall regions. Consequently, the design radial work gradients for the NAS3-7603 slotted rotor blading did not compensate for the high loss gradients that were measured near the walls, which resulted in a highly three-dimensional flow with low total pressure ratio and efficiency near the walls. These factors indicated that advanced compressor design concepts for the increase of allowable stage loading and stable, low-loss operating range should be addressed to the problem of secondary flow and associated high losses near the wall.

A single stage compressor investigation was initiated with the following three approaches to reduce large secondary flow losses and improve blade element performance in the wall region of highly-loaded compressor blade rows:

1. Addition of blade end slots (upstream of the existing slots), and secondary flow fences to rotor 3 and stator 3 of Contract NAS3-7603
2. Design and test of two new stages (designated 4 and 5) with relatively high work input near the walls to compensate for high losses
3. Addition of blade slots and secondary flow fences or wall vortex generators to stages 4 and 5 to reduce the wall-associated losses.

Discussion of the design modifications for, and the experimental results obtained with, modified rotor 3 and stator 3 are presented in Reference 2.

The aerodynamic and mechanical design of stages 4 and 5, and the design of blade slots and wall vortex generators for stage 4, are the subject of this report. Failure of rotor 5 during the baseline test without slots or vortex generators precluded further testing of stage 5; therefore slot and vortex generator design information for stage 5 are not included in this report. Stages 4 and 5, each consisting of a rotor and stator blade row, were designed with different work levels and correspondingly different radial gradients of work input. Slotted rotor and stator blading test data from References 3 through 8 were used as the basis for the selection of loss coefficient, deviation angle, and incidence angle distributions.

AERODYNAMIC ANALYSIS AND DESIGN

General Criteria for Stage Selection

The primary definition of the stages is given in table 2.

Table 2. Approximate Design Goals

Pressure Ratio	1.35
Rotor Tip Velocity, ft/sec (m/sec)	800 (243.83)
Hub/Tip Ratio	0.8
Tip Solidity	1.0 (minimum)

In addition to the goals given in table 2, the designs were intended to meet seven other conditions, as follows:

1. In order to reduce the effects attributable to the interaction of inlet guide vane wakes with the rotor and stator, inlet guide vanes were not to be employed
2. Stator discharge flow direction should be axial
3. The average axial velocity ratio should be maintained near unity across all blade rows to ensure that blade diffusion-loading is achieved as a result of work input only.

4. The rotor tip (10% span) inlet relative Mach number should be approximately 0.8 to avoid high losses due to shock wave induced boundary layer separation in the rotor blade rows

5. The stages were to be designed for two different levels of aerodynamic loading. The hub (90% span from tip) diffusion factor for the most highly-loaded rotor should be between 0.7 to 0.8 to ensure that this stage is in advance of current technology

6. A single flow path should be used for both stages

7. The stage exit total pressure should be constant across the span.

Stage Aerodynamic Design Procedure

The initial phase of the design was the correlation of slotted rotor and stator blade element performance data from References 3 through 8. These data, which were used in the design of the two subject compressor stages, were comprised of loss parameter, diffusion factor, deviation angle, and reference incidence angle data.

Loss Correlation

Rotor and stator loss parameter data for 90, 100, and 110 percent of design rotor speed from References 3 through 8 were plotted versus diffusion factor. Minimum loss data were used whenever a minimum loss was clearly defined. Where a minimum loss was not clearly defined, the point corresponding to the midpoint of incidences tested was selected. Curves were drawn through the loss parameter data at each percent span. Cross-plots were made of loss parameter vs percent span at constant diffusion factor values of 0.5 and 0.7 to check the spanwise loss gradient at constant diffusion factor. The loss correlation curves were modified slightly to obtain a smooth distribution of loss parameter with span. In anticipation of reduced losses due to blade slots and secondary flow

fences or wall vortex generators, it was necessary to select design loss curves for stages 4 and 5 at loss levels lower than the correlated data. The correlation curves for 50% span in figures 1 and 2 were assumed to represent the closest approximation of a two-dimensional flow environment possible in a high hub-tip ratio compressor. Although these curves are above the indicated two-dimensional cascade loss curves in the figures, they represent reasonable extrapolations of the single stage compressor data from Reference 9, which are also indicated in the figures. It was therefore assumed that the midspan loss curves represent a limiting loss for other span locations. The design curves selected for stages 4 and 5 consisted of the loci of midpoints between the loss level at each spanwise location and the midspan loss level, since a 50% improvement between the secondary flow losses and the low limit of loss was considered to be a reasonable goal for slots and fences or vortex generators. The loss data correlation curves and the selected design loss curves for stages 4 and 5 are compared in figures 1 and 3a through 3d for rotors, and figures 2 and 4a through 4d for stators.

Deviation Angle Correlation

Plots denoting the difference between predicted and measured deviation angle versus diffusion factor at each percent span were made from the data in References 3 through 8 to determine if any adjustment to the NASA deviation angle correlation (Reference 9) was necessary. Composite plots of the deviation angle data are presented in figures 5 and 6 for rotors and stators, respectively, with percent spans from the tip indicated. The rotor data (figure 5) generally centered around zero difference at all stations across the span and it was decided that no adjustment was required. The stator data in figure 6 exhibit a larger scatter than the rotor data, the general level of the deviation difference being approximately -3 deg (-0.05236 rad). In view of the scatter and because the stator deviation angle affects only the discharge flow direction and not the stage performance, it was decided that no correction based on these data should be applied. Additional data, generated during the tests of stages 4 and 5, will be used to better define the stator deviation angle.

Reference Incidence Correlation

Correlation techniques similar to those used on the loss coefficient and deviation angle data were applied to the reference incidence angle data to determine if any adjustment to the Pratt & Whitney Aircraft reference incidence correlation was necessary. Composite plots of reference incidence angle adjustment for rotors and stators with percent spans from tip noted are given in figures 7 and 8. Data scatter prevented correlation of incidence angle adjustment versus loading at each percent span. However, if extreme rotor and stator data points were eliminated, the average difference is approximately -2 (-0.03491 rad) and 0 degree for rotors and stators, respectively. Consequently, rotors 4 and 5 were designed with 2 deg (0.03491 rad) less than reference incidence across the span, and stators 4 and 5 were designed at the reference incidence angle.

Stage Selection Process

Following the correlation of data from References 3 through 8, the stage selection was made through successive iterations until the design goals previously outlined were satisfied. The stage selection process is illustrated in figure 9. The iteration procedure required the loss coefficient distribution to be input into the axisymmetric flow calculation computer program in accordance with the calculated diffusion factor distribution from the previous iteration and the design loss parameter curves described earlier. During these iterations, the flow path was altered by varying the outer wall in order to maintain a nearly constant average axial velocity. The tip speed was controlled to maintain the desired (0.8) tip Mach number, and the stage specific flow was held constant at 33 lb/sec/ft^2 (161.11 kg/sec/m^2), a value that is representative of current middle stage design practice. The design pressure ratio was varied to bring the loading to the desired levels ($D_{F,\ max}$ = 0.7 for rotor 4 and $D_{F,\ max}$ = 0.8 for rotor 5) and thus produce two stages with varying degrees of difficulty. Differing work gradients for the two design pressure ratios resulted because, as average work coefficient and hence diffusion factor increases, the radial work gradient must be greater to compensate for the increasing slope of the design loss curves. Since the stator exit total pressure radial profile

was held approximately constant by varying rotor radial work distribution to compensate for both rotor and stator losses, the discharge from the stage is similar to the inlet flow, as both are of constant total pressure and axial flow direction. The discharge total temperature profile, however, will not be uniform.

Design Velocity Diagram Data and Predicted Performance

Design velocity diagram data and predicted performance of the stages selected to fulfill the design intent are summarized in table 3. Stages 4 and 5 have design pressure ratios of 1.325 and 1.375, respectively, at a design rotor tip velocity of approximately 757 ft/sec (230.73 m/sec).

Diffusion factor distributions for the two stages are presented in figure 10. The average level of loading for rotor 4 and stator 5 are similar to those of rotor 3 and stator 3, (Reference 8), which were the most highly-loaded rotor and stator under the NAS3-7603 contract investigation of slotted blading. The stage 4 and 5 blading, however, is comprised of a proportionally more highly loaded hub when compared to the rotor 3 and stator 3 loading distribution.

Spanwise loss coefficient distributions are presented in figure 11 for both rotors and stators. The combined effects of the loading gradient and the radial gradient of loss coefficient are readily noted in figure 11. The small variation of loading with radius in the tip region of the rotor results in a positive radial loss gradient at the tip, while the negative radial diffusion factor gradient of the stator tip results in an almost constant tip loss.

The flow path of the two stages is depicted schematically in figure 12. The area contraction from rotor and stator leading to trailing edge is 7.6 and 6.5 percent respectively. The tip contour for the stages of Reference 1 is shown for comparison.

Blading Selection

Stages 4 and 5 represent a continuation of the work in Reference 1, therefore, NACA 65-series airfoil sections were also selected for both rotors and stators of stages 4 and 5. The number of rotor and stator blades selected were 60 and 58, respectively. Table 4 lists those geometric variables arbitrarily determined or directly related to the selection of flow path and blade number.

Table 3a. Rotor 4 Blade Element Design Data Along Design Streamlines (English Units)

GEOMETRY DATA

Airfoil: NACA 65 (A = 1.0)
No. of Blades: 60

Aspect Ratio: 1.820
Chord Length: 2.21 in.

Percent Span From Tip Leading Edge	Trailing Edge	κ_{1e} (deg)	κ_{te} (deg)	ϕ (deg)	$\gamma°$ (deg)	0/0*	σ	t/c
97.01	96.90	56.43	-8.50	64.93	23.97	1.286	1.276	0.078
91.02	91.02	56.22	-3.50	59.72	26.36	1.270	1.258	0.076
86.71	86.60	56.28	-0.20	56.48	28.04	1.259	1.243	0.074
71.02	69.60	57.70	9.75	47.95	33.73	1.224	1.197	0.068
50.06	49.10	61.29	16.40	44.89	38.85	1.194	1.143	0.060
29.59	28.40	65.85	19.10	46.75	42.48	1.177	1.093	0.052
14.02	13.50	70.18	19.28	50.90	44.73	1.147	1.060	0.046
9.23	8.80	71.89	19.05	52.84	45.47	1.134	1.050	0.044
3.36	3.36	73.85	18.65	55.20	46.25	1.119	1.040	0.042

VELOCITY DIAGRAM DATA

Corrected Rotor Speed: 4210 rpm

Corrected Weight Flow: 110 lb/sec

Percent Span From Tip Leading Edge	Trailing Edge	V'_{1e} (ft/sec)	V_{z1e} (ft/sec)	$V'_{\theta 1e}$ (ft/sec)	β'_{1e} (deg)	U_{1e} (ft/sec)	V'_{te} (ft/sec)	V_{zte} (ft/sec)	$V'_{\theta te}$ (ft/sec)	β'_{te} (deg)	U_{te} (ft/sec)
97.01	96.90	780.00	489.20	605.10	51.23	604.9	438.80	437.50	37.9	4.82	607.9
91.02	91.02	788.35	490.09	616.70	51.53	615.7	453.25	447.70	71.2	8.95	616.2
86.71	86.60	794.20	492.80	623.60	51.78	624.2	463.90	454.20	95.9	11.75	622.6
71.02	69.60	814.30	496.00	647.80	52.74	647.7	498.40	466.75	174.9	20.40	645.5
50.06	49.10	837.40	488.25	679.80	54.30	680.0	527.25	471.65	234.9	26.47	675.8
29.59	28.40	855.20	473.70	711.30	56.28	711.7	546.75	472.70	272.3	29.83	705.3
14.02	13.50	865.10	454.60	735.00	58.17	735.0	556.80	472.05	292.3	31.55	726.3
9.23	8.80	867.50	446.65	742.65	58.85	742.5	560.30	472.20	297.9	32.05	733.1
3.36	3.36	870.05	436.25	751.80	59.72	751.7	565.75	473.75	303.8	32.58	740.2

Table 3a. Rotor 4 Blade Element Design Data Along Design Streamlines (English Units) (Continued)

DESIGN PERFORMANCE DATA

Pressure Ratio: 1.349

Efficiency: 89.5%

Percent Span From Tip Leading Edge	Trailing Edge	$\Delta\beta'$ (deg)	M'_{1e}	i_m (deg)	D_F	$\bar{\omega}$	Loss Parameter	$\delta°$ (deg)	P_{te} (psia)	T_{te} (°R)
97.01	96.90	46.41	0.713	-5.20	0.722	0.176	0.069	13.32	20.197	576.59
91.02	91.02	42.58	0.720	-4.69	0.697	0.149	0.058	12.45	20.116	574.41
86.71	86.60	40.03	0.726	-4.50	0.681	0.131	0.052	11.95	20.057	573.16
71.02	69.60	28.64	0.744	-4.96	0.632	0.089	0.034	10.65	19.834	569.53
50.06	49.10	27.83	0.765	-6.99	0.603	0.073	0.029	10.07	19.766	568.50
29.59	28.40	26.45	0.780	-9.57	0.598	0.094	0.037	10.73	19.762	569.58
14.02	13.50	26.62	0.789	-12.01	0.600	0.127	0.051	12.27	19.719	571.30
9.23	8.80	26.80	0.790	-13.04	0.600	0.139	0.056	13.00	19.714	571.87
3.36	3.36	27.14	0.792	-14.13	0.599	0.155	0.063	13.93	19.683	572.54

Rotor 4 Blade Element Design Data Along Design Streamlines (Metric Units)

GEOMETRY DATA

Airfoil: NACA 65 (A=1.0)
No. of Blades: 60

Aspect Ratio: 1.820
Chord Length: 0.0561 m

Percent Span From Tip Leading Edge	Trailing Edge	κ_{1e} (rad)	κ_{te} (rad)	ϕ (rad)	$\gamma°$ (rad)	0/0*	σ	t/c
97.01	96.90	0.9849	-0.1484	1.133	0.4183	1.286	1.276	0.078
91.02	91.02	0.9812	-0.0611	1.042	0.4601	1.270	1.258	0.076
86.71	86.60	0.9823	-0.0035	0.9857	0.4894	1.259	1.243	0.074
71.02	69.60	1.007	0.1702	0.8369	0.5887	1.224	1.197	0.068
50.06	49.10	1.070	0.2862	0.7835	0.6780	1.194	1.143	0.060
29.59	28.40	1.149	0.3334	0.8159	0.7414	1.177	1.093	0.052
14.02	13.50	1.225	0.3365	0.8884	0.7807	1.147	1.060	0.046
9.23	8.80	1.255	0.3325	0.9222	0.7936	1.134	1.050	0.044
3.36	3.36	1.289	0.3255	0.9634	0.8072	1.119	1.040	0.042

Table 3a. Rotor 4 Blade Element Design Data Along Design Streamlines (Metric Units) (Continued)

VELOCITY DIAGRAM DATA

Corrected Rotor Speed: 440.87 rad/sec

Corrected Weight Flow: 49.89 kg/sec

Percent Span From Tip Leading Edge	Trailing Edge	V'_{1e} (m/sec)	V_{z1e} (m/sec)	$V'_{\theta 1e}$ (m/sec)	β'_{1e} (rad)	U_{1e} (m/sec)	V'_{te} (m/sec)	V_{zte} (m/sec)	$V'_{\theta te}$ (m/sec)	β'_{te} (rad)	U_{te} (m/sec)
97.01	96.90	237.74	149.10	184.43	0.8941	184.37	133.74	133.35	11.55	0.0841	185.28
91.02	91.02	240.28	149.37	187.97	0.8994	187.66	138.15	136.45	21.70	0.1562	187.81
86.71	86.60	242.07	150.20	190.07	0.9037	190.25	141.39	138.44	29.23	0.2051	189.76
71.02	69.60	248.19	151.18	197.44	0.9205	197.41	151.91	142.26	53.31	0.3560	196.74
50.06	49.10	255.23	148.81	207.20	0.9477	207.26	160.70	143.75	71.60	0.4620	205.98
29.59	28.40	260.66	144.38	216.80	0.9823	216.92	166.64	144.07	83.00	0.5206	214.97
14.02	13.50	263.68	138.56	224.02	1.015	224.02	169.71	143.88	89.09	0.5506	221.37
9.23	8.80	264.41	136.13	226.35	1.027	226.31	170.77	143.92	90.80	0.5594	223.44
3.36	3.36	265.19	132.96	229.14	1.042	229.11	172.44	144.39	92.60	0.5686	225.61

DESIGN PERFORMANCE DATA

Pressure Ratio: 1.349

Efficiency: 89.5%

Percent Span From Tip Leading Edge	Trailing Edge	$\Delta\beta'$ (rad)	M_{1e}	i_m (rad)	D_F	$\bar{\omega}$	Loss Parameter	δ° (rad)	$P_{te} \times 10^{-6}$ (N/m^2)	T_{te} (°K)
97.01	96.90	0.8100	0.713	-0.0908	0.722	0.176	0.069	0.2325	0.1393	320.33
91.02	91.02	0.7431	0.720	-0.0819	0.697	0.149	0.058	0.2173	0.1387	319.11
86.71	86.60	0.6986	0.726	-0.0785	0.681	0.131	0.052	0.2086	0.1383	318.42
71.02	69.60	0.4999	0.744	-0.0866	0.632	0.089	0.034	0.1859	0.1367	316.40
50.06	49.10	0.4857	0.765	-0.1220	0.603	0.073	0.029	0.1758	0.1363	315.83
29.59	28.40	0.4616	0.780	-0.1670	0.598	0.094	0.037	0.1873	0.1363	316.43
14.02	13.50	0.4646	0.789	-0.2096	0.600	0.127	0.051	0.2141	0.1360	317.39
9.23	8.80	0.4677	0.790	-0.2276	0.600	0.139	0.056	0.2269	0.1359	317.70
3.36	3.36	0.4734	0.792	-0.2466	0.599	0.155	0.063	0.2431	0.1357	318.08

Table 3b. Stator 4 Blade Element Design Data Along Design Streamlines (English Units)

GEOMETRY DATA

Airfoil: NACA 65 (A = 1.0)
No. of Vanes: 58

Aspect Ratio: 1.689
Chord Length: 2.182 in.
Thickness Ratio, t/c: 0.090

Percent Span From Tip Leading Edge	Trailing Edge	κ_{1e} (deg)	κ_{te} (deg)	ϕ (deg)	$\gamma°$ (deg)	0/0*	σ
94.87	94.87	53.81	-16.48	70.29	18.67	1.324	1.214
90.07	90.07	51.87	-15.59	67.46	18.14	1.310	1.200
85.00	84.85	50.23	-14.62	64.85	17.81	1.297	1.187
70.27	69.98	47.18	-12.52	59.70	17.33	1.265	1.151
50.40	49.95	46.30	-11.67	57.97	17.32	1.236	1.105
30.27	29.25	48.75	-12.52	61.27	18.12	1.216	1.063
15.27	14.60	52.40	-14.12	66.52	19.14	1.196	1.032
10.27	9.70	53.92	-14.95	68.87	19.49	1.194	1.021
5.00	4.60	55.80	-15.95	71.75	19.93	1.199	1.010

VELOCITY DIAGRAM DATA

Percent Span From Tip Leading Edge	Trailing Edge	V_{1e} (ft/sec)	V_{z1e} (ft/sec)	$V_{\theta 1e}$ (ft/sec)	β_{1e} (deg)	V_{te} (ft/sec)	V_{zte} (ft/sec)	$V_{\theta te}$ (ft/sec)	β_{te} (deg)
94.87	94.87	735.2	474.2	561.2	49.71	469.0	468.9	0.0	0.0
90.07	90.07	725.0	482.9	540.2	48.15	468.9	468.8	0.0	0.0
85.00	84.85	715.2	491.2	520.4	46.68	468.7	468.7	0.0	0.0
70.27	69.98	690.0	501.1	474.3	43.45	468.9	468.8	0.0	0.0
50.40	49.95	667.9	498.9	443.2	41.59	477.0	476.4	0.0	0.0
30.27	29.25	649.6	481.0	435.2	42.07	489.9	489.9	0.0	0.0
15.27	14.60	631.2	454.8	436.8	43.77	504.9	503.7	0.0	0.0
10.27	9.70	623.8	443.5	437.8	44.52	511.1	510.2	0.0	0.0
5.00	4.60	615.3	429.9	438.5	45.40	518.7	517.5	0.0	0.0

Table 3b. Stator 4 Blade Element Design Data Along Design Streamlines (English Units) (Continued)

DESIGN PERFORMANCE DATA

Stage Pressure Ratio: 1.324 Stage Efficiency: 83.8%

Percent Span From Tip Leading Edge	Trailing Edge	$\Delta\beta$ (deg)	M 1e	i_m (deg)	D_F	$\bar{\omega}$	Loss Parameter	δ° (deg)	P_{te} (psia)
94.87	94.87	49.71	0.652	-4.105	0.676	0.142	0.058	16.48	19.455
90.07	90.07	48.15	0.644	-3.730	0.663	0.132	0.055	15.59	19.455
85.00	84.85	46.68	0.634	-3.555	0.652	0.121	0.051	14.62	19.455
70.27	69.98	43.45	0.612	-3.730	0.620	0.094	0.041	12.52	19.418
50.40	49.95	41.59	0.591	-4.710	0.588	0.072	0.033	11.67	19.440
30.27	29.25	42.07	0.574	-6.680	0.563	0.073	0.034	12.52	19.469
15.27	14.60	43.77	0.557	-8.630	0.537	0.066	0.032	14.12	19.484
10.27	9.70	44.52	0.549	-9.400	0.526	0.062	0.030	14.95	19.484
5.00	4.60	45.40	0.541	-10.405	0.511	0.056	0.028	15.95	19.492

Stator 4 Blade Element Design Data Along Design Streamlines (Metric Units)

GEOMETRY DATA

Airfoil: NACA 65 (A = 1.0)
No. of Vanes: 58

Aspect Ratio: 1.689
Chord Length: 0.0554 m
Thickness Ratio, t/c: 0.090

Percent Span From Tip Leading Edge	Trailing Edge	κ_{1e} (rad)	κ_{te} (rad)	ϕ (rad)	γ° (rad)	0/0*	σ
94.87	94.87	0.9391	-0.2876	1.227	0.3258	1.324	1.214
90.07	90.07	0.9053	-0.2721	1.177	0.3166	1.310	1.200
85.00	84.85	0.8767	-0.2552	1.132	0.3108	1.297	1.187
70.27	69.98	0.8234	-0.2185	1.042	0.3025	1.265	1.151
50.40	49.95	0.8081	-0.2037	1.012	0.3023	1.236	1.105
30.27	29.25	0.8508	-0.2185	1.069	0.3162	1.216	1.063
15.27	14.60	0.9145	-0.2464	1.161	0.3341	1.196	1.032
10.27	9.70	0.9411	-0.2609	1.202	0.3402	1.194	1.021
5.00	4.60	0.9739	-0.2784	1.252	0.3478	1.199	1.010

Table 3b. Stator 4 Blade Element Design Data Along Design Streamlines (Metric Units) (Continued)

VELOCITY DIAGRAM DATA

Percent Span From Tip Leading Edge	Trailing Edge	V_{1e} (m/sec)	V_{z1e} (m/sec)	$V_{\theta 1e}$ (m/sec)	β_{1e} (rad)	V_{te} (m/sec)	V_{zte} (m/sec)	$V_{\theta te}$ (m/sec)	β_{te} (rad)
94.87	94.87	224.08	144.53	171.05	0.8676	142.95	142.92	0.0	0.0
90.07	90.07	220.98	147.18	164.65	0.8404	142.92	142.89	0.0	0.0
85.0	84.85	217.99	149.71	158.61	0.8147	142.85	142.85	0.0	0.0
70.27	69.98	210.31	152.73	144.56	0.7583	142.92	142.89	0.0	0.0
50.40	49.95	203.57	152.06	135.08	0.7259	145.38	145.20	0.0	0.0
30.27	29.25	197.99	146.60	132.64	0.7342	149.32	149.32	0.0	0.0
15.27	14.60	192.38	138.62	133.13	0.7639	153.89	153.52	0.0	0.0
10.27	9.70	190.13	135.17	133.44	0.7770	155.78	155.50	0.0	0.0
5.0	4.60	187.54	131.03	133.65	0.7924	158.09	157.73	0.0	0.0

DESIGN PERFORMANCE DATA

Stage Pressure Ratio: 1.324 Stage Efficiency: 83.8%

Percent Span From Tip Leading Edge	Trailing Edge	$\Delta\beta$ (rad)	M_{1e}	i_m (rad)	D_f	$\bar{\omega}$	Loss Parameter	δ° (rad)	$P_{te} \times 10^{-6}$ (N/m^2)
94.87	94.87	0.8676	0.625	-0.0716	0.676	0.142	0.058	0.2876	0.1341
90.07	90.07	0.8404	0.644	-0.0651	0.663	0.132	0.055	0.2721	0.1341
85.0	84.85	0.8147	0.634	-0.0620	0.652	0.121	0.051	0.2552	0.1341
70.27	69.98	0.7583	0.612	-0.0651	0.620	0.094	0.041	0.2185	0.1339
50.40	49.95	0.7259	0.591	-0.0822	0.588	0.072	0.033	0.2037	0.1340
30.27	29.25	0.7342	0.574	-0.1166	0.563	0.073	0.034	0.2185	0.1342
15.27	14.60	0.7639	0.557	-0.1506	0.537	0.066	0.032	0.2464	0.1343
10.27	9.70	0.7770	0.549	-0.1641	0.526	0.062	0.030	0.2609	0.1343
5.0	4.60	0.7924	0.541	-0.1816	0.511	0.056	0.028	0.2784	0.1344

Table 3c. Rotor 5 Blade Element Design Data Along Design Streamlines (English Units)

GEOMETRY DATA

Airfoil: NASA 65 (A = 1.0)
No. of Blades: 60

Aspect Ratio: 1,820
Chord Length: 2.21 in.

Percent Span From Tip Leading Edge	Trailing Edge	κ_{1e} (deg)	κ_{te} (deg)	ϕ (deg)	γ° (deg)	0/0*	σ	t/c
96.41	94.75	60.40	-31.00	91.40	14.70	1.039	1.276	0.078
91.20	89.25	59.90	-22.60	82.50	18.65	1.060	1.258	0.076
86.77	84.80	59.70	-17.00	76.70	21.35	1.079	1.243	0.074
70.84	69.00	60.37	- 2.40	62.77	28.99	1.142	1.197	0.068
50.30	49.40	63.22	7.00	56.22	35.11	1.194	1.143	0.060
29.94	29.75	68.07	9.85	58.22	38.96	1.229	1.093	0.052
13.65	14.40	72.80	10.40	62.40	41.60	1.266	1.060	0.046
9.22	10.00	74.35	10.20	64.15	42.28	1.277	1.050	0.044
3.41	4.70	76.60	9.65	66.95	43.13	1.293	1.040	0.042

VELOCITY DIAGRAM DATA

Corrected Rotor Speed: 4210 rpm

Corrected Weight Flow: 110 lb/sec

Percent Span From Tip Leading Edge	Trailing Edge	V'_{1e} (ft/sec)	V_{z1e} (ft/sec)	$V'_{\theta 1e}$ (ft/sec)	β'_{1e} (deg)	U_{1e} (ft/sec)	V'_{te} (ft/sec)	V_{zte} (ft/sec)	$V'_{\theta te}$ (ft/sec)	β'_{te} (deg)	U_{te} (ft/sec)
96.41	94.75	779.4	485.6	609.1	51.44	608.5	429.2	422.5	- 77.0	-10.30	610.7
91.20	89.25	786.3	487.3	617.3	51.70	616.6	440.6	439.0	- 32.0	- 4.40	618.8
86.77	84.80	792.9	488.7	624.2	51.92	623.7	449.3	449.2	2.0	- 0.00	625.0
70.84	69.00	813.3	491.5	648.3	52.84	648.0	478.4	468.5	96.0	11.40	647.5
50.30	49.40	837.4	488.2	680.2	54.27	680.0	499.8	475.4	167.0	19.40	675.3
29.94	29.75	855.6	474.3	710.8	56.15	711.0	515.3	472.0	202.0	23.40	703.6
13.65	14.40	866.2	455.2	735.3	58.17	736.7	520.8	468.0	221.0	25.30	725.2
9.22	10.00	868.1	448.5	742.8	58.79	743.0	522.9	467.5	227.0	25.70	731.8
3.41	4.70	870.6	437.5	752.0	59.65	752.3	525.2	467.0	233.0	26.20	739.2

Table 3c. Rotor 5 Blade Element Design Data Along Design Streamlines (English Units) (Continued)

DESIGN PERFORMANCE DATA

Pressure Ratio: 1.414

Efficiency = 89.3%

Percent Span From Tip Leading Edge	Trailing Edge	$\Delta\beta'$ (deg)	M'_{le}	i_m (deg)	D_F	$\bar{\omega}$	Loss Parameter	δ° (deg)	P_{te} (psia)	T_{te} (°R)
96.41	94.75	61.74	0.712	- 8.96	0.796	0.200	0.077	20.70	21.550	588.47
91.20	89.25	56.10	0.719	- 8.20	0.770	0.173	0.069	18.20	21.328	585.51
86.77	84.80	51.92	0.724	- 7.78	0.750	0.153	0.062	17.00	21.168	583.38
70.84	69.00	41.44	0.743	- 7.53	0.696	0.107	0.044	13.80	20.788	578.35
50.30	49.40	34.87	0.766	- 8.95	0.665	0.082	0.034	12.40	20.627	575.76
29.94	29.75	32.75	0.780	-11.92	0.668	0.107	0.045	13.55	20.616	576.90
13.65	14.40	32.87	0.789	-14.63	0.678	0.141	0.060	14.90	20.608	579.23
9.22	10.00	33.09	0.791	-15.56	0.680	0.154	0.066	15.50	20.601	580.96
3.41	4.70	33.45	0.792	-16.95	0.682	0.170	0.073	16.55	20.589	580.94

Rotor 5 Blade Element Design Data Along Design Streamlines (Metric Units)

GEOMETRY DATA

Airfoil: NASA 65 (A = 1.0)
No. of Blades: 60

Aspect Ratio: 1.820
Chord Length: 0.05613 m

Percent Span From Tip Leading Edge	Trailing Edge	κ_{le} (rad)	κ_{te} (rad)	ϕ (rad)	γ° (rad)	0/0*	σ	t/c
96.41	94.75	1.054	-0.5410	1.595	0.2566	1.039	1.276	0.078
91.20	89.25	1.045	-0.3944	1.440	0.3255	1.060	1.258	0.076
86.77	84.80	1.042	-0.2967	1.339	0.3726	1.079	1.243	0.074
70.84	69.00	1.054	-0.0419	1.096	0.5060	1.142	1.197	0.068
50.30	49.40	1.103	0.1222	0.9812	0.6128	1.194	1.143	0.060
29.94	29.75	1.188	0.1719	1.016	0.6800	1.229	1.093	0.052
13.65	14.40	1.271	0.1815	1.089	0.7260	1.266	1.060	0.046
9.22	10.00	1.298	0.1780	1.120	0.7379	1.277	1.050	0.044
3.41	4.70	1.337	0.1684	1.168	0.7527	1.293	1.040	0.042

Table 3c. Rotor 5 Blade Element Design Data Along Design Streamlines (Metric Units) (Continued)

VELOCITY DIAGRAM DATA

Corrected Rotor Speed: 440.87 rad/s

Corrected Weight Flow: 49.894 kg/sec

Percent Span From Tip Leading Edge	Trailing Edge	V'_{1e} (m/sec)	V_{z1e} (m/sec)	$V'_{\theta 1e}$ (m/sec)	β'_{1e} (rad)	U_{1e} (m/sec)	V'_{te} (m/sec)	V_{zte} (m/sec)	$V'_{\theta te}$ (m/sec)	β'_{te} (rad)	U_{te} (m/sec)
96.41	94.75	237.56	148.01	185.65	0.8978	185.47	130.82	128.77	-23.47	-0.1798	186.14
91.20	89.25	239.66	148.52	188.15	0.9023	187.93	134.29	133.80	- 9.75	-0.0768	188.61
86.77	84.80	241.67	148.95	190.25	0.9062	190.10	136.94	136.91	0.6122	0.0000	190.50
70.84	69.00	247.89	149.80	197.60	0.9222	197.51	145.81	142.79	29.26	0.1990	197.35
50.30	49.40	255.23	148.80	207.32	0.9472	207.26	152.33	144.90	50.90	0.3386	205.83
29.94	29.75	260.78	144.56	216.65	0.9800	216.71	157.06	143.86	61.57	0.4084	214.45
13.65	14.40	264.01	138.74	224.11	1.015	224.54	158.73	142.64	67.36	0.4416	221.04
9.22	10.00	264.59	136.70	226.40	1.026	226.46	159.37	142.49	69.19	0.4485	223.05
3.41	4.70	265.35	133.35	229.20	1.041	229.30	160.08	142.34	71.02	0.4573	225.30

DESIGN PERFORMANCE DATA

Pressure Ratio: 1.414

Efficiency: 89.3%

Percent Span From Tip Leading Edge	Trailing Edge	$\Delta\beta'$ (rad)	M'_{1e}	i_m (deg)	D_F	$\bar{\omega}$	Loss Parameter	δ° (rad)	$P_{te} \times 10^{-6}$ (N/m^2)	T_{te} ($^\circ K$)
96.41	94.75	1.0776	0.712	-0.1564	0.796	0.200	0.077	0.3613	0.1486	326.93
91.20	89.25	0.9791	0.719	-0.1431	0.770	0.173	0.069	0.3176	0.1471	325.28
86.77	84.80	0.9062	0.724	-0.1358	0.750	0.153	0.062	0.2967	0.1459	324.10
70.84	69.00	0.7232	0.743	-0.1314	0.696	0.107	0.044	0.2409	0.1433	321.30
50.30	49.40	0.6086	0.766	-0.1562	0.665	0.082	0.034	0.2164	0.1422	319.86
29.94	29.75	0.5716	0.780	-0.2080	0.668	0.107	0.045	0.2365	0.1421	320.50
13.65	14.40	0.5734	0.789	-0.2553	0.678	0.141	0.060	0.2600	0.1421	321.79
9.22	10.00	0.5775	0.791	-0.2716	0.680	0.154	0.066	0.2705	0.1420	322.75
3.41	4.70	0.5837	0.792	-0.2958	0.682	0.170	0.073	0.2888	0.1420	322.74

Table 3d. Stator 5 Blade Element Design Data Along Design Streamlines (English Units)

GEOMETRY DATA

Airfoil: NACA 65 (A = 1.0)
No. of Vanes: 58

Aspect Ratio: 1.689
Chord Length: 2.182 in.
Thickness Ratio t/c: 0.090

Percent Span From Tip Leading Edge	Trailing Edge	κ_{1e} (deg)	κ_{te} (deg)	ϕ (deg)	γ° (deg)	0/0*	σ
94.74	94.9	66.30	-22.42	88.72	21.94	1.311	1.214
90.13	90.4	62.35	-20.42	82.77	20.97	1.255	1.200
84.87	85.0	59.20	-18.60	77.80	20.30	1.201	1.187
70.39	70.2	53.65	-15.12	68.77	19.27	1.126	1.151
50.66	49.8	51.95	-13.80	65.75	19.08	1.101	1.105
30.92	30.0	55.03	-15.17	70.20	19.93	1.131	1.063
15.79	15.0	59.20	-17.22	76.42	20.99	1.188	1.032
10.53	10.0	61.10	-18.15	79.25	21.48	1.212	1.021
5.13	5.0	63.30	-19.40	82.70	21.95	1.238	1.010

VELOCITY DIAGRAM DATA

Percent Span From Tip Leading Edge	Trailing Edge	V_{1e} (ft/sec)	V_{z1e} (ft/sec)	$V_{\theta 1e}$ (ft/sec)	β_{1e} (deg)	V_{te} (ft/sec)	V_{zte} (ft/sec)	$V_{\theta te}$ (ft/sec)	β_{te} (deg)
94.74	94.9	821.5	453.1	687.1	56.90	457.1	457.0	0.0	0.0
90.13	90.4	800.5	468.7	655.8	54.50	457.8	457.8	0.0	0.0
84.87	85.0	787.0	481.5	622.5	52.35	458.4	458.3	0.0	0.0
70.39	70.2	747.5	500.0	558.0	48.00	459.2	459.0	0.0	0.0
50.66	49.8	716.0	503.5	510.0	45.40	464.3	464.0	0.0	0.0
30.92	30.0	697.0	482.1	503.0	46.14	474.8	474.6	0.0	0.0
15.79	15.0	680.5	463.8	505.0	47.94	488.2	487.5	0.0	0.0
10.53	10.0	673.0	440.0	506.2	48.77	493.8	493.0	0.0	0.0
5.13	5.0	664.5	426.2	508.0	49.85	500.0	499.2	0.0	0.0

Table 3d. Stator 5 Blade Element Design Data Along Design Streamlines (English Units) (Continued)

DESIGN PERFORMANCE DATA

Stage Pressure Ratio: 1.375
Stage Efficiency: 81.7%

Percent Span From Tip Leading Edge	Trailing Edge	$\Delta\beta$ (deg)	M_{1e}	i_m (deg)	D_F	$\bar{\omega}$	Loss Parameter	$\delta°$ (deg)	P_{te} (psia)
94.74	94.9	56.90	0.728	- 9.40	0.789	0.215	0.089	22.42	20.175
90.13	90.4	54.50	0.712	- 7.85	0.771	0.193	0.080	20.42	20.189
84.87	85.0	52.35	0.695	- 6.85	0.751	0.167	0.070	18.60	20.204
70.39	70.2	48.00	0.662	- 5.65	0.710	0.116	0.050	15.12	20.189
50.66	49.8	45.40	0.633	- 6.55	0.676	0.090	0.041	13.80	20.175
30.92	30.0	46.14	0.614	- 8.89	0.659	0.092	0.043	15.17	20.175
15.79	15.0	47.94	0.597	-11.26	0.643	0.096	0.047	17.22	20.182
10.53	10.0	48.77	0.590	-12.33	0.636	0.097	0.048	18.15	20.189
5.13	5.0	49.85	0.582	-13.45	0.626	0.098	0.049	19.40	20.175

Stator 5 Blade Element Design Data Along Design Streamlines (Metric Units)

GEOMETRY DATA

Airfoil: NACA 65 (A = 1.0)
No. of Vanes: 58

Aspect Ratio: 1.689
Chord Length: 0.0554 m
Thickness Ratio, t/c: 0.090

Percent Span From Tip Leading Edge	Trailing Edge	κ_{1e} (rad)	κ_{te} (rad)	ϕ (rad)	$\gamma°$ (rad)	0/0*	σ
94.74	94.9	1.157	-0.3913	1.548	0.3829	1.311	1.214
90.13	90.4	1.088	-0.3564	1.445	0.3660	1.255	1.200
84.87	85.0	1.033	-0.3246	1.358	0.3543	1.201	1.187
70.39	70.2	0.9364	-0.2639	1.200	0.3363	1.126	1.151
50.66	49.8	0.9067	-0.2409	1.148	0.3330	1.101	1.105
30.92	30.0	0.9604	-0.2648	1.225	0.3478	1.131	1.063
15.79	15.0	1.033	-0.3005	1.334	0.3663	1.188	1.032
10.53	10.0	1.066	-0.3168	1.383	0.3749	1.212	1.021
5.13	5.0	1.105	-0.3386	1.443	0.3831	1.238	1.010

Table 3d. Stator 5 Blade Element Design Data Along Design Streamlines (Metric Units) (Continued)

VELOCITY DIAGRAM DATA

Percent Span From Tip Leading Edge	Trailing Edge	V_{1e} (m/sec)	V_{z1e} (m/sec)	$V_{\theta 1e}$ (m/sec)	β_{1e} (rad)	V_{te} (m/sec)	V_{zte} (m/sec)	$V_{\theta te}$ (m/sec)	β_{te} (rad)
94.74	94.9	250.39	138.10	209.42	0.9931	139.32	139.29	0.0	0.0
90.13	90.4	243.99	142.85	199.88	0.9512	139.53	139.53	0.0	0.0
84.87	85.0	239.87	146.76	189.73	0.9137	139.72	139.68	0.0	0.0
70.39	70.2	227.83	152.39	170.07	0.8377	139.96	139.90	0.0	0.0
50.66	49.8	218.23	153.46	155.47	0.7924	141.51	141.42	0.0	0.0
30.92	30.0	212.44	146.94	153.31	0.8053	144.71	144.65	0.0	0.0
15.79	15.00	207.41	141.36	153.92	0.8367	148.80	148.58	0.0	0.0
10.53	10.0	205.13	134.11	154.22	0.8512	150.51	150.26	0.0	0.0
5.13	5.0	202.53	129.90	154.83	0.8700	152.39	152.15	0.0	0.0

DESIGN PERFORMANCE DATA

Percent Span From Tip Leading Edge	Trailing Edge	$\Delta\beta$ (rad)	M_{1e}	i_m (rad)	D_F	$\overline{\omega}$	Loss Parameter	δ°, (rad)	$P_{te} \times 10^{-6}$ (N/m^2)
94.74	94.9	0.9931	0.728	-0.1641	0.789	0.215	0.089	0.3913	0.1391
90.13	90.4	0.9512	0.712	-0.1370	0.771	0.193	0.080	0.3564	0.1392
84.87	85.0	0.9137	0.695	-0.1196	0.751	0.167	0.070	0.3246	0.1393
70.39	70.2	0.8377	0.662	-0.0986	0.710	0.116	0.050	0.2639	0.1392
50.66	49.8	0.7924	0.633	-0.1143	0.676	0.090	0.041	0.2409	0.1391
30.92	30.0	0.8053	0.614	-0.1552	0.659	0.092	0.043	0.2648	0.1391
15.79	15.0	0.8367	0.597	-0.1965	0.643	0.096	0.047	0.3005	0.1392
10.53	10.0	0.8512	0.590	-0.2152	0.636	0.097	0.048	0.3168	0.1392
5.13	5.0	0.8700	0.582	-0.2347	0.626	0.098	0.049	0.3386	0.1391

Table 4. Geometry Selections

	Rotor		Stator	
	Hub	Tip	Hub	Tip
Solidity	1.285	1.025	1.226	0.994
Thickness ratio, t/c	0.08	0.04	0.09	0.09
Chord, in. (meters)	2.21(0.05613)	2.21	2.18(0.05537)	2.18

The blade chord angle and camber were determined by satisfying the velocity diagram values, the correlations of data previously described, and the camber, deviation angle, and incidence angle correlations presented as equations 286, 287, and 288 of Reference 9.

The resultant radial distributions of rotor and stator camber and blade chord angle are presented in figures 13 and 14. The data pertaining to the blading geometry are presented in terms of an equivalent circular arc meanline of the same maximum camber as the actual (A = 1.0) meanline of the 65-Series blade sections. In addition, the leading and trailing edge blade angles based on the equivalent circular arc meanline are provided for reference in figures 15 and 16. Rotor and stator incidence and deviation angles are presented in figures 17 and 18. Hub, midspan, and tip sections of the stage 4 and 5 blading are shown in figures 19 and 20. Blade element data are summarized in table 3.

Predicted Overall Performance Without Slots Or Vortex Generators

The overall performance of stages 4 and 5 was predicted for the design blading geometry, operating with losses equal to those of the original data correlations in figures 1 through 4. This gives the approximate performance that would be expected without any improvement due to slots and fences or vortex generators. For this calculation it was assumed that the rotor deviation angle distribution would be the same as the design distribution, and that any slight change in stator incidence angle would not affect stator minimum losses. The resulting predicted overall performance is given in table 5.

Table 5. Predicted Overall Performance Without Slots or Vortex Generators

	Pressure Ratio	Adiabatic Efficiency, %
Rotor 4	1.335	86.8
Rotor 5	1.401	87.3
Stage 4	1.305	79.7
Stage 5	1.353	78.1

Design of Slots and Vortex Generators for Stage 4

The design of blade slots and the selection and design of wall vortex generators for stage 4 were based on a preliminary analysis of the data from the stage 4 baseline tests and the results of the modified stage 3 tests of Reference 1. Vortex generators were chosen over secondary flow fences because the fences did not provide any apparent performance improvement for stage 3 (Reference 2). Although compressors that utilize vortex generators have not been found in the open literature, the effectiveness of vortex generators in other applications (and criteria for their design) are well documented.

Slot Design

Four factors were considered for the selection of rotor and stator slot configurations:

- Spanwise extent
- Chordal location
- Number
- Geometry

Spanwise extent, chordal location, and the number of slots were based on the stage 4 baseline test results obtained at near design point operation conditions. Slot geometry was based on the results of a two-dimensional potential flow analysis.

The estimated stalled regions on the rotor and stator suction surfaces at near design operating conditions are illustrated in figure 21. The spanwise extent of the stalled regions were estimated on the basis of the axial velocity and loss coefficient distributions shown in the figure; and the shape of the stalled regions generally

conforms to secondary flow patterns that have been observed on cascade airfoils. The maximum spanwise extent of the slots was selected to cover the estimated spanwise extent of the stalled regions on the suction surfaces. The chordal location of the slots was selected so that all of the slot flow would enter the suction surface flow ahead of the estimated flow separation line. Because of the larger radial flow gradients indicated by the axial velocity distribution for the rotor (as opposed to those indicated for the stator), two rows of slots were specified for the rotor. The upstream row (of lesser spanwise extent) is intended to move the starting point of the stalled region beyond the downstream row.

Any improvement in the rotor exit velocity distribution by means of the rotor slots implies improvement to the stator inlet velocity distribution. The increase in axial velocity near the walls will be accompanied by a reduced radial flow shift through the stator. Based on this anticipated increase in axial velocity and the accompanying reduction in the stalled region on the stator, only one row of slots was considered necessary for the stator. The chordal location of the upstream rotor slot, and the stator slot, favors operation above design incidence, as one of the program objectives is to extend the stable operating range of compressor stages. Also, all of the slot rows (at the suction surface) are either at or downstream of the minimum pressure point for operation between design and stall incidence; thus the slot flow should not adversely affect the stabilizing influence of the favorable pressure gradient on the suction surface. Slot locations for the rotor and stator are summarized in table 6.

Table 6. Rotor and Stator Slot Location

	Chordal Location (Percent Chord)	Spanwise Extent (Percent from Tip)
Rotor	20	0-20 ; 80-100
	45	0-30 ; 70-100
Stator	20	0-30 ; 80-100

Slot geometry was evaluated on the basis of calculated pressure coefficient distributions for the airfoil section at 85% span from the tip of stator 4. Two-dimensional, steady, incompressible, and inviscid

potential flow was assumed for these calculations. The 85% span section was selected as being representative of both the rotor and stator section geometry near the wall. Slot geometries for the rotor hub and tip and the stator tip sections were made geometrically similar to the configuration selected for the stator at 85% span.

The slot is required to transfer a specified amount of flow from the pressure surface to the suction surface as efficiently as possible, and with as much acceleration as practical without introducing severe adverse pressure gradients on the slot walls. The slot design that evolved from the annular cascade tests of Reference 10 was evaluated initially. The pressure coefficient distribution for this slot, located at 20% chord in the 85% span section of stator 4, is shown in figure 22. The slight diffusion on the forward wall of the slot and the high rate of diffusion immediately downstream of the slot were considered unacceptable. Subsequent changes were made to the surface curvature on the forward and rear walls of the slot to provide a smooth pressure distribution through the slot without severe local adverse pressure gradients. Eight configurations were analyzed. The high degree of convergence in the initial configuration led to diffusion on the pressure surface ahead of the slot. The revised slot had essentially zero convergence, and gave a smoother transition through the slot. The selected configuration and associated pressure distribution are shown in figure 23. The slight spike in pressure coefficient on the rear wall of the slot is not considered to be of any consequence because of the large acceleration after the spike.

Slots at 50% chord were evaluated with the selected slot at 20% chord. The selected configuration of the second slot, and the pressure coefficient distribution with both slots in the airfoil, are shown in figure 24. Final slot configuration and locations are shown for several spanwise sections of the rotor in figures 25a and 25b, and for the stator in figure 26.

Vortex Generator Design

Baseline test results indicated severe secondary flows in the end regions of both the rotor and stator blade rows and therefore, it was concluded that vortex generators should be designed for the inner and

outer walls of both blade rows. The vortex generators are intended, by means of turbulent mixing, to induce high momentum air from the mainstream into the wall boundary layer flow and low momentum air from the wall region into the mainstream flow. This mixing helps to unload the blades in the wall region and load the midspan region.

Vortex generator design criteria presented in References 11 and 12 were used as a guideline for the design of these wall vortex generators. The vortex generators for the rotor were located approximately 20 boundary layer thicknesses upstream of the rotor leading edge and positioned symmetrically in pairs to produce counter-rotating vortices. A boundary layer thickness of 0.41 in. (0.010 m) was determined from rotor inlet total pressure traverse data obtained during the baseline tests. Vortex generator height was set equal to 1.1 boundary layer thicknesses, and they were equally spaced 2.7 heights apart at 25% chord. The chord length was set equal to approximately twice the height. The resulting configuration is shown in figures 27a and 27b. Based on the above criteria, a chord of 0.910 in. (0.0231 m) was desired. Sixty-five series airfoil stock with a 0.983 in. (0.02497 m) chord was available, and was used to expedite fabrication. This strip stock had a maximum thickness-to-chord ratio of 9%, and a camber (based on an equivalent circular arc meanline) of 25 deg (0.4363 rad). To produce the maximum lift-drag ratio, an angle of attack of 14 deg (0.2443 rad) was selected.

Design of the stator vortex generators was not straight-forward because no clearly defined boundary layer exists downstream of the rotor, and the upstream distance from a "separation" point (such as the stalled regions on the stator vanes) for placement of the generators is limited. A pseudo-boundary layer thickness was therefore defined as one-twentieth of the maximum distance available for generator placement upstream of the stator mid-chord. Thus, with the vortex generator height set at 1.1 boundary thicknesses, the required distance for turbulent mixing is provided between the generators and the "separation" point (stator mid-chord, in this case). One pair of counter-rotating vortex generators was provided for each stator vane passage. The vortex generator chord length was twice the height, and they were equally spaced at 25% chord. These vortex generators will be fabricated from 0.020 in. (0.000508 m) sheet stock

because of their small size. They will be cambered 20 deg (0.3491 rad) and installed at an angle of attack of 10 deg (0.1745 rad). The chord angle will be set based on the stator inlet air angles measured during the testing of slotted stage 4 with inlet vortex generators. The resulting configuration is shown in figure 27c.

MECHANICAL DESIGN

Steady-State Stress Analysis

A steady-state stress analysis was performed for rotors 4 and 5 and stators 4 and 5 for design point conditions. A computer program that calculates airload, section properties, and the resulting stress distributions was used in this analysis. The stator was treated as a guided, cantilevered beam because slight movement of the stator inner shroud is possible, and this definition resulted in larger stresses than those for a beam fixed rigidly at both ends. The influence of centrifugal forces on gas bending loads was accounted for in the rotor stress calculation. Hub section bending stresses were evaluated at the leading and trailing edge and at the point of maximum thickness on the convex surface.

Calculated steady-state blade stress distributions for rotor 4 and 5 are presented in figure 28. The combined stresses shown are the sum of the net gas bending and the centrifugal tensile stress. The maximum stress for rotor 4 was 19,800 psi (0.1365×10^9 N/m^2) at the trailing edge of the hub section. The maximum stress for rotor 5 was 17,300 psi (0.1193×10^9 N/m^2) at the trailing edge 90% of span from the tip. The calculated stress for rotor 4 with two slots was 27,500 psi (0.1896×10^9 N/m^2) and occurred at the leading edge of the middle airfoil segment in the hub section. The section of primary interest for stator stress evaluation was the junction of the airfoil and attachment trunnion. For this section the calculated bending stresses were 33,700 psi (0.2324×10^9 N/m^2) and 40,100 psi (0.2765×10^9 N/m^2) for stators 4 and 5 respectively. Stator 4 slots did not affect the stresses since their location did not alter the airfoil/trunnion interface section modulus. Both the rotor and stator blading will be machined from materials having a 0.2% yield strength of 110,000 psi (0.7584×10^9 N/m^2); the above calculated stresses are well within the design limits for these materials.

Design analyses of rotor disk stresses, rotor and stator blade attachment stresses, and rotor critical speed were not performed because the rotor and stator assemblies are similar to those reported in Reference 1. The blade attachment stress analysis in Reference 13 thus applies to the stage 4 and 5 blading.

Vibration Analysis

Bending and torsional vibration frequencies were calculated for the stage 4 and 5 blading and the results are presented in terms of frequency versus rotor speed in figures 29 and 30. Lines representing factors of rotor frequency (E) are shown in the figures to permit identification of any excitation frequencies within the planned operating range. As indicated in figure 29, the calculated rotor blade natural frequencies are greater than six times that of rotor frequency for speeds between zero and 110% design corrected rotor speed. This level of frequency is considered adequate for safe rotor operation as no disturbances are expected at this frequency level. The calculated stator first bending frequencies, shown in figure 30, do not indicate resonance at the rotor passing frequency for the planned range of operating conditions, therefore no vibration problems are anticipated for the stator. Values were not calculated for the slotted blading because the change in frequency has been noted in other similar calculations to be within the accuracy of the calculation (Reference 13).

Blade vibration and fatigue life bench tests were conducted to determine the actual natural frequencies, the locus of maximum stress points, and the fatigue life of the blading. The measured vibration frequencies are summarized in table 7 and shown in figure 29 for comparison with the calculated values.

Table 7. Measured Vibration Frequencies

	First Bending Frequency		First Torsion Frequency	
	Unslotted	Slotted	Unslotted	Slotted
Configuration	cps (rad/sec)	cps (rad/sec)	cps (rad/sec)	cps (rad/sec)
Rotor 4	443 (2783.4)	403 (2532.1)	1465 (9204.8)	1360 (8545.1)
Rotor 5	490 (3078.7)	-	1500 (9424.8)	-
Stator 4	-	2100 (13194)	-	-
Stator 5	-	-	-	-

The measured bending frequencies for rotors 4 and 5 are lower than the calculated frequencies at zero rpm (figure 29). Assuming that the actual blade frequency will have a similar distribution with rotor speed as the calculated blade frequency, rotor 4 would closely approximate a 6E resonance at design corrected rotor speed. Although there are six support struts in the compressor inlet flowpath, the 6E vibration frequency was of little concern because the struts are unequally spaced and their wakes are substantially dissipated ahead of the rotor. The measured torsional mode vibration frequencies at design speed are not close to any apparent excitation frequencies.

The results of the fatigue life tests are presented in table 8. These fatigue test results were obtained by imposing bending or torsional stresses at the predetermined natural frequencies starting with 35,000 psi (0.2413×10^9 N/m^2) and increasing the level in 5,000 psi (0.3447×10^8 N/m^2) increments after 10×10^6 cycles (0.6238×10^8 rad) until failure occurred.

The calculated stresses and fatigue test results indicate that both the slotted and unslotted rotor and stator blading have sufficient strength to withstand the loads anticipated during the test program.

Flutter Analysis

The bending and torsional stall flutter characteristics of rotors 4 and 5 were analyzed and calculated flutter variables were compared with correlated experimental flutter data. The flutter variables are a reduced velocity parameter, defined as

$$K = \frac{3.82 V_1'}{c \omega}$$

and incidence parameter, defined as

$$f(i_m) = \frac{i_m - i_{m\ ref}}{\text{Low-Loss Incidence Range}}$$

Where V_1', c, i_m, $i_{m\ ref}$ and low-loss incidence range are the values for airfoil sections located at 25% span from the tip. The low-loss incidence range and $i_{m\ ref}$ were determined from the P&WA cascade data correlation.

The flutter variables, calculated for design operating conditions and for the estimated negative and positive incidence operating limits, are shown in relationship to correlated flutter data for first bending and

first torsional vibration frequencies in figures 31 and 32, respectively. The region labeled "possible $-i_m$ flutter region" is not well defined by experimental data and the boundary indicated is simply a mirror image of the stall flutter boundary. Neither the design points nor the operating envelopes appear to indicate a flutter problem with respect to the flutter regions shown in the figures.

Table 8. Airfoil Fatigue Test Summary

Airfoil	Slot Configuration: Percent Span From Tip	Slot Configuration: Percent Chord	Mode	Frequency, cps (rad/sec)	Stress At Failure, psi (N/m^2)	Cycles To Failure x 10^{-6}	Failure Location
Stator 4	0-30 80-100	20 20	First Bending	2100 (13914)	No Test	———	Airfoil Not Considered Critical, Therefore No Fatigue Test Conducted.
Rotor 4	0-7 10-20 80-100 0-11 14-30 70-100	20 20 20 45 45 45	First Bending	396 (2488.1)	75,000 (0.517×10^9)	1.4 (8.796)	The Failure Was In The Tip Radius of the 80 To 100% Span, 20% Chord Slot and Extended Toward the Leading Edge.
Rotor 4	0-7 10-20 80-120 0-11 14-30 70-100	20 20 20 45 45 45	First Torsion	1360 (8545.1)	45,000 (0.3103×10^9)	5 (31.416)	The Failure Was In the 11 to 14% Span, 45% Chord Bridge.
Rotor 5	None	None	First Bending	490 (3078.7)	50,000 (0.3447×10^9)	3.7 (23.247)	The Failure Was 1/8 Inch Above the Platform In the Leading Edge On Concave Surface.
Rotor 4	None	None	First Bending	430 (2701.7)	60,000 (0.4137×10^9)	0.6 (3.77)	The Failure Was 3/4 Inch Above the Platform In the Leading Edge.

REFERENCES

1. Rockenbach, R. W., "Single Stage Experimental Evaluation of Slotted Rotor and Stator Blading, Part IX - Final Report," NASA CR-54553, PWA FR-2289, 26 September 1968.

2. Rockebach, R. W., "Single Stage Experimental Evaluation of Compressor Blading with Slots and Wall Flow Fences," NASA CR-72635, PWA FR-3597.

3. Linder, C. G., and B. A. Jones, "Single Stage Experimental Evaluation of Slotted Rotor and Stator Blading, Part III - Data and Performance for Slotted Rotor I," NASA CR-54546, PWA FR-2110, February 1967.

4. Linder, C. G., and B. A. Jones, "Single Stage Experimental Evaluation of Slotted Rotor and Stator Blading, Part IV - Data and Performance for Slotted Rotor 2," NASA CR-54547, PWA FR-2111, February 1967.

5. Linder, C. G. and B. A. Jones, "Single Stage Experimental Evaluation of Slotted Rotor and Stator Blading, Part V - Data and Performance for Slotted Rotor 3 - Slotted Stator 2," NASA CR-54548, PWA FR-2285, August 1967.

6. Linder, C. G., and B. A. Jones, "Single Stage Experimental Evaluation of Slotted Rotor and Stator Blading, Part VI - Data and Performance for Slotted Stator 1," NASA CR-54549, PWA FR-2286, July 1967.

7. Linder, C. G., and B. A. Jones, "Single Stage Experimental Evaluation of Slotted Rotor and Stator Blading, Part VII - Data and Performance for Slotted Stator 2," NASA CR-54550, PWA FR-2287, September 1967.

8. Linder, C. G., and B. A. Jones, "Single Stage Experimental Evaluation of Slotted Rotor and Stator Blading, Part VIII - Data and Performance for Slotted Stator 3," NASA CR-54551, PWA FR-2288, October 1967.

9. Aerodynamic Design of Axial Flow Compressors (Revised), NASA SP-36, 1965.

10. Linder, C. G., and B. A. Jones, "Single Stage Experimental Evaluation of Slotted Rotor and Stator Blading, Part II - Annular Cascade Investigation of Slot Location and Geometry," NASA CR-54545, PWA FR-1669, October 1966.

11. Taylor, H. D., "Application of Vortex Generator Mixing Principle to Diffusers - Concluding Report." United Aircraft Research Department Report R-15064-5, December 1948.

12. Brown, A. C., H. F. Nawrocki, and P. N. Paley, "Subsonic Diffusers Designed Integrally with Vortex Generators," Journal of Aircraft, Vol. 5, No. 3, May-June, 1968, pp. 221-229.

13. Linder, C. G., and B. A. Jones, "Single Stage Experimental Evaluation of Slotted Rotor and Stator Blading, Part I - Analysis and Design," NASA CR-54544, PWA FR-1713, July 1966.

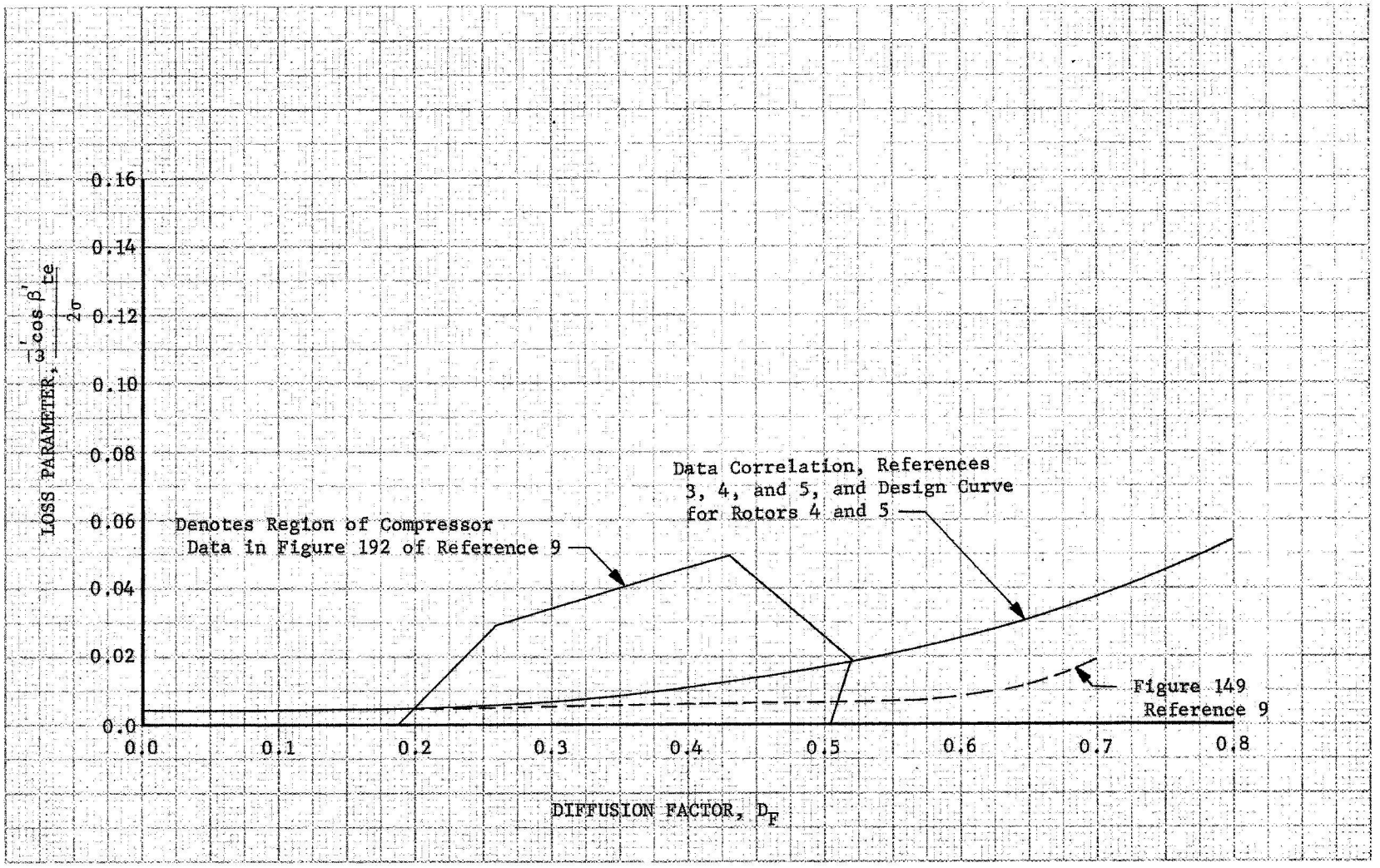

DF 78770

Figure 1. Rotor Loss Correlation, 50% Span From Tip

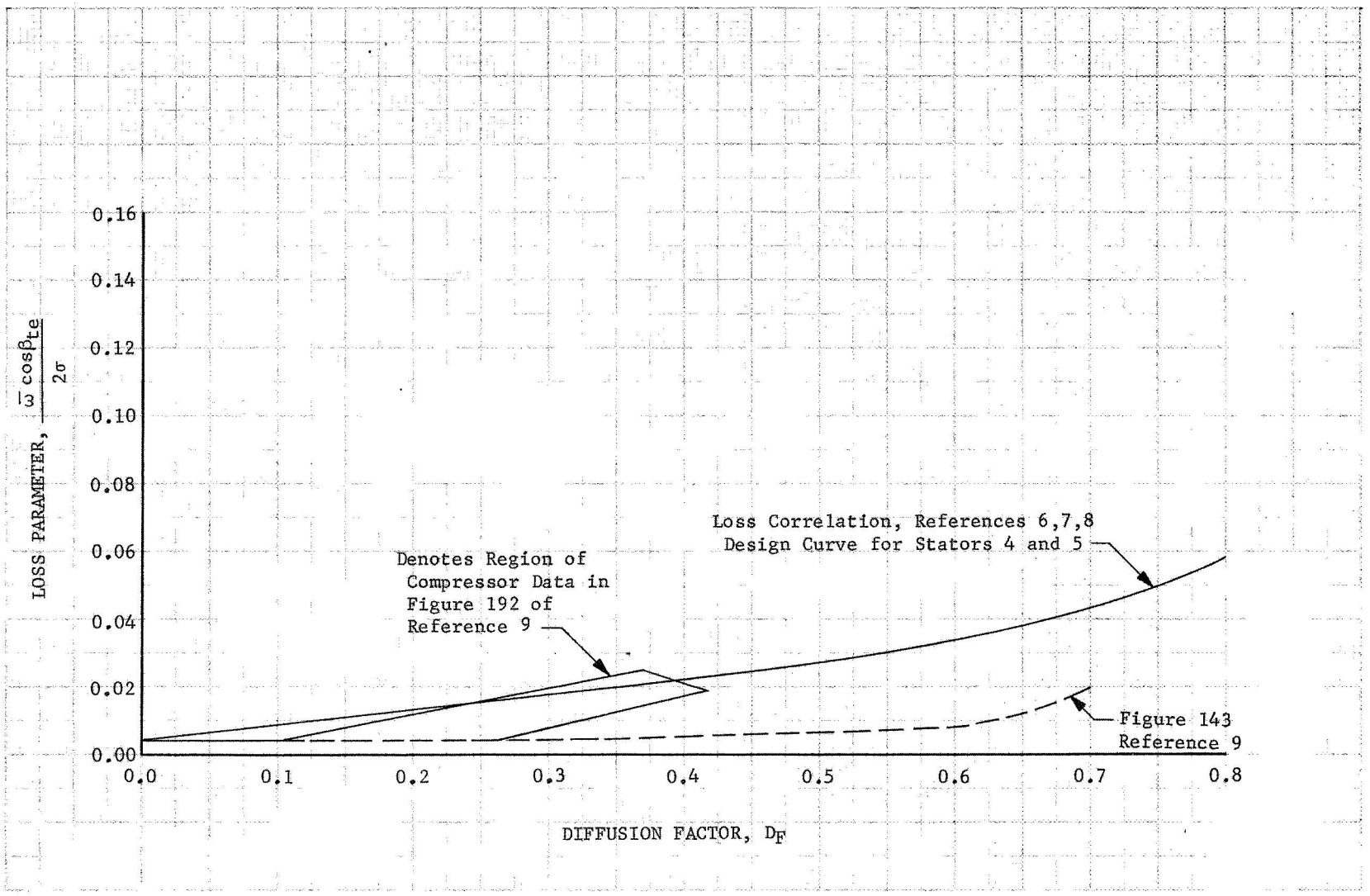

Figure 2. Stator Loss Correlation, 50% Span From Tip

DF 78785

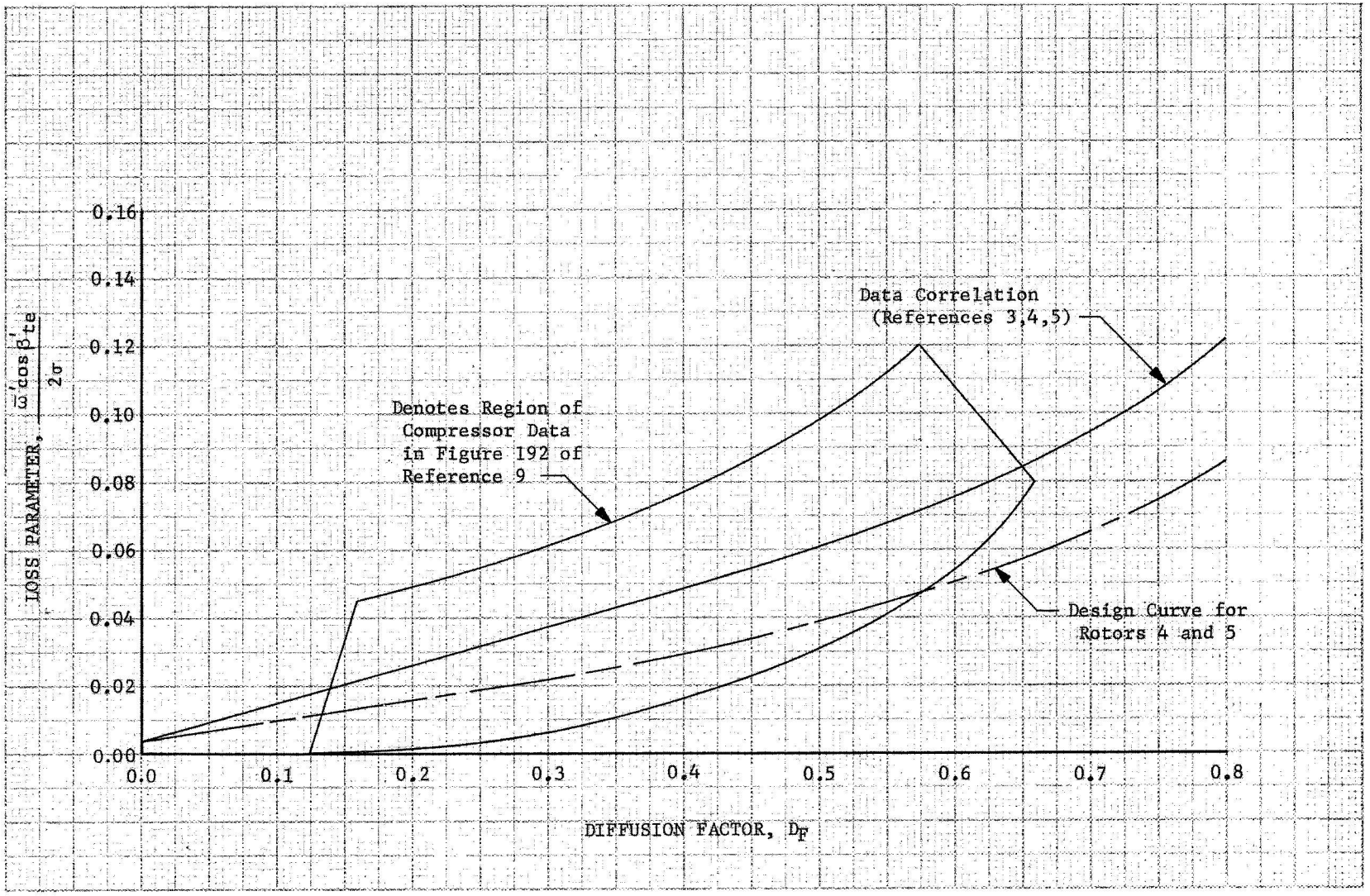

Figure 3a. Rotor Loss Correlation, 10% Span From Tip

DF 78784

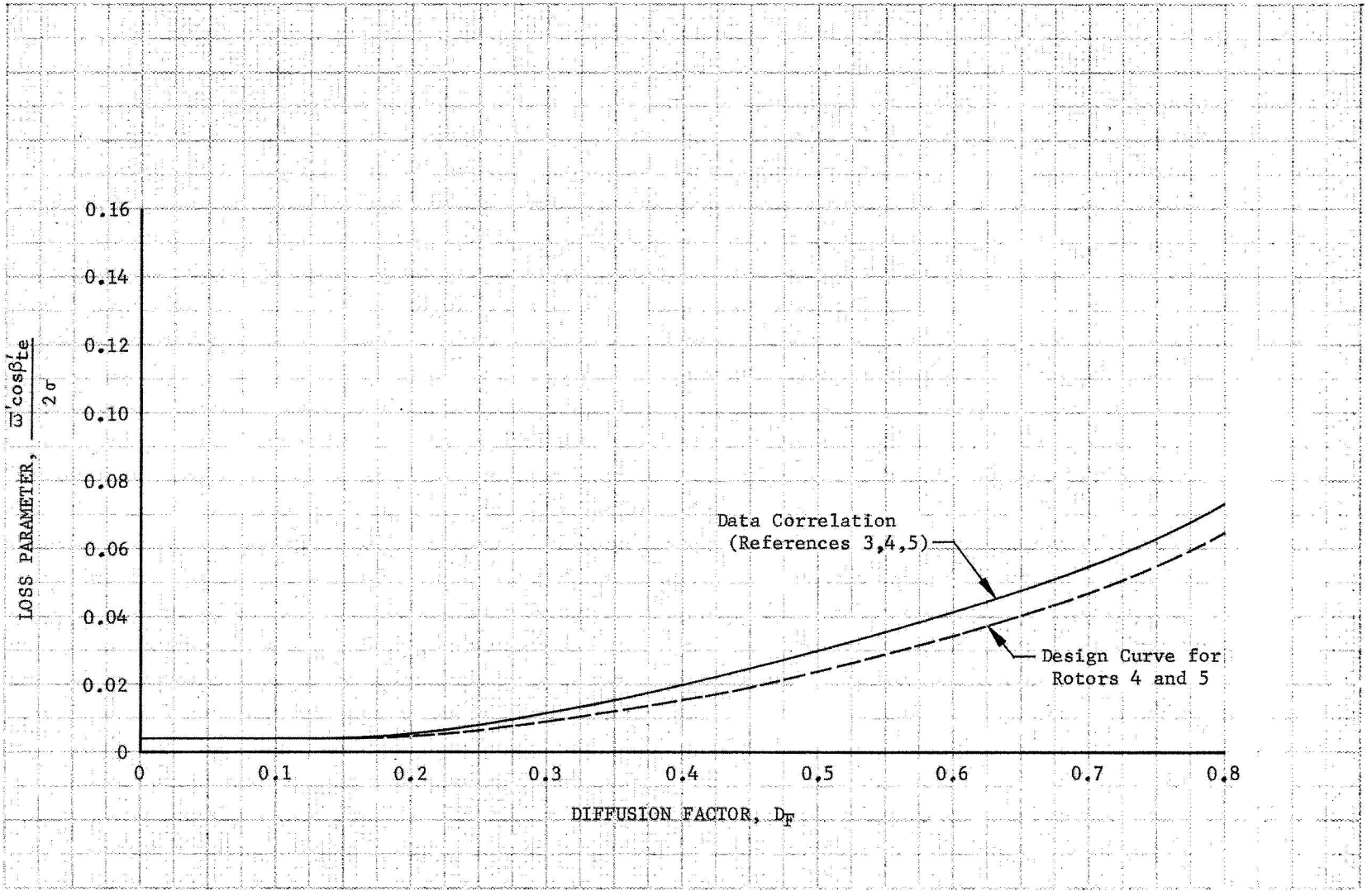

DF 78783

Figure 3b. Rotor Loss Correlation, 30% Span From Tip

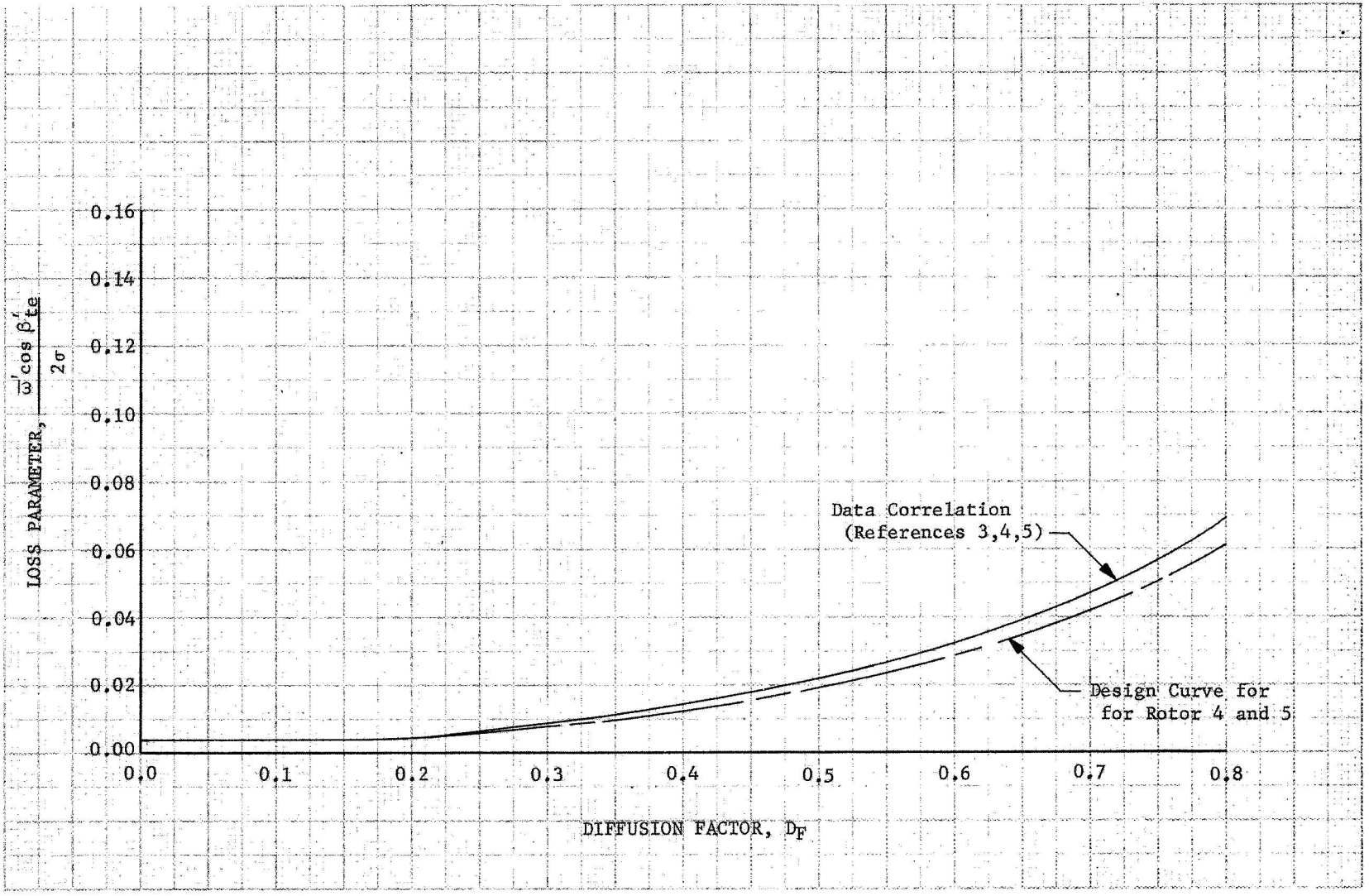

DF 78782

Figure 3c. Rotor Loss Correlation, 70% Span From Tip

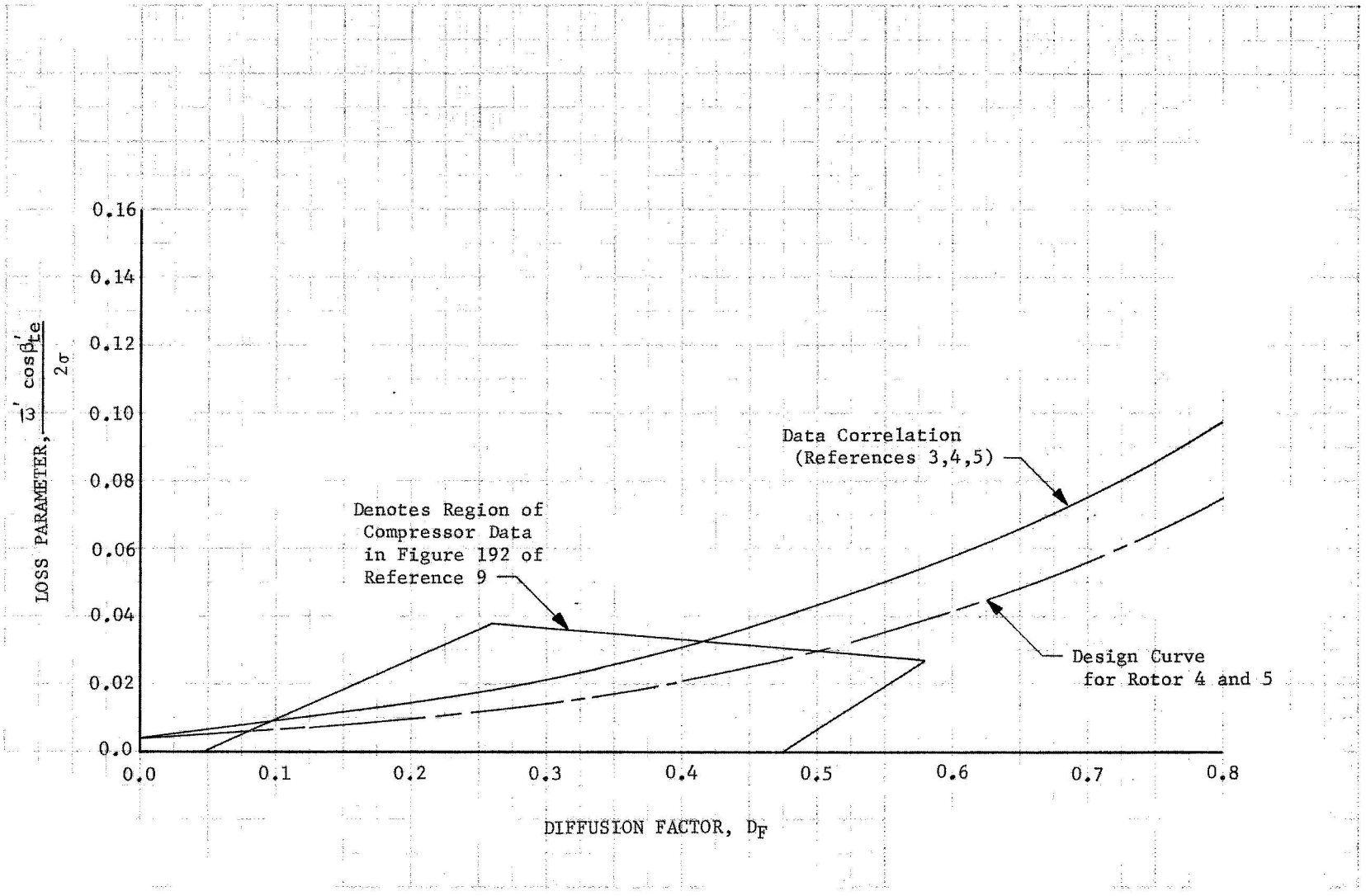

Figure 3d. Rotor Loss Correlation, 90% Span From Tip

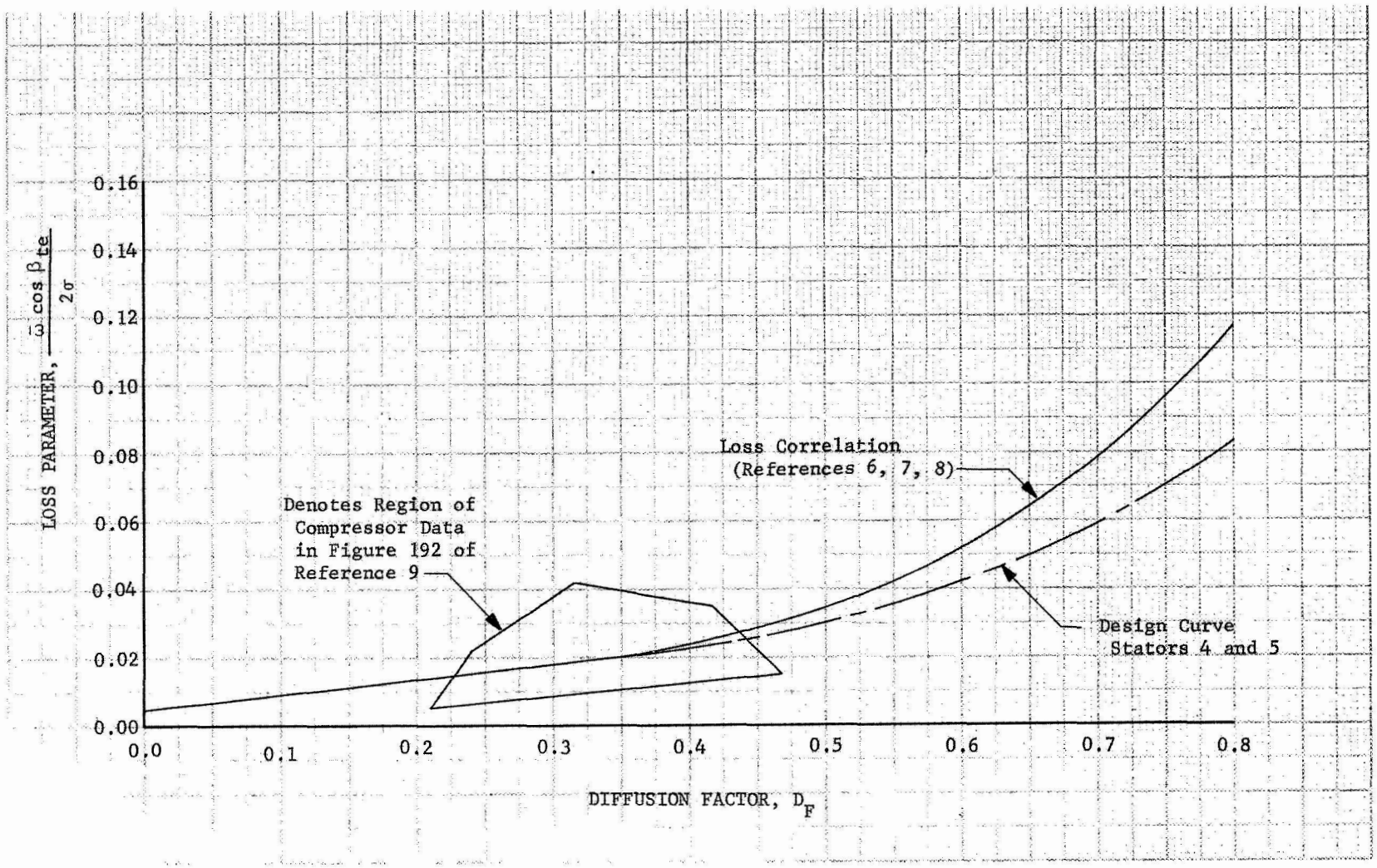

DF 78780

Figure 4a. Stator Loss Correlation, 10% Span From Tip

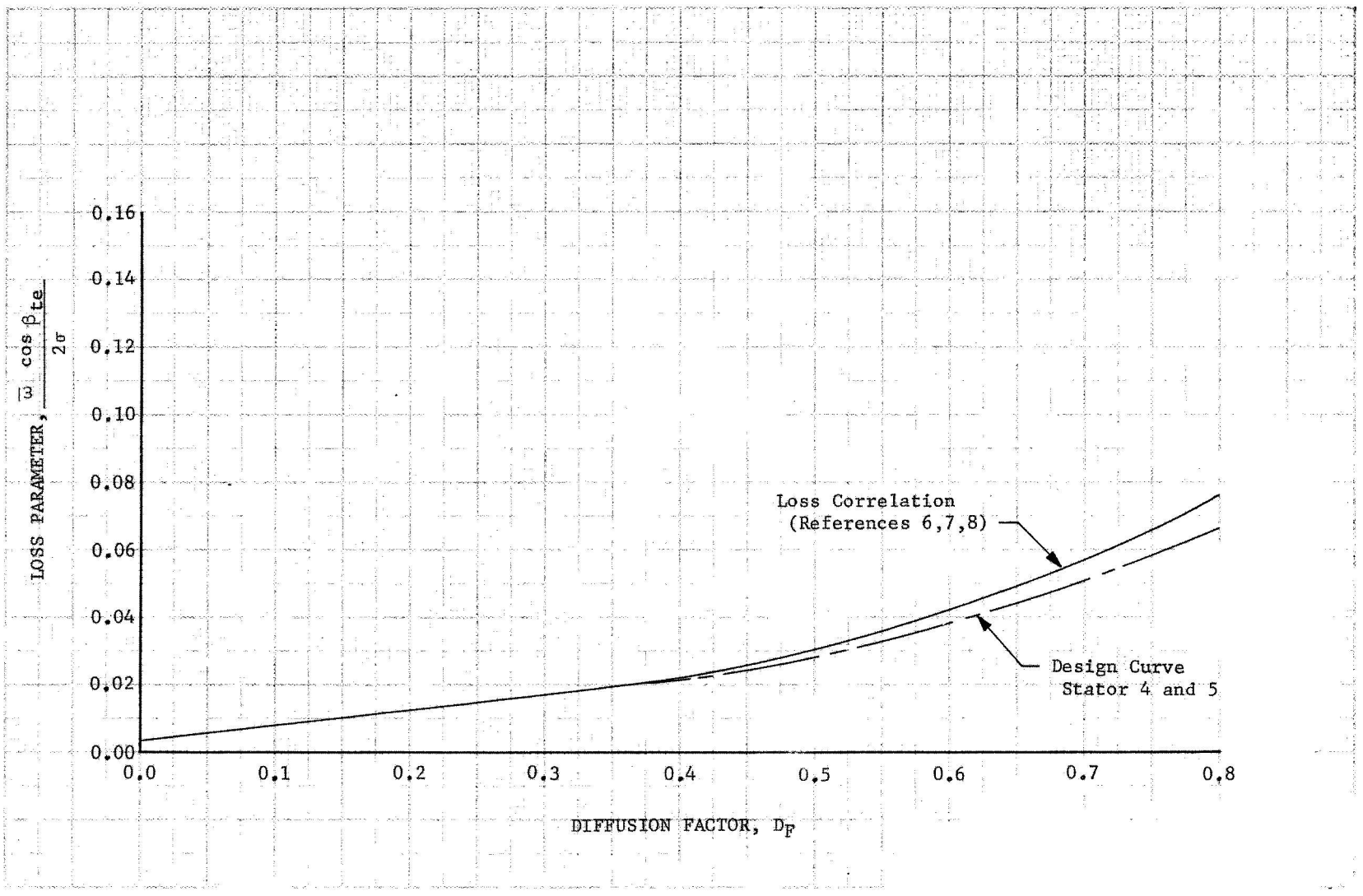

Figure 4b. Stator Loss Correlation, 30% Span From Tip

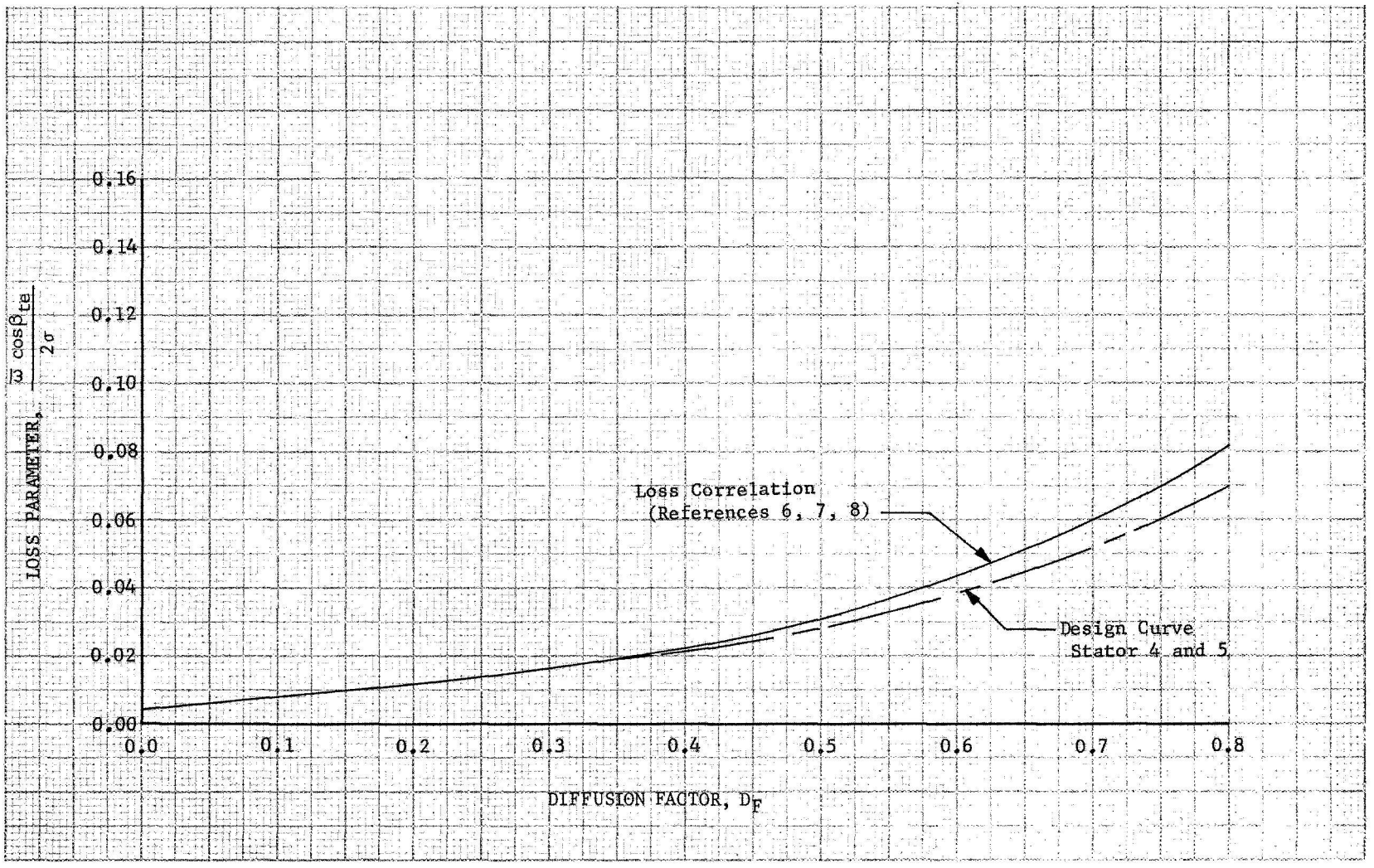

Figure 4c. Stator Loss Correlation, 70% Span From Tip

DF 78778

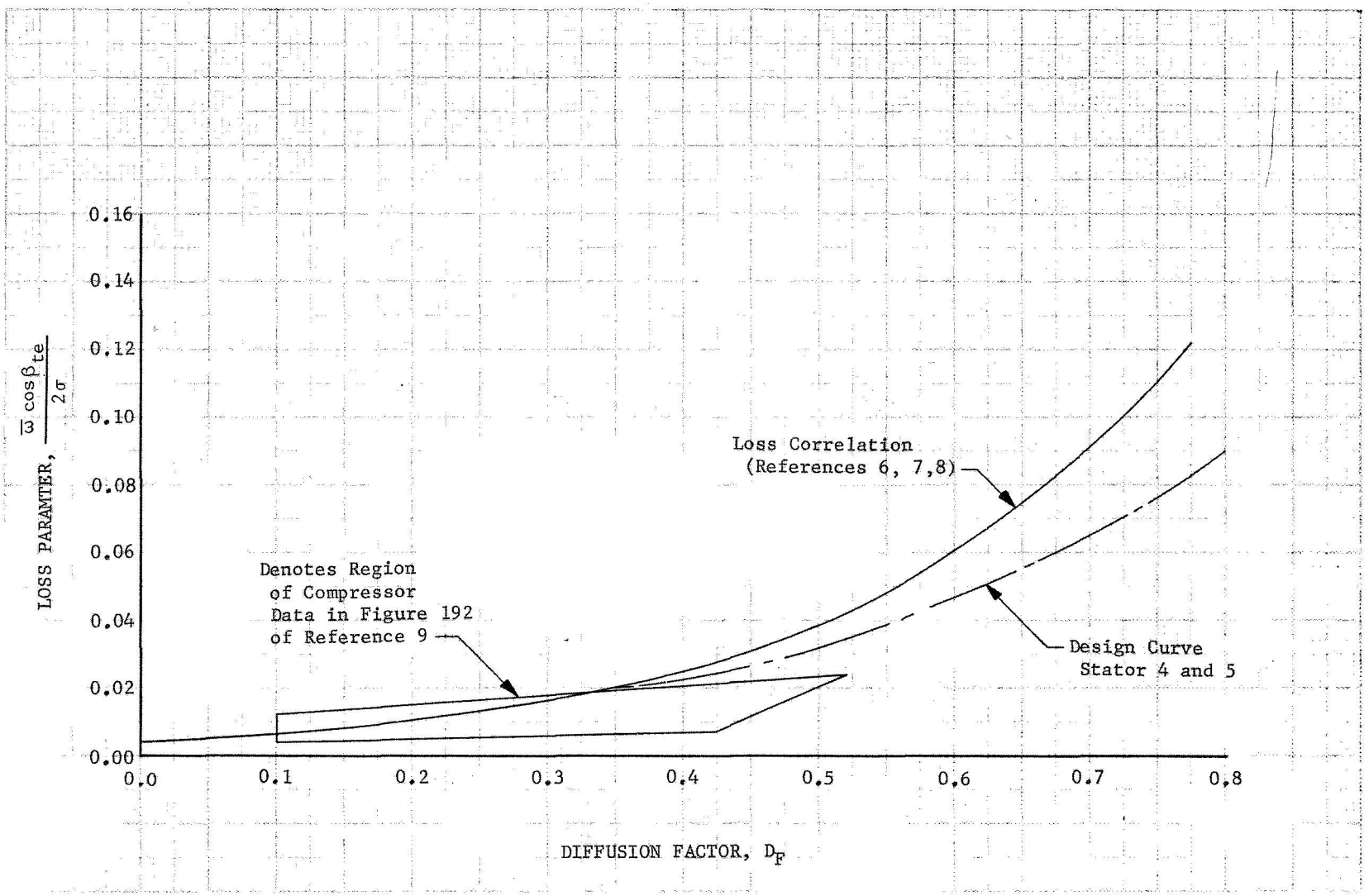

Figure 4d. Stator Loss Correlation, 90% Span From Tip

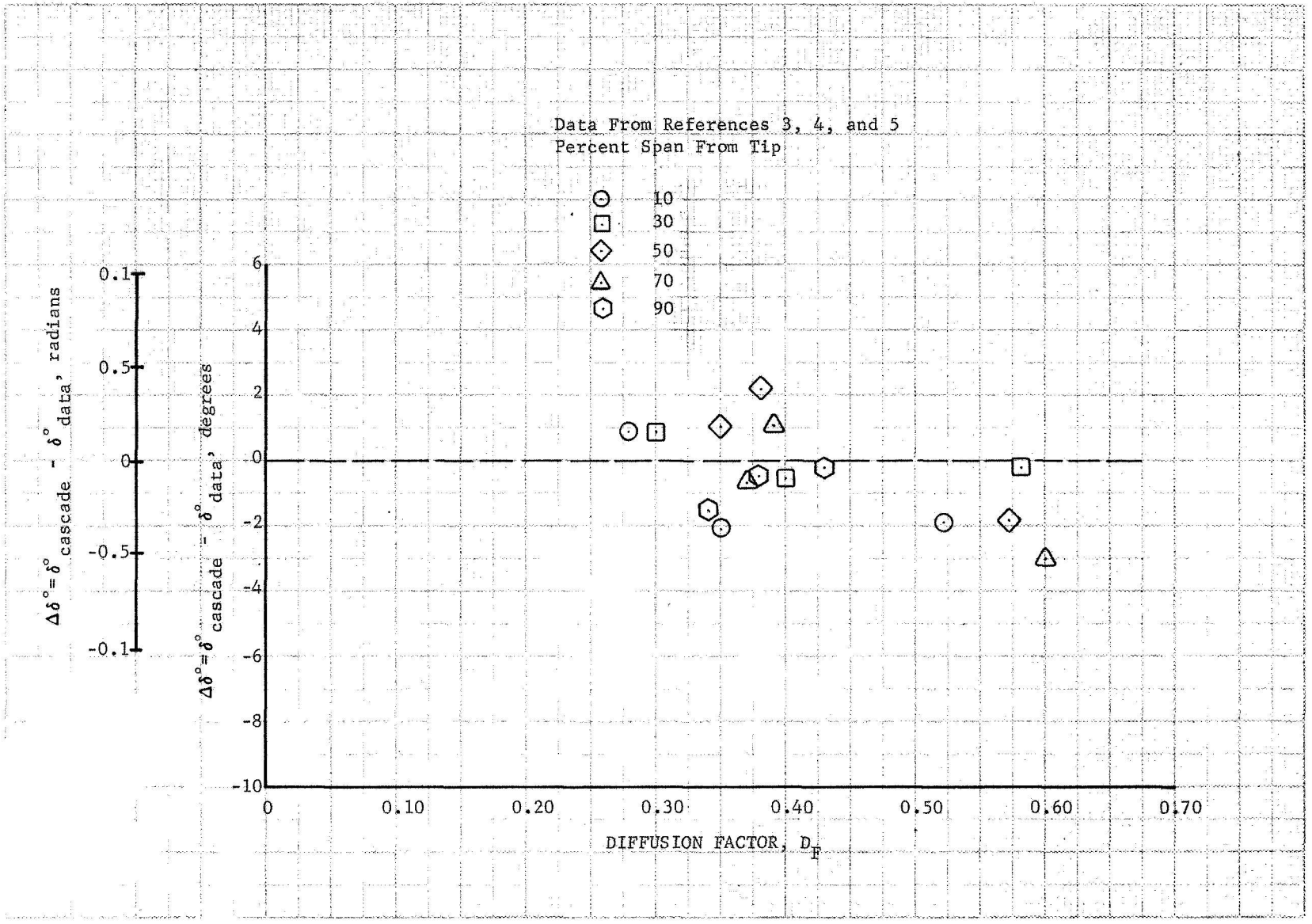

Figure 5. Rotor Deviation Angle Correlation

DF 78772

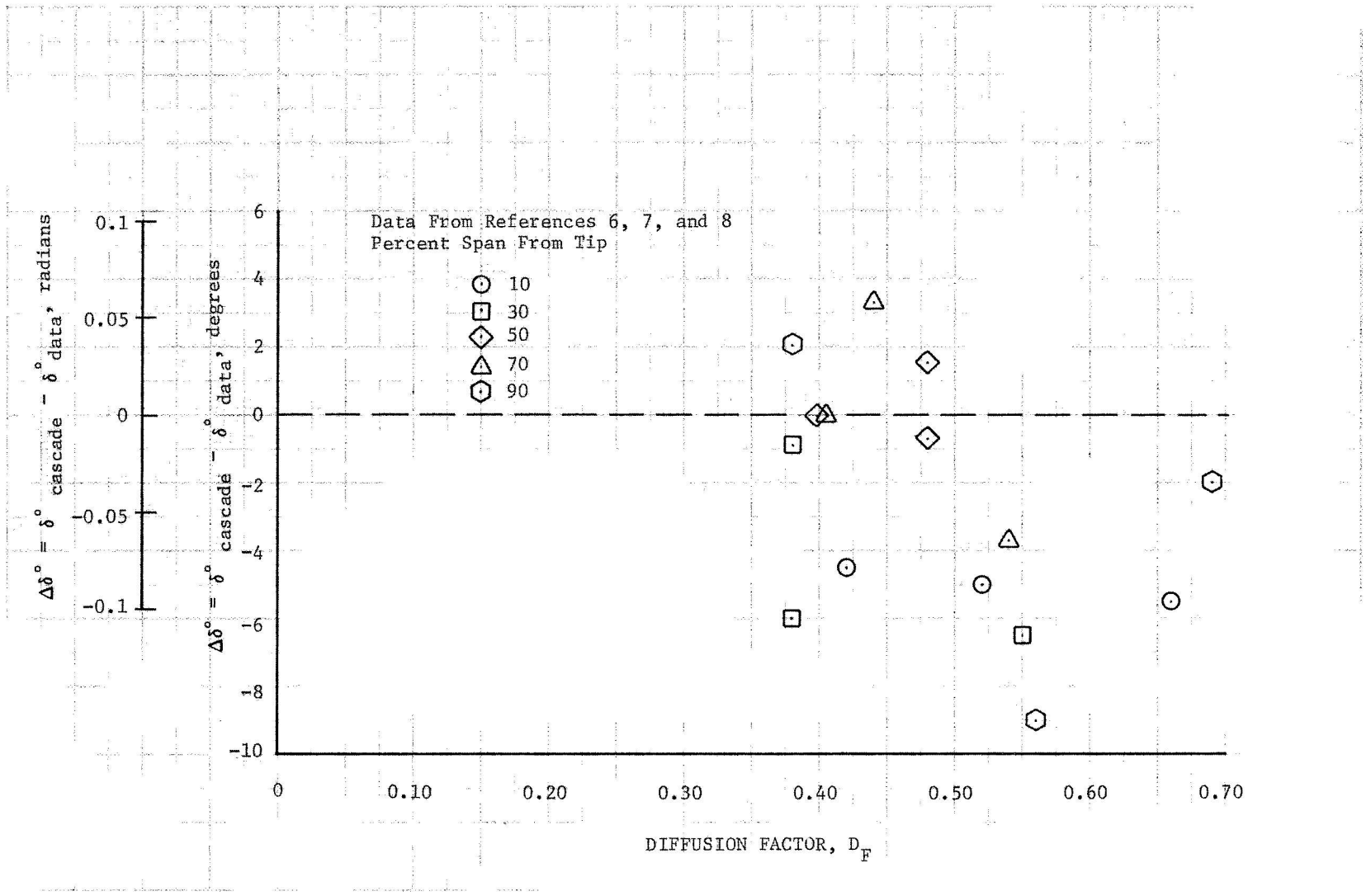

Figure 6. Stator Deviation Angle Correlation

DF 78773

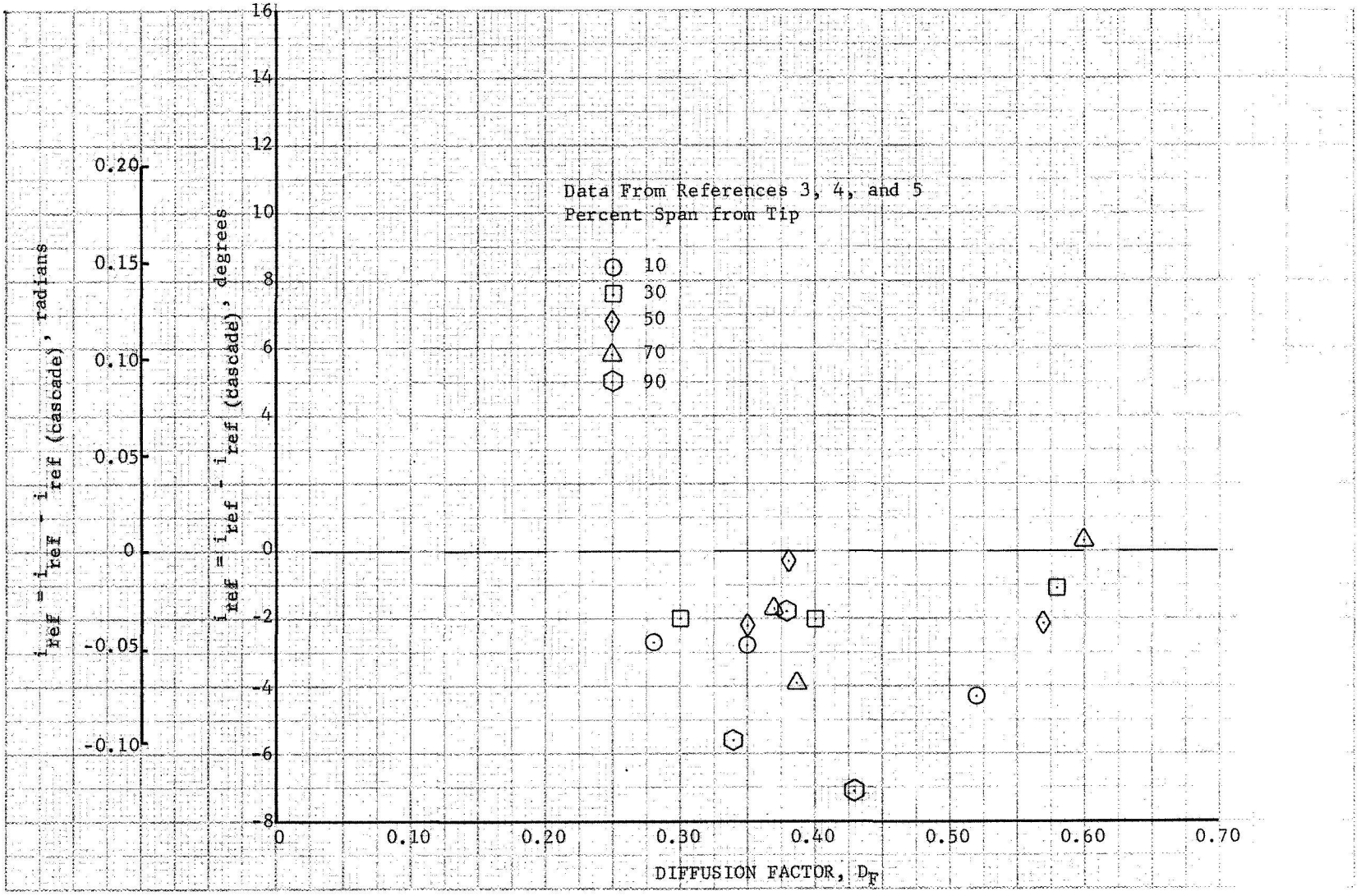

Figure 7. Rotor Reference Incidence Angle Adjustment

DF 78777

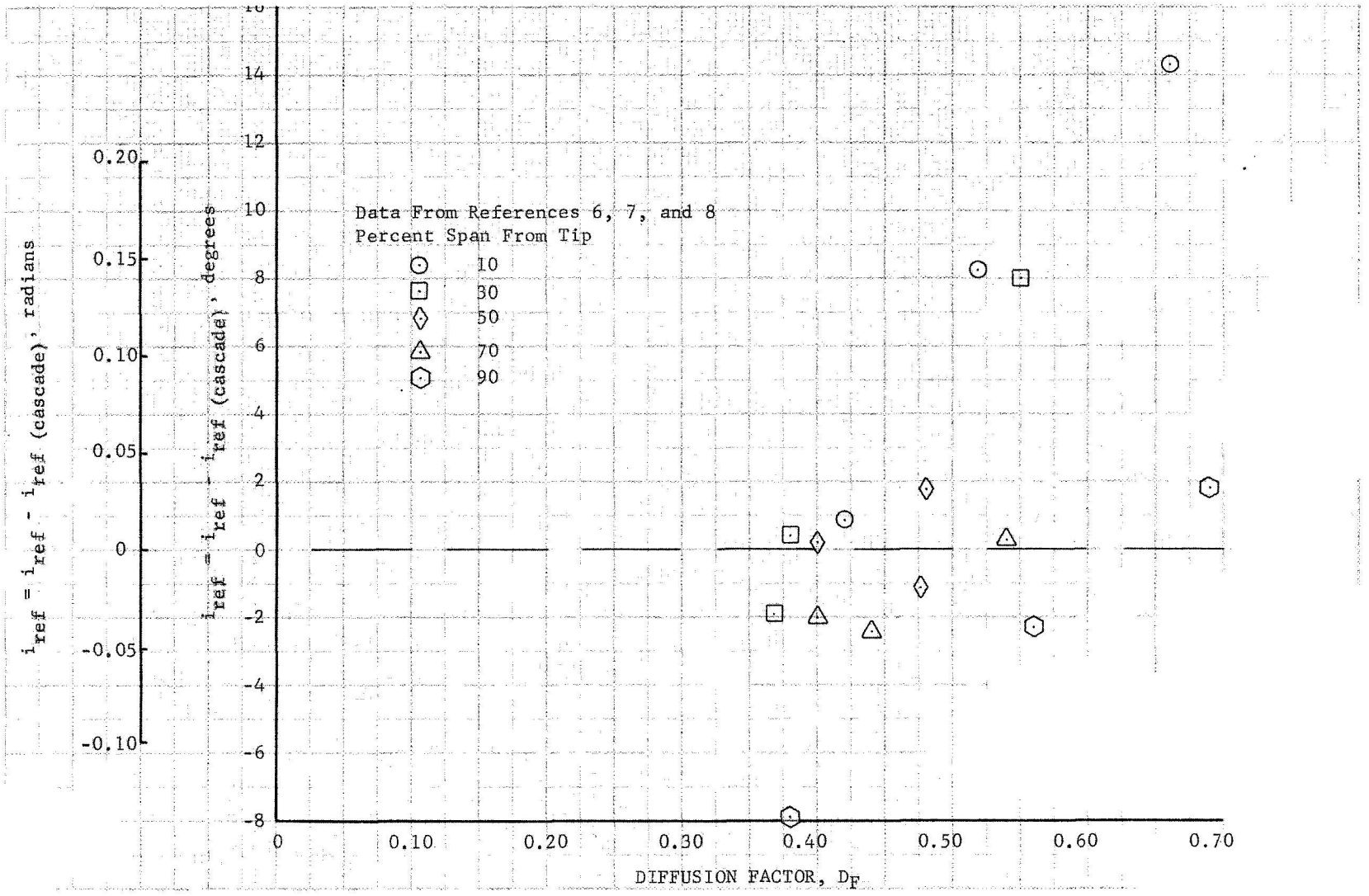

DF 78776

Figure 8. Stator Reference Incidence Angle Adjustment

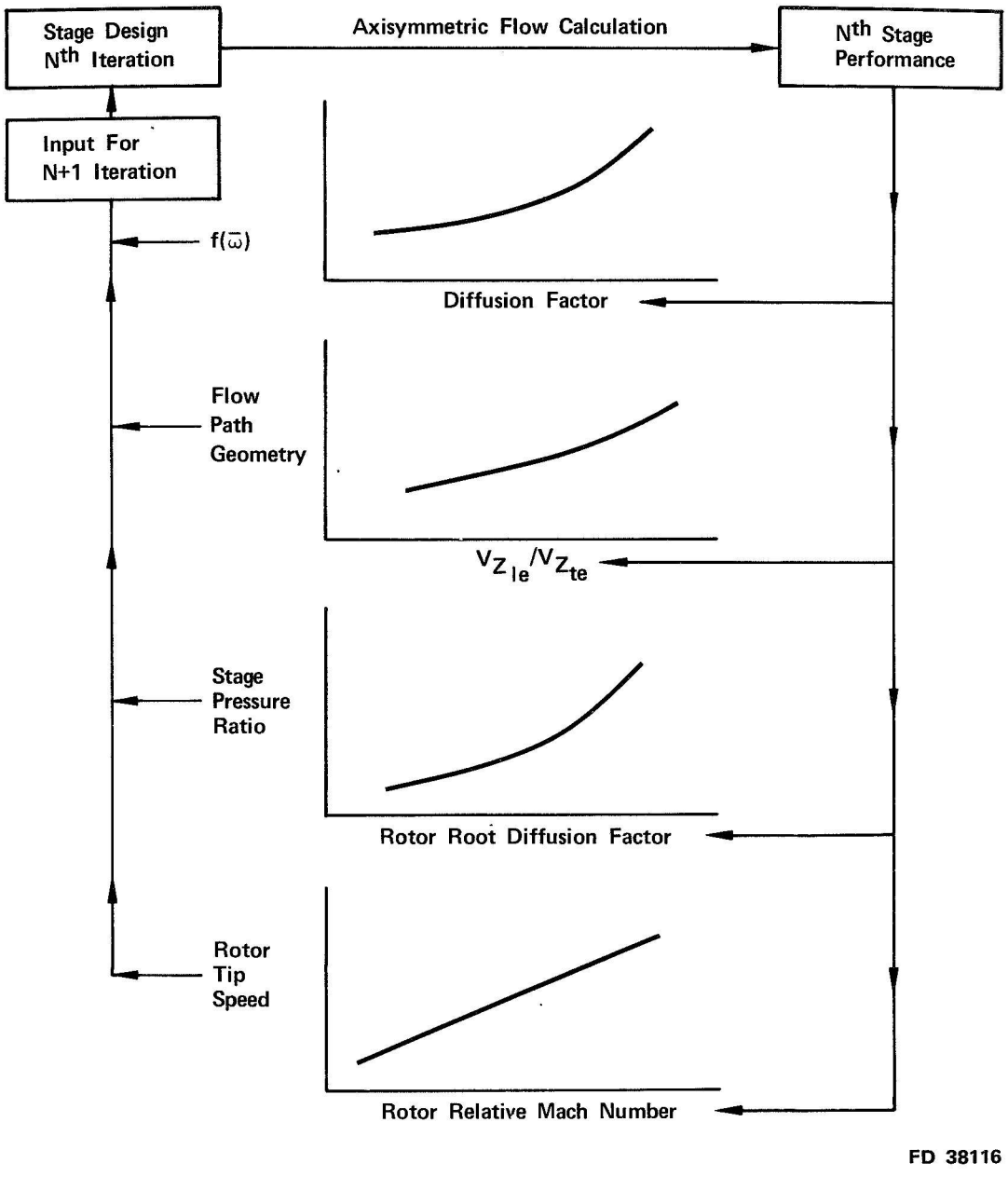

Figure 9. Stage Selection Process

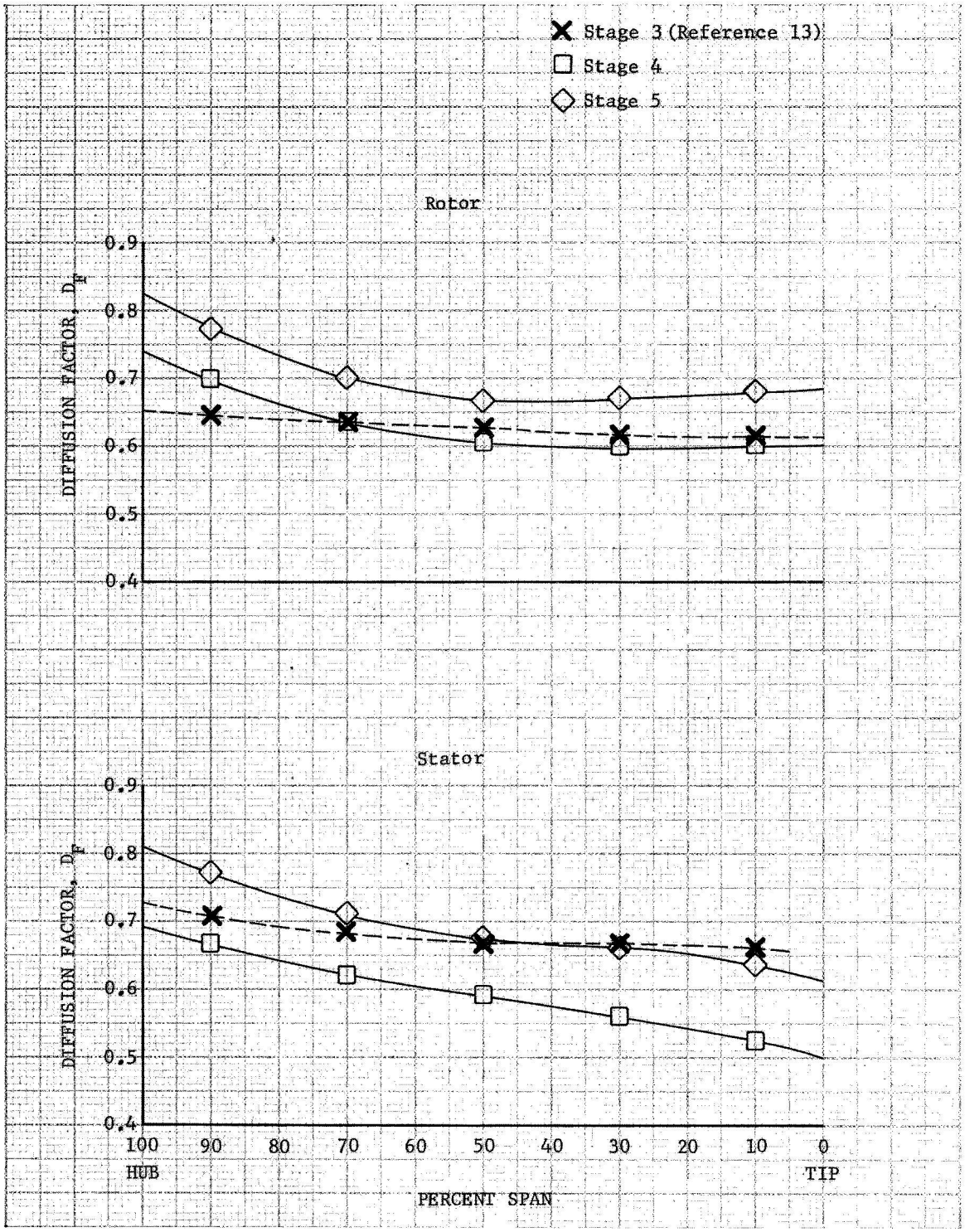

DF 78775

Figure 10. Rotor and Stator Diffusion Factor Distributions

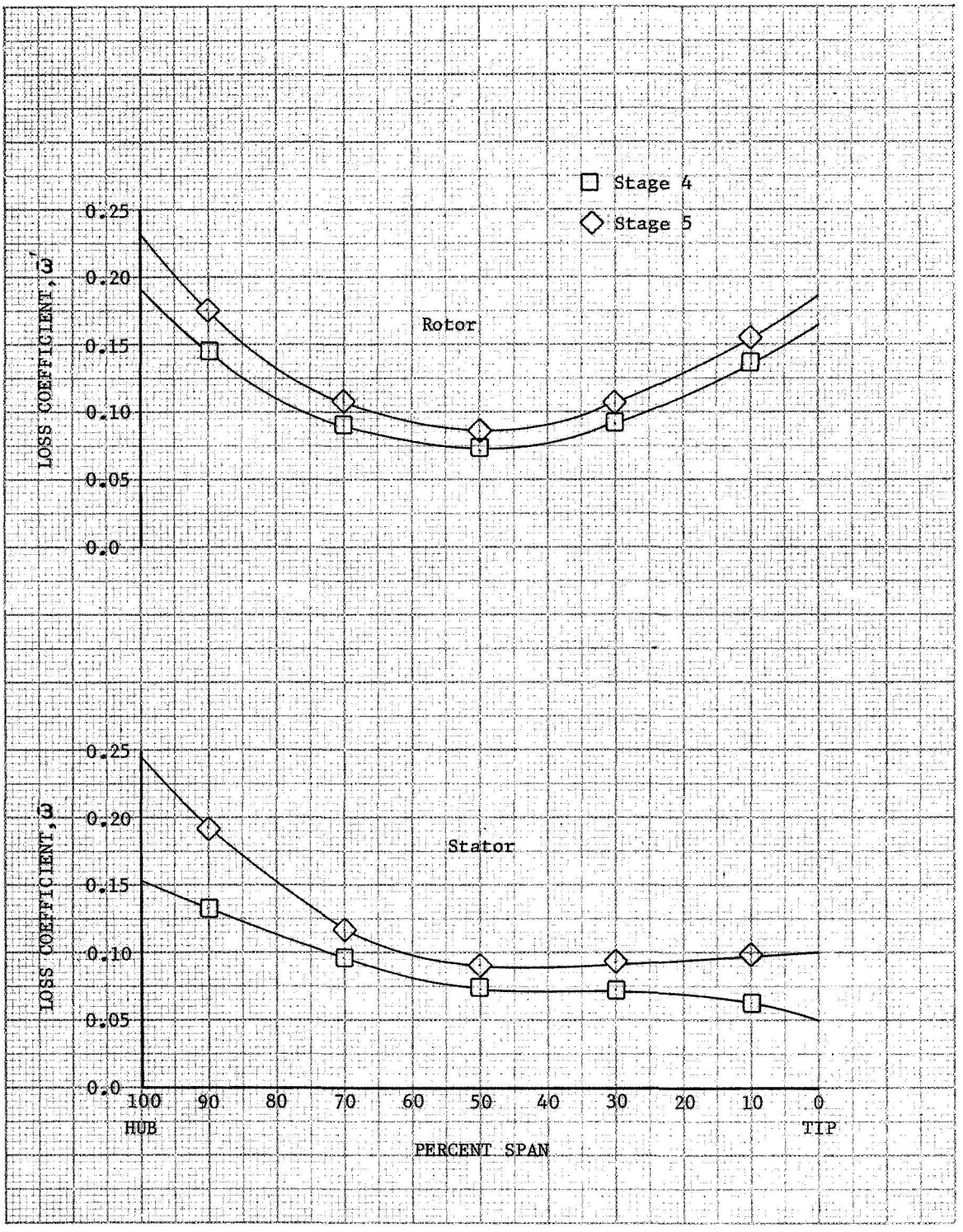

Figure 11. Rotor and Stator Loss Distributions

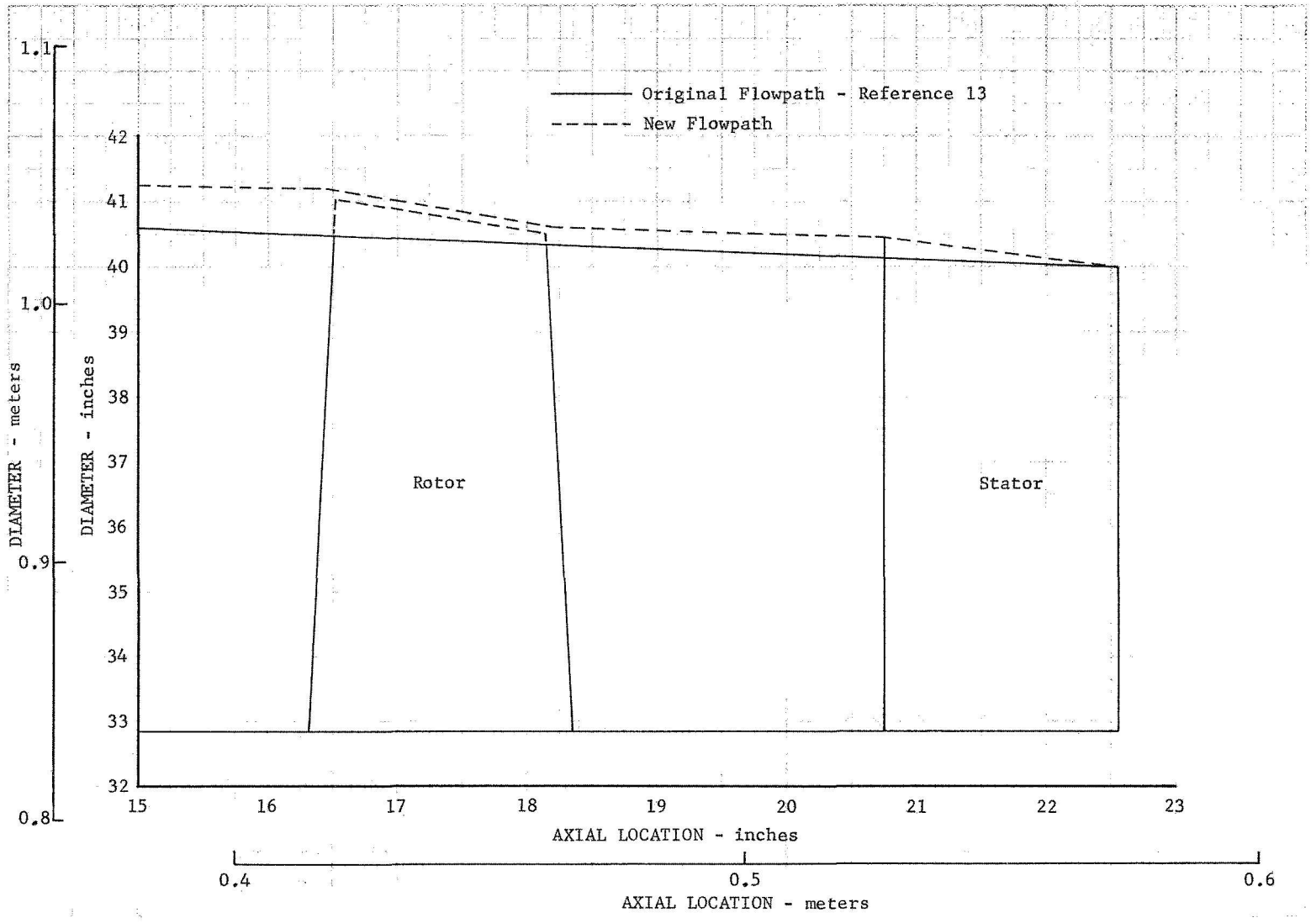

Figure 12. Flowpath Comparison

DF 78791

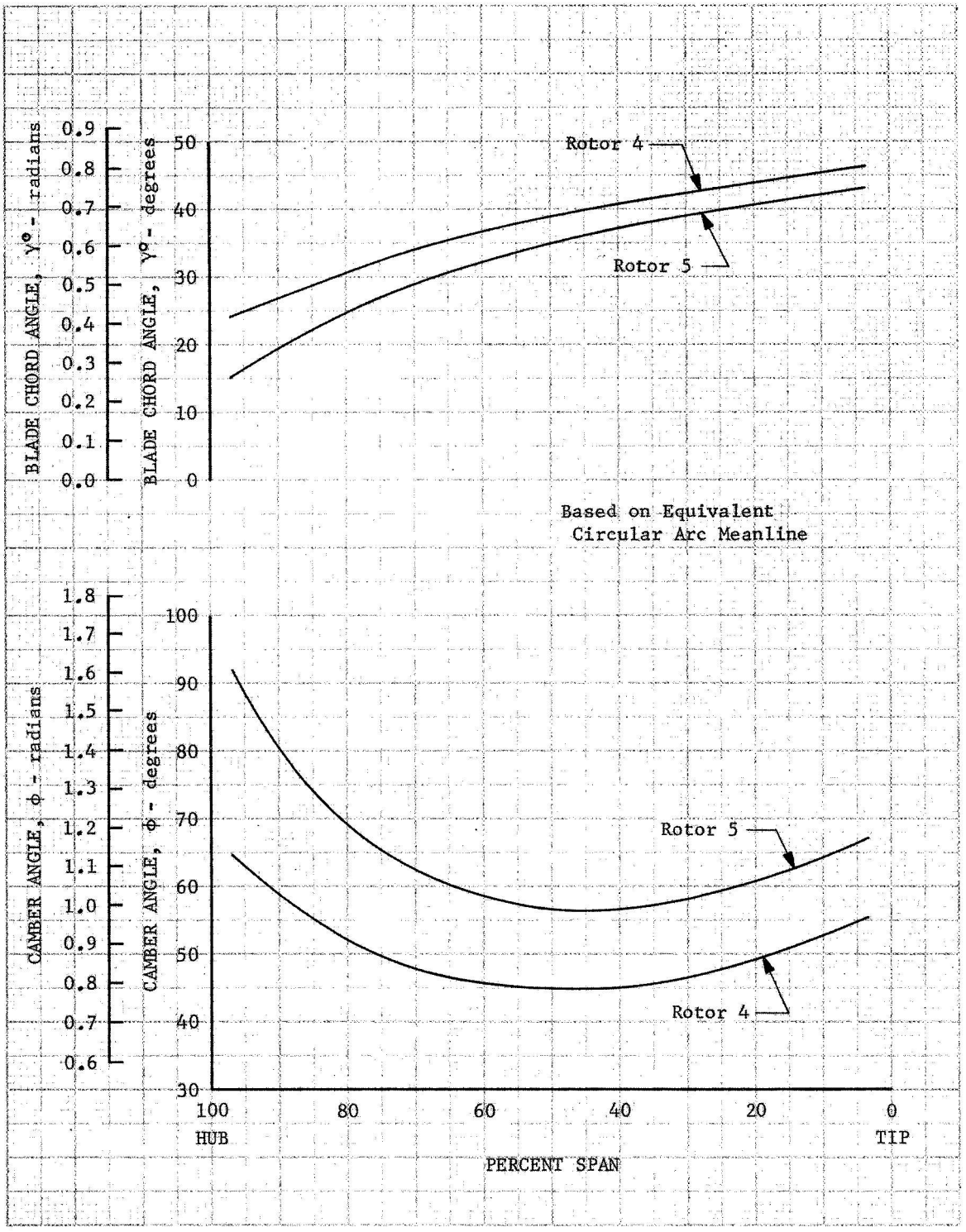

Figure 13. Rotor Camber and Blade Chord Angle Distributions

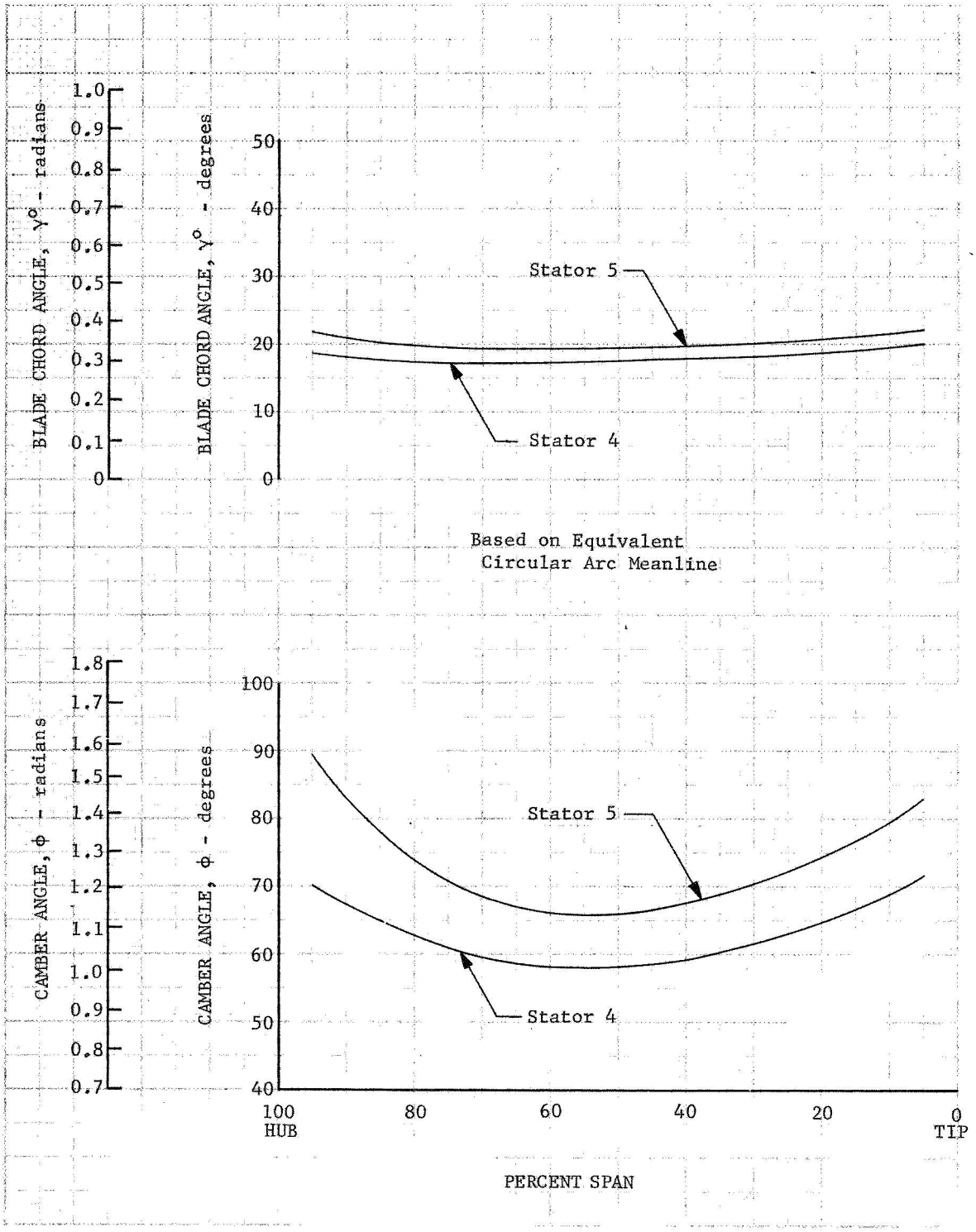

Figure 14. Stator Camber and Blade Chord Angle Distributions

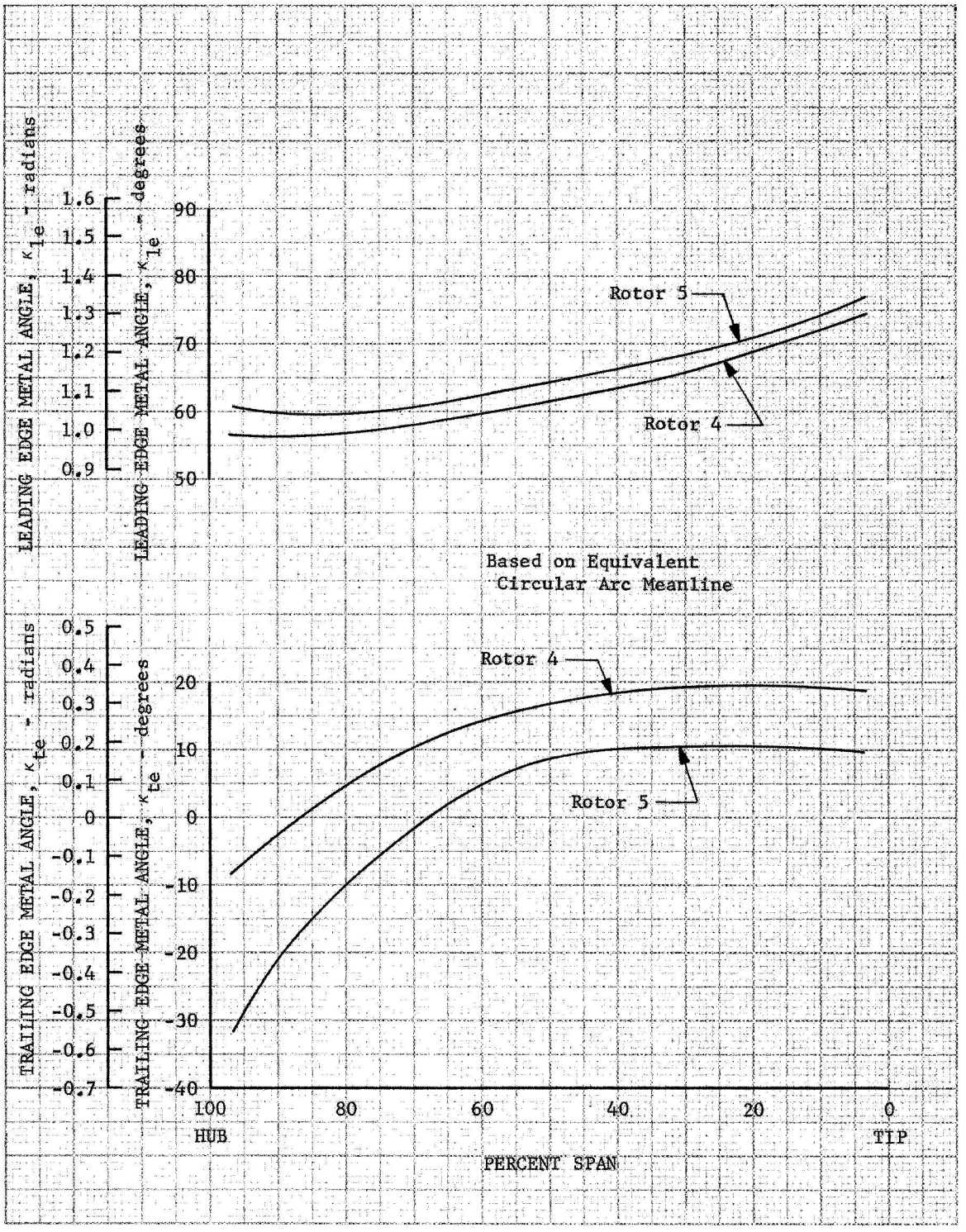

DF 78792

Figure 15. Rotor Leading and Trailing Edge Metal Angle Distributions

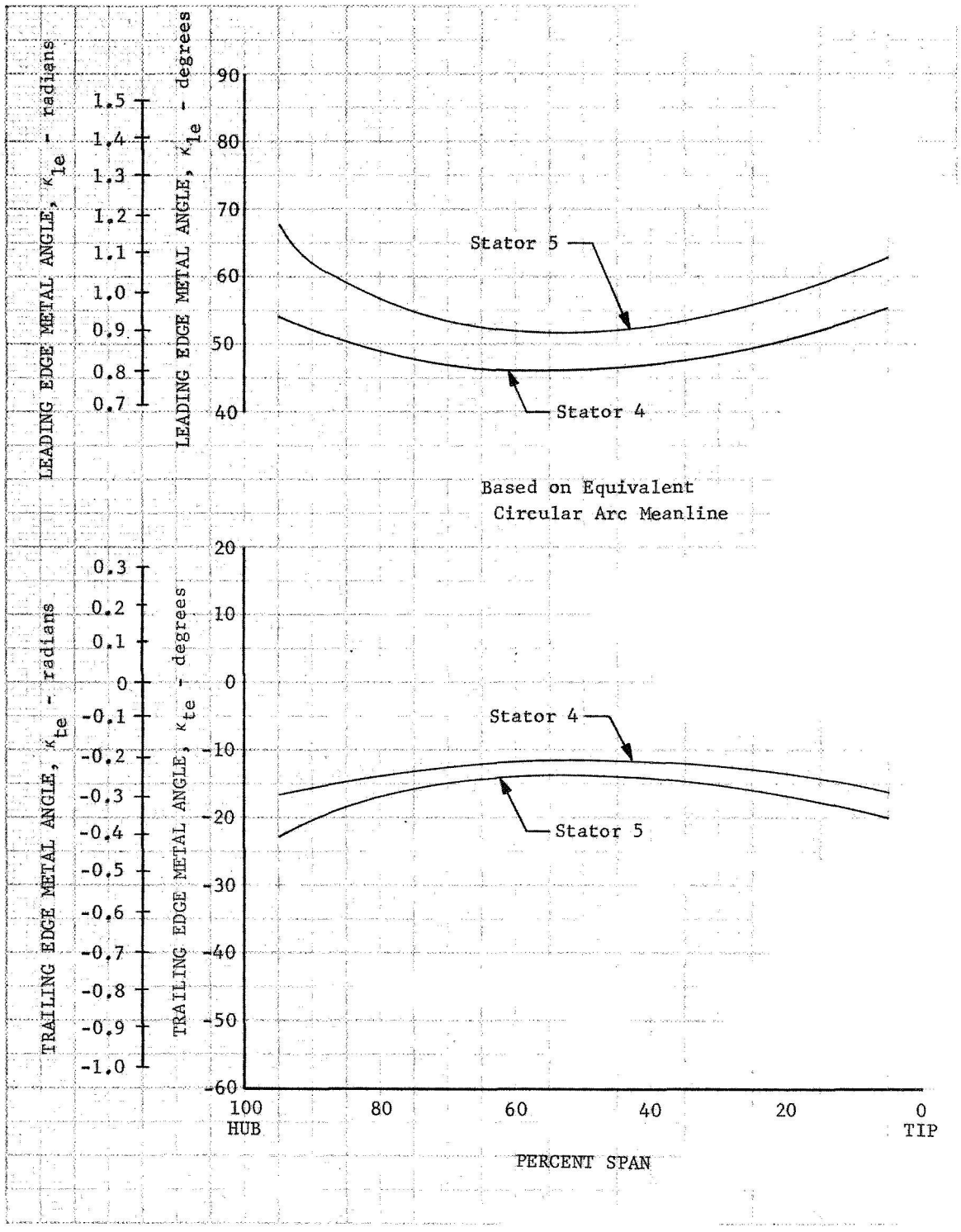

Figure 16. Stator Leading and Trailing Edge Metal Angle Distributions

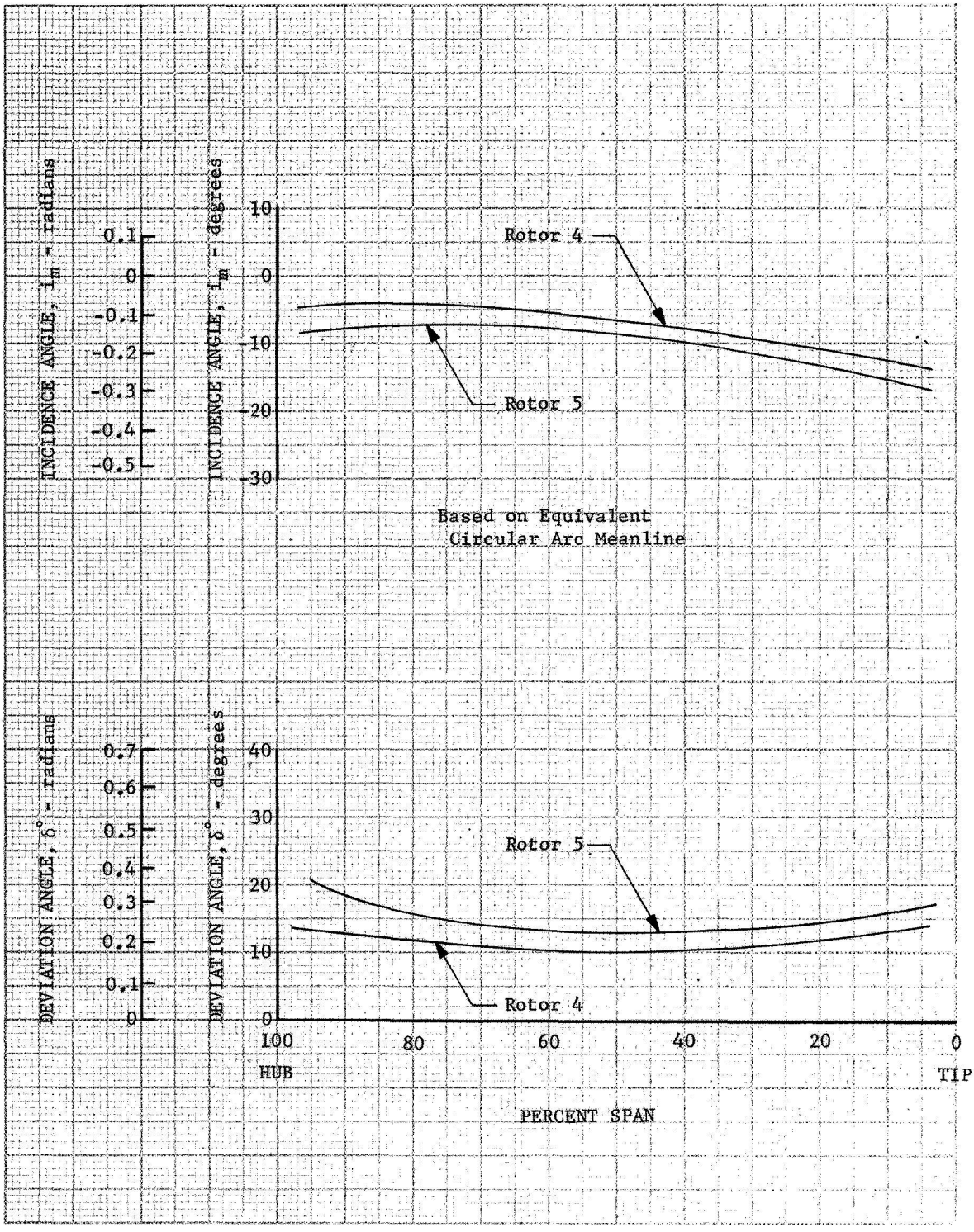

Figure 17. Rotor Incidence and Deviation Angle Distributions

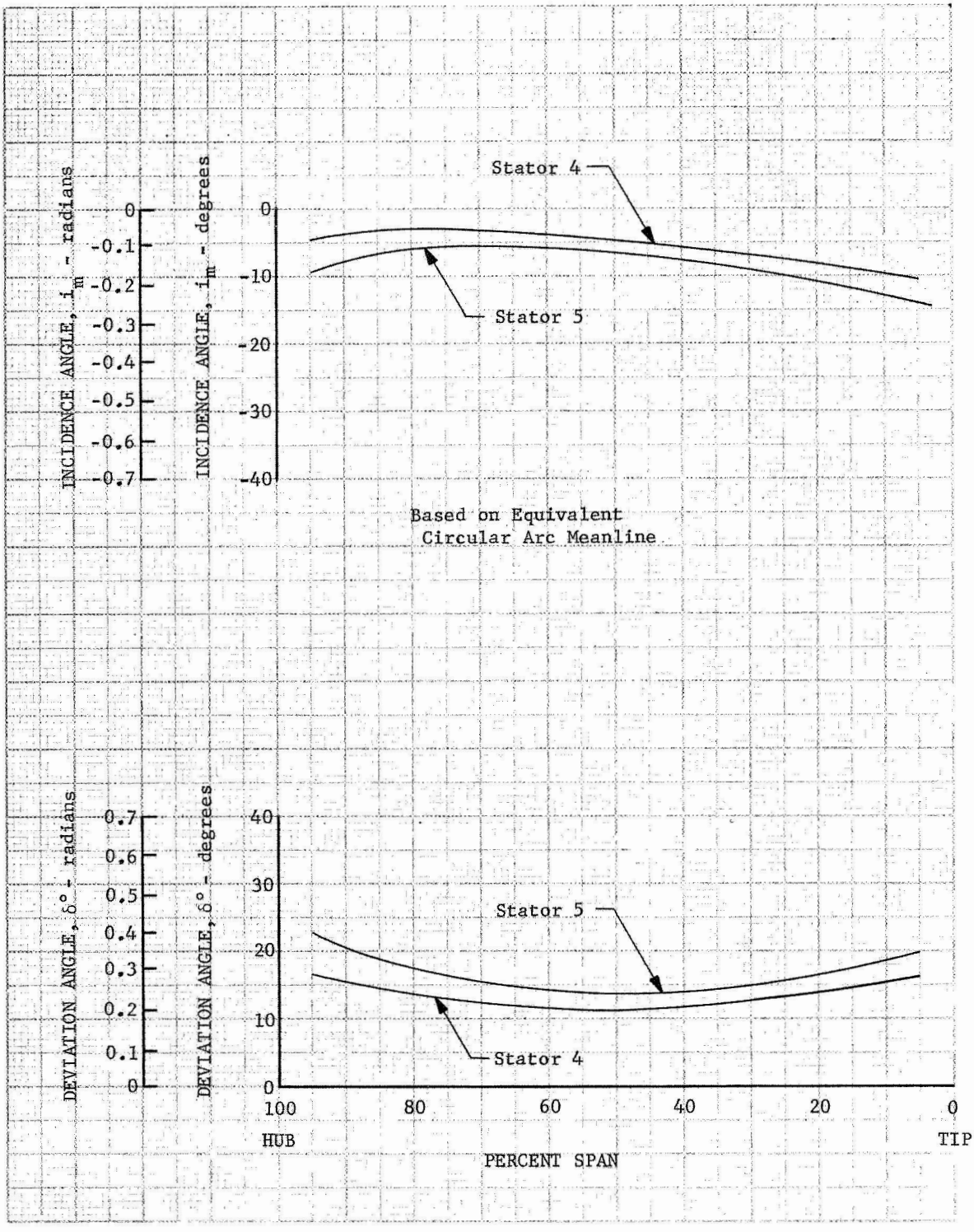

Figure 18. Stator Incidence and Deviation Angle Distributions

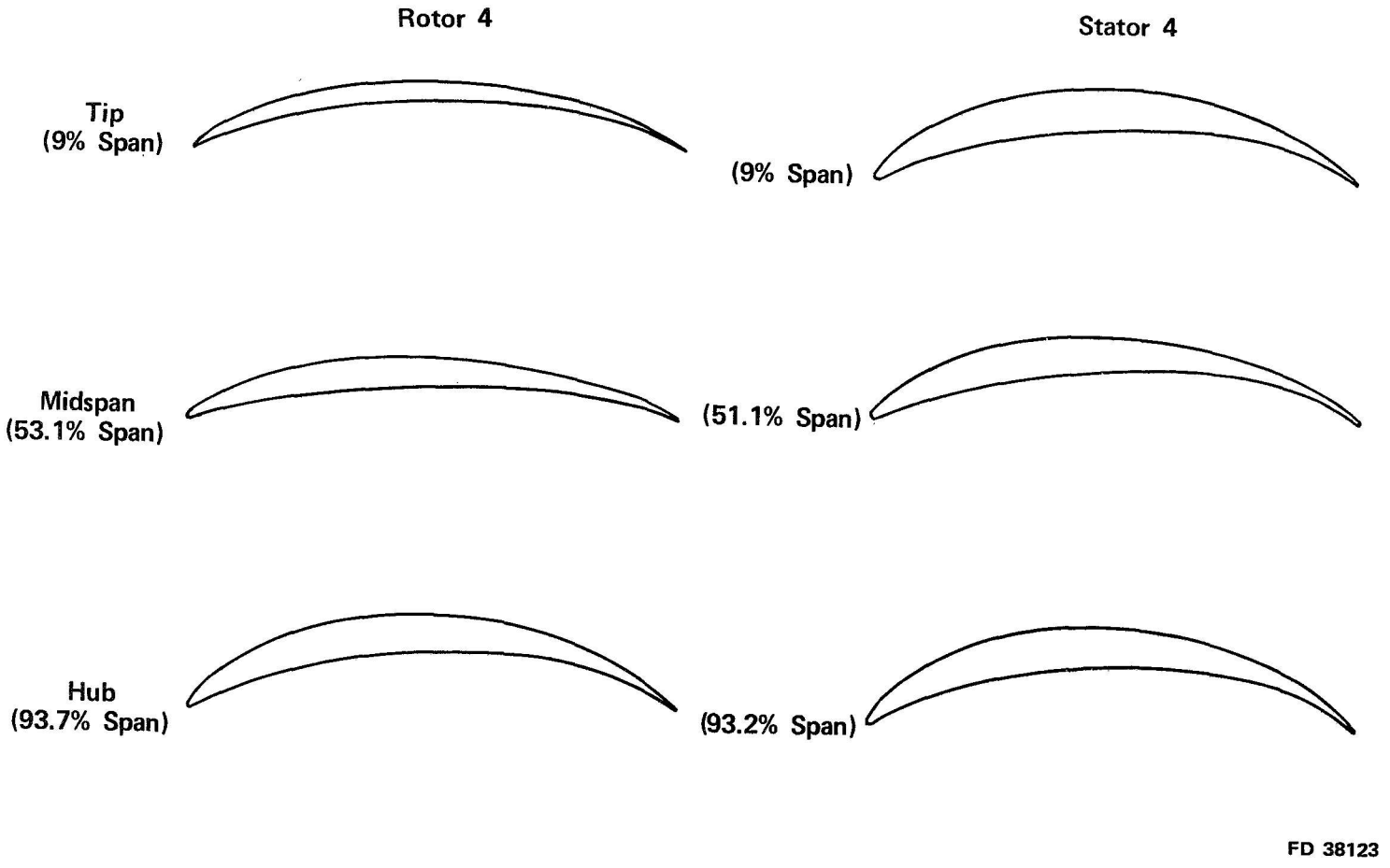

Figure 19. Stage 4 Blading Section Geometry

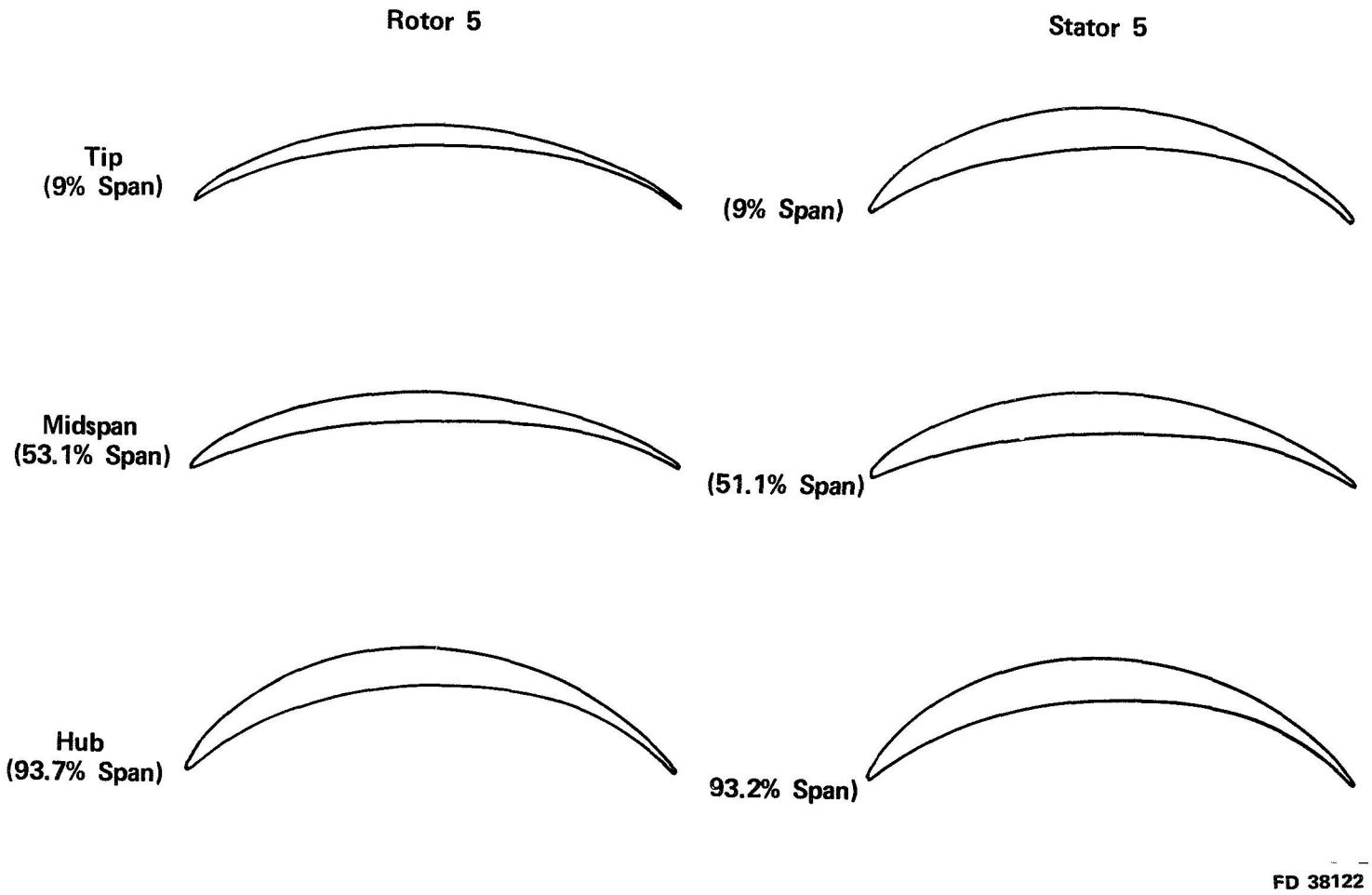

Figure 20. Stage 5 Blading Section Geometry

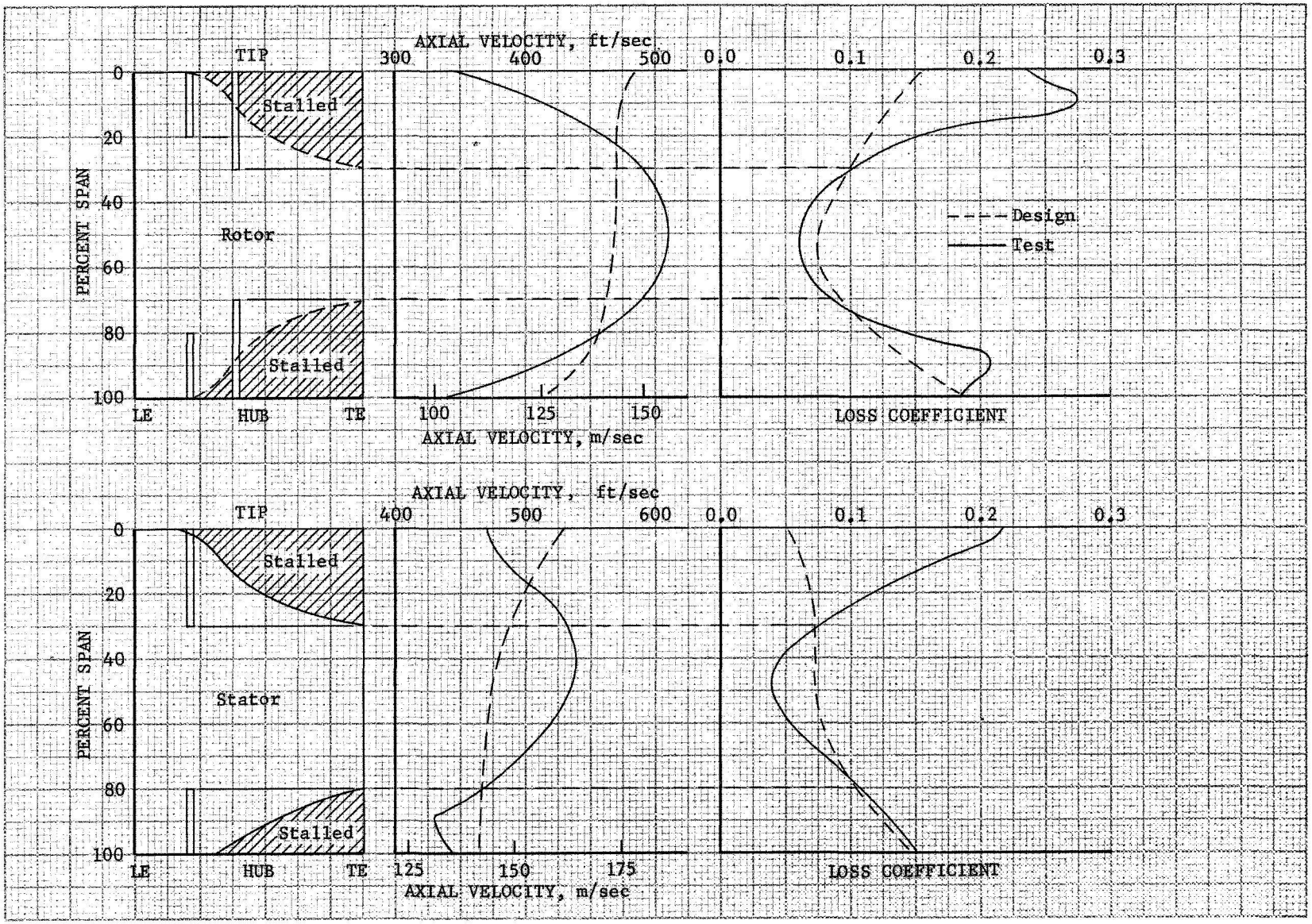

DF 78788

Figure 21. Baseline Test Results

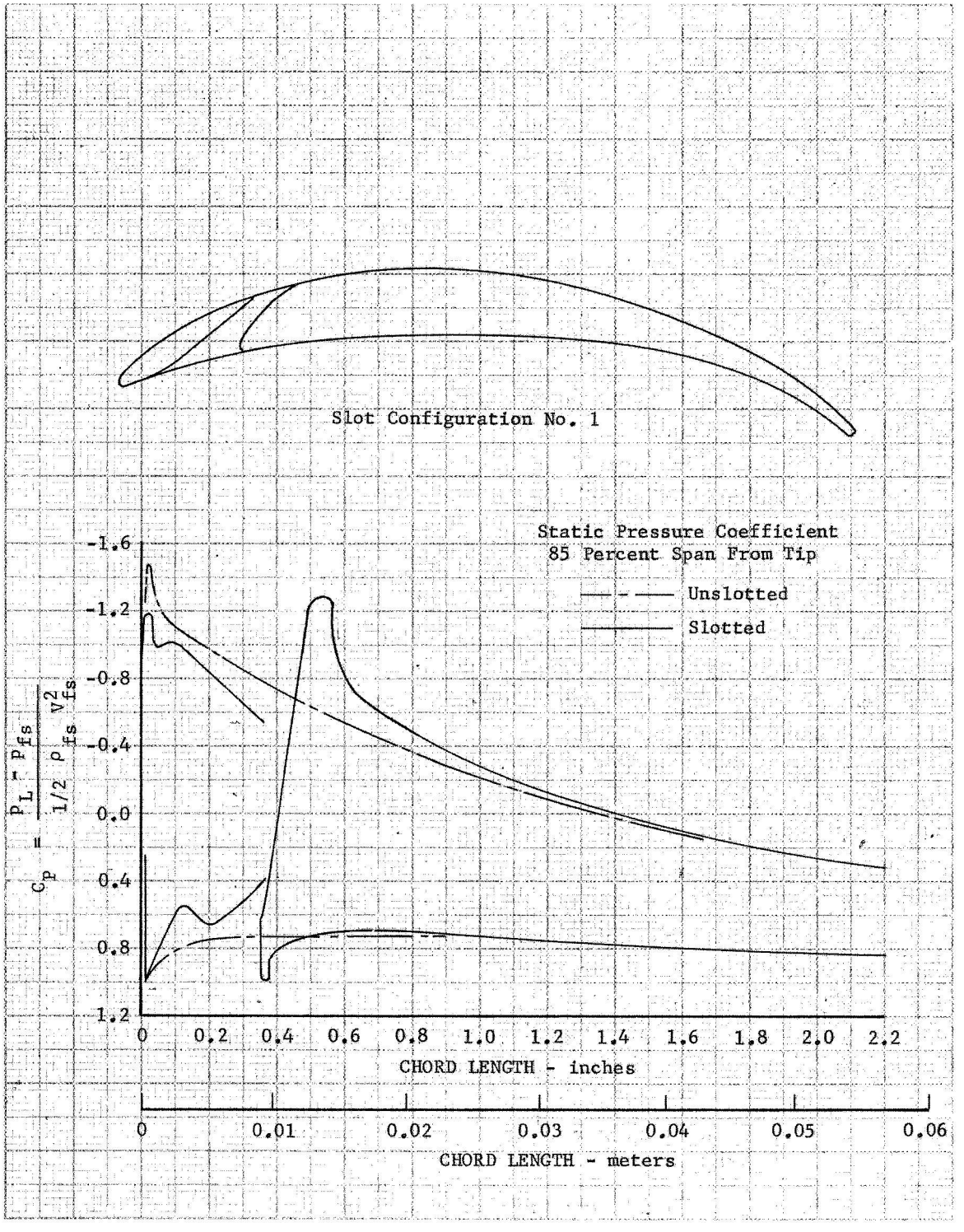

Figure 22. Pressure Coefficient Distribution for Slotted Stator 4, Configuration 1

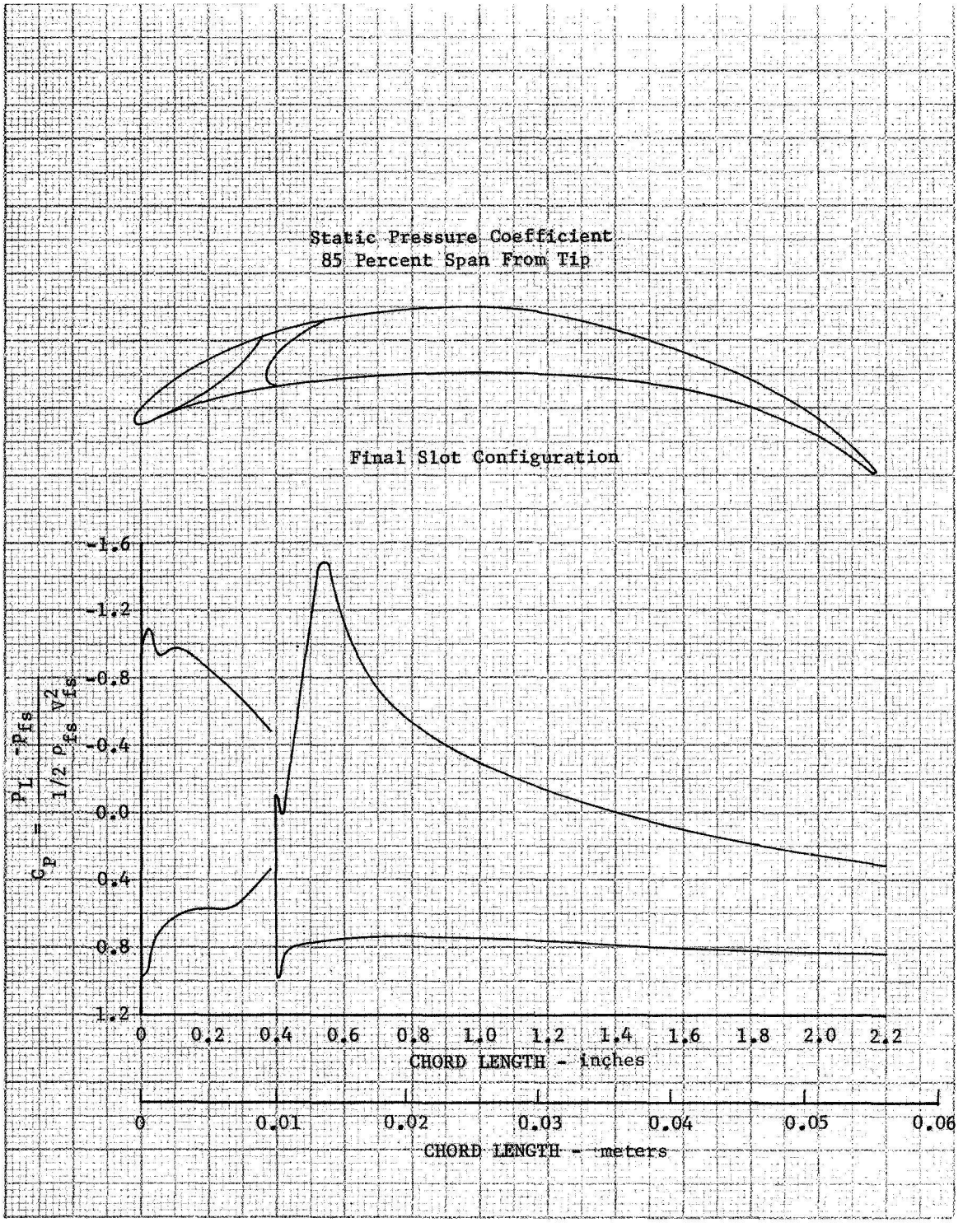

Figure 23. Pressure Coefficient Distributions for Slotted Stator 4, Final Slot Configuration

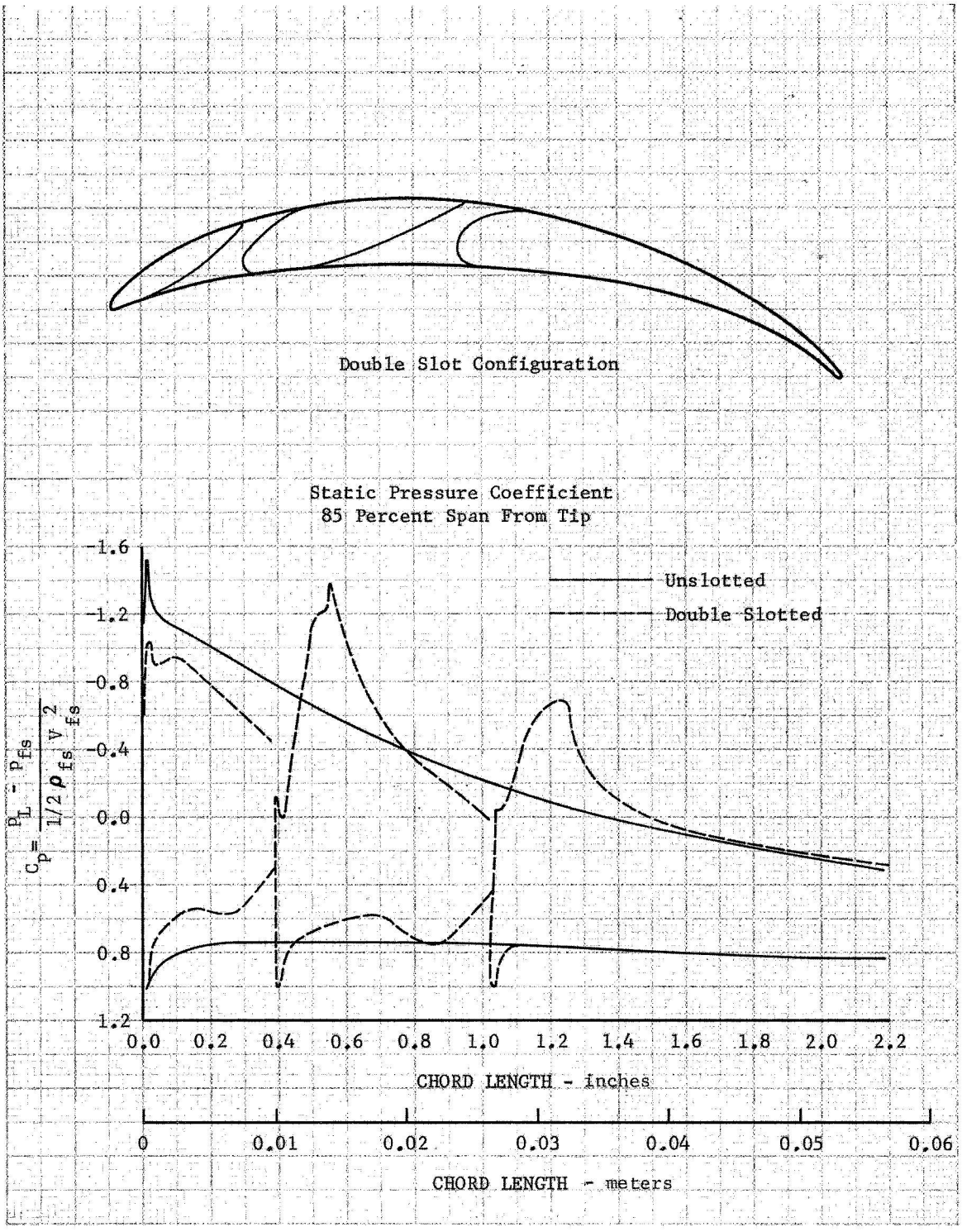

Figure 24. Pressure Coefficient Distribution for Double Slot Configuration

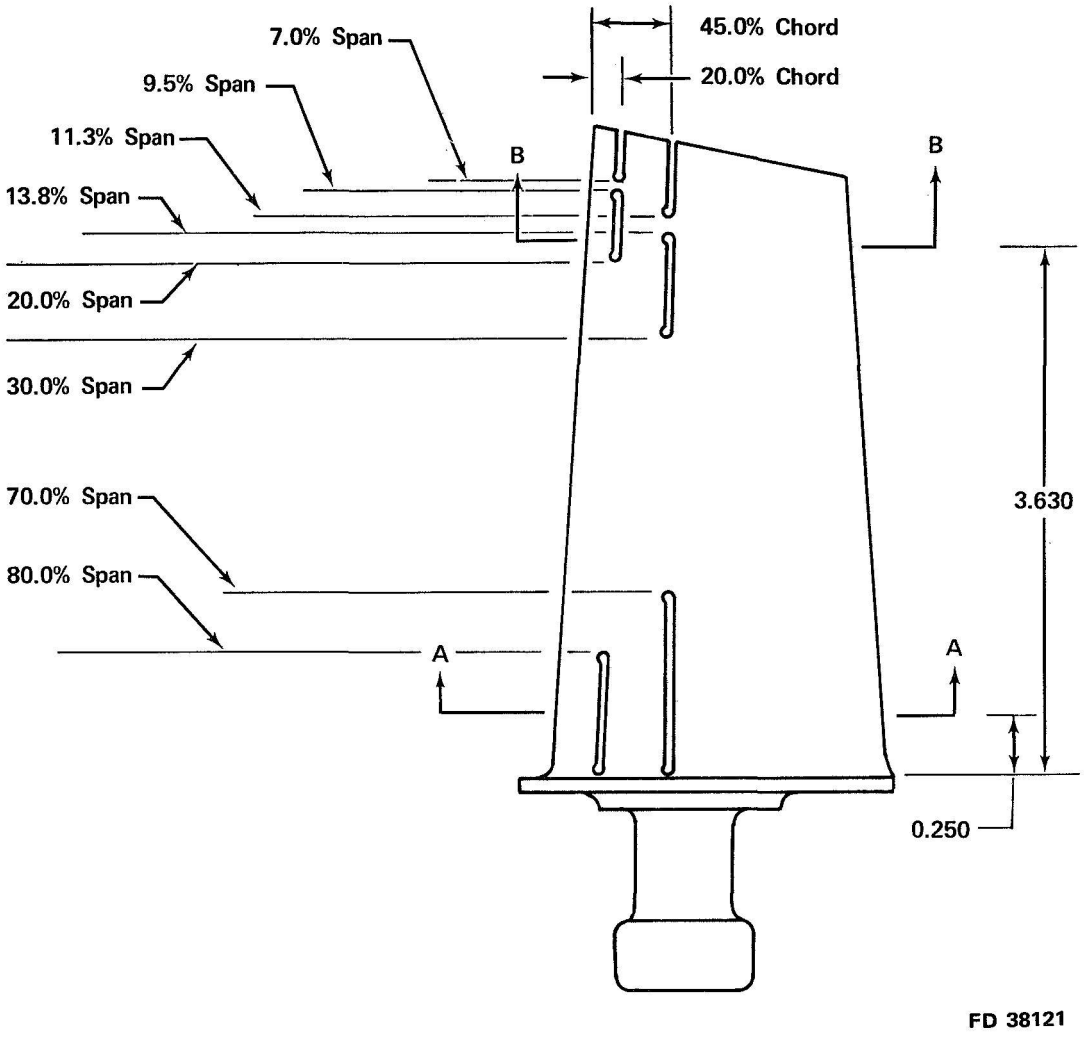

Figure 25a. Rotor 4 Slot Location

(Reference Figure 25a)

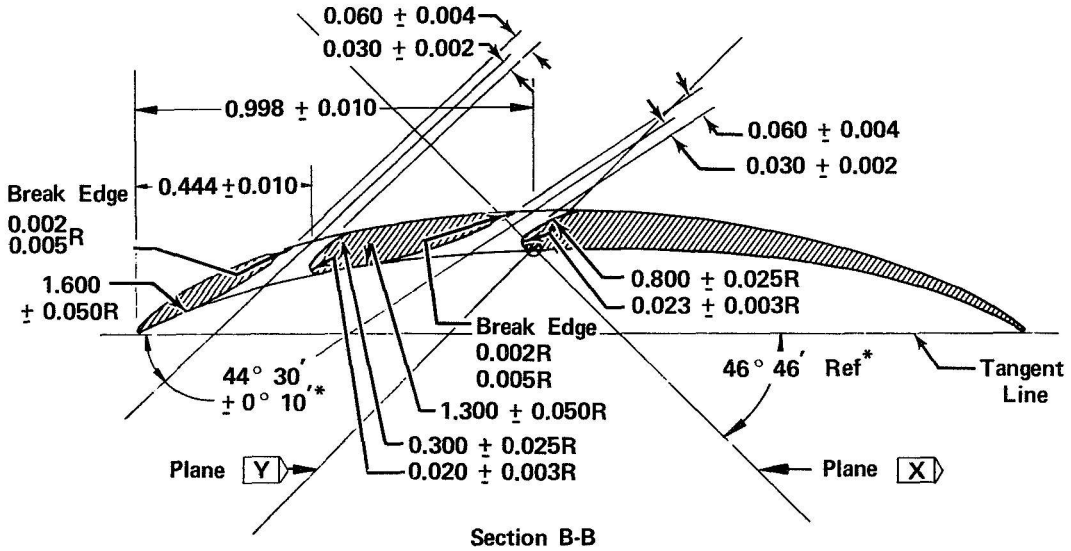

Section B-B
Typical Tip Slot Geometry

Dimensions Are in Inches

*Dimensions Applicable Section B-B Only

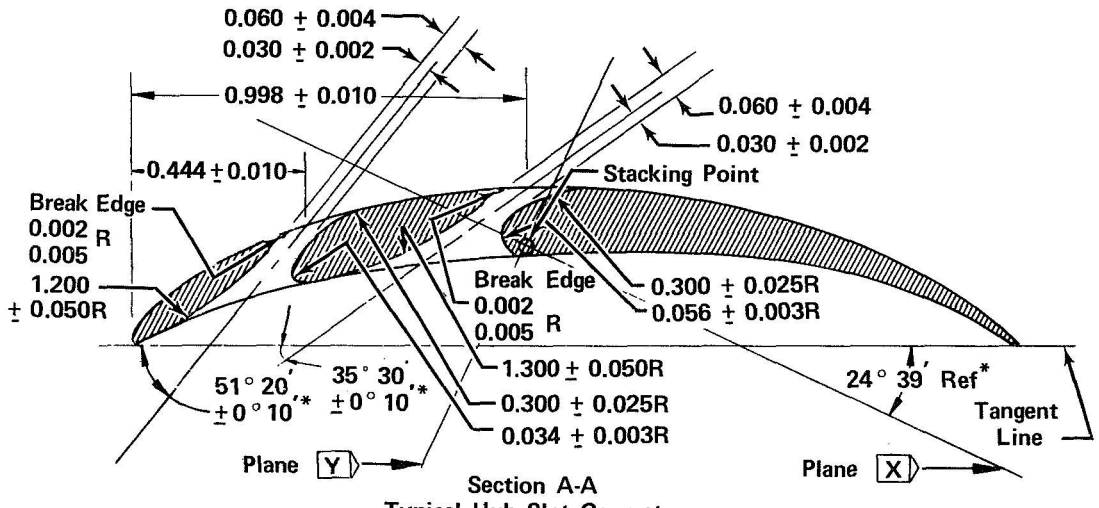

Section A-A
Typical Hub Slot Geometry

Dimensions Are in Inches

*Dimensions Applicable Section A-A Only

FD 38124

Figure 25b. Rotor 4 Slot Configuration

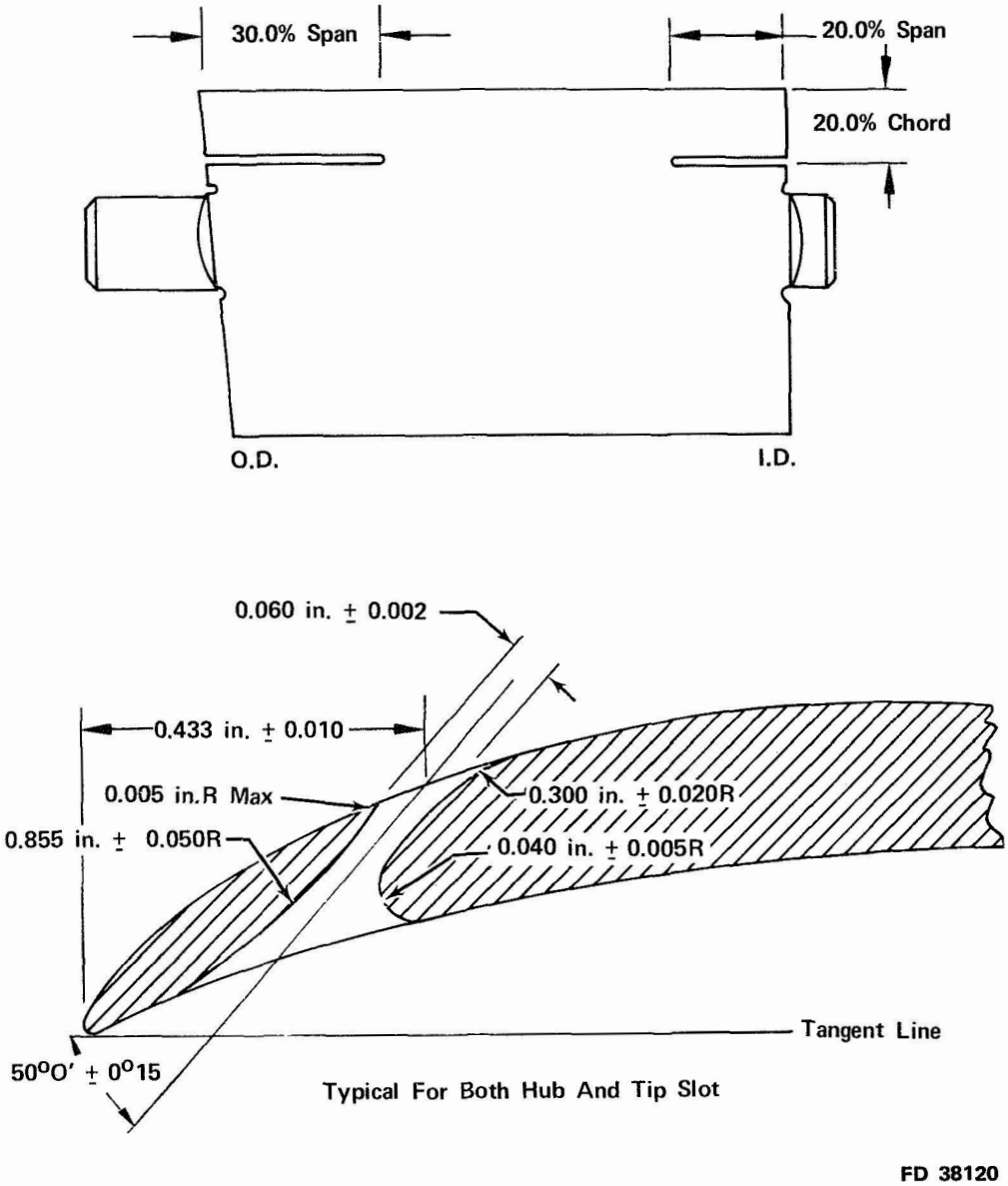

Figure 26. Stator 4 Slot Configuration

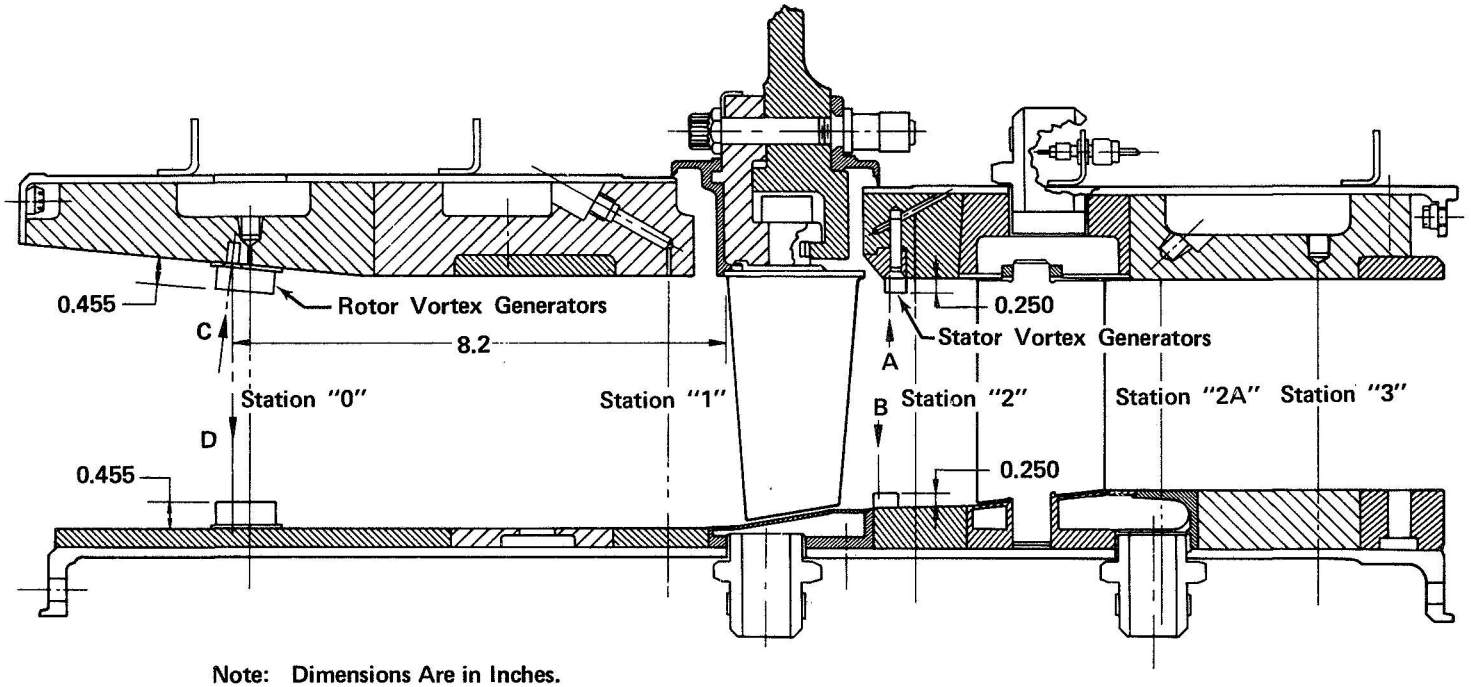

Figure 27a. Vortex Generator Locations

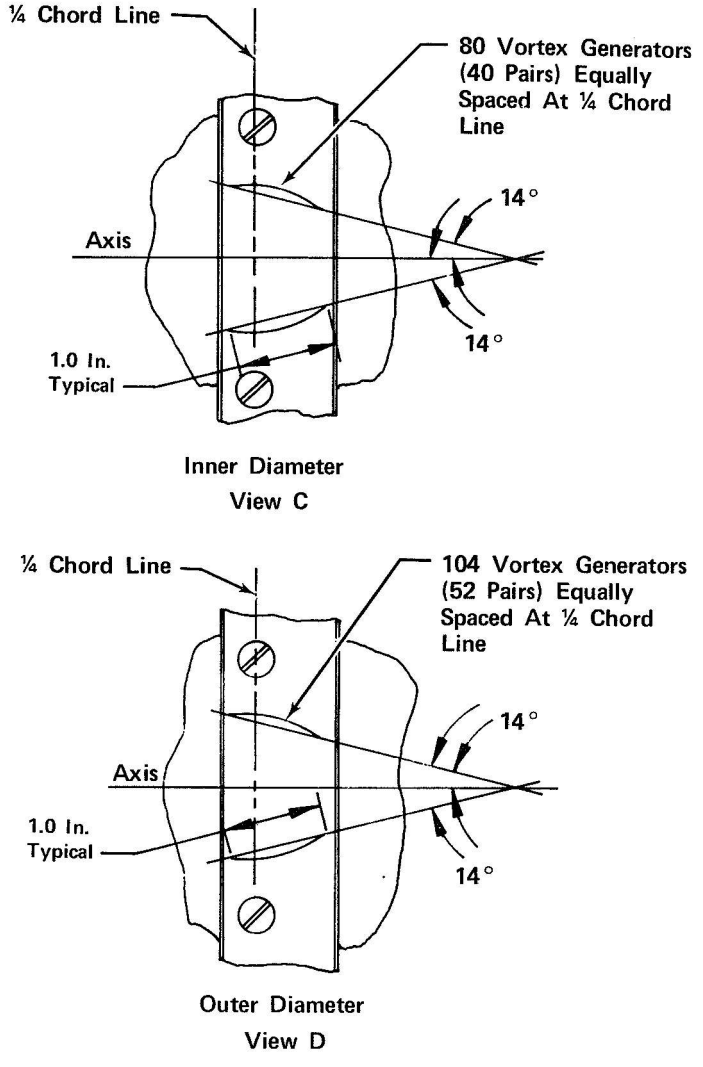

Figure 27b. Rotor Vortex Generator Design

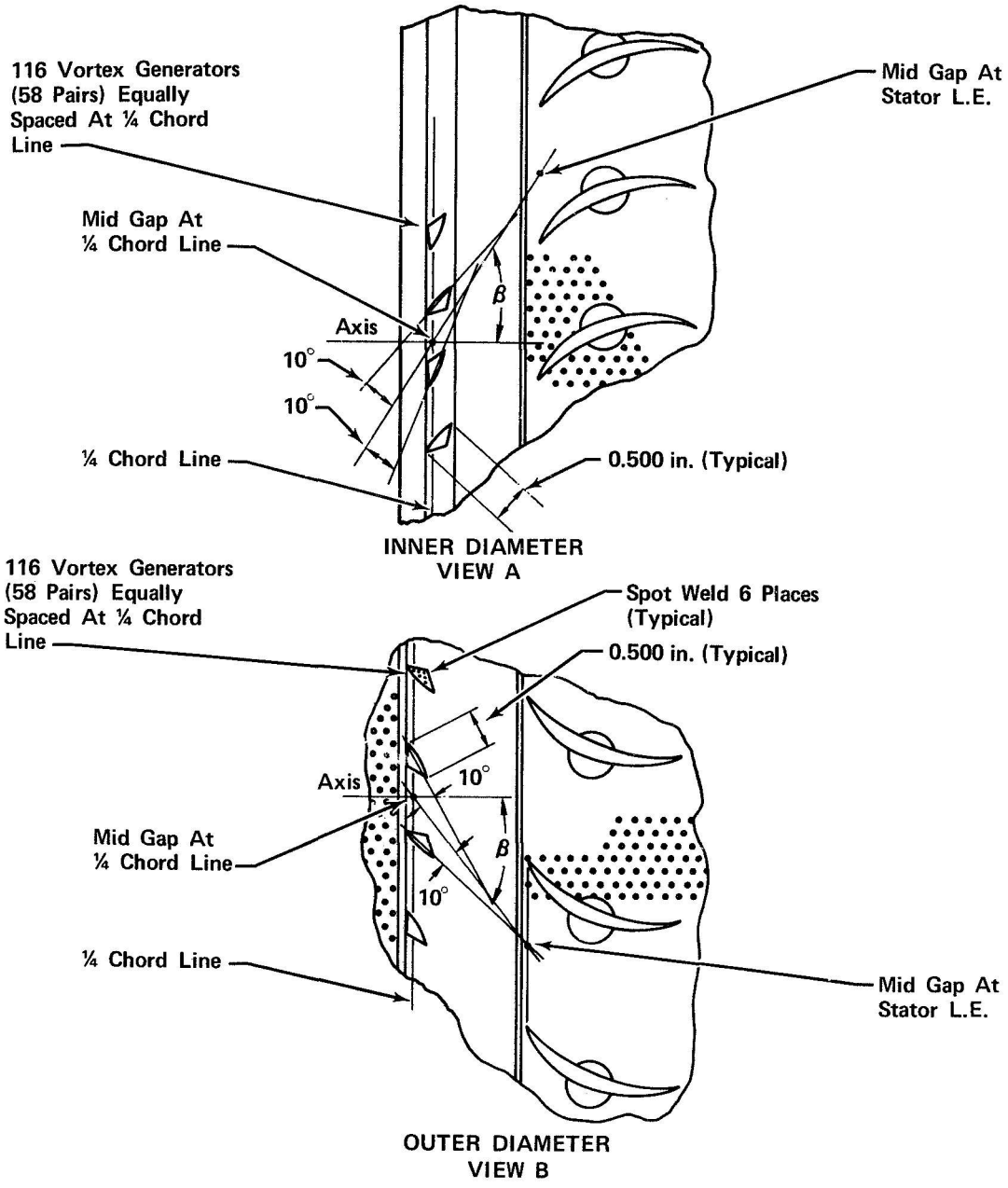

FD 38117

Figure 27c. Stator Vortex Generator Design

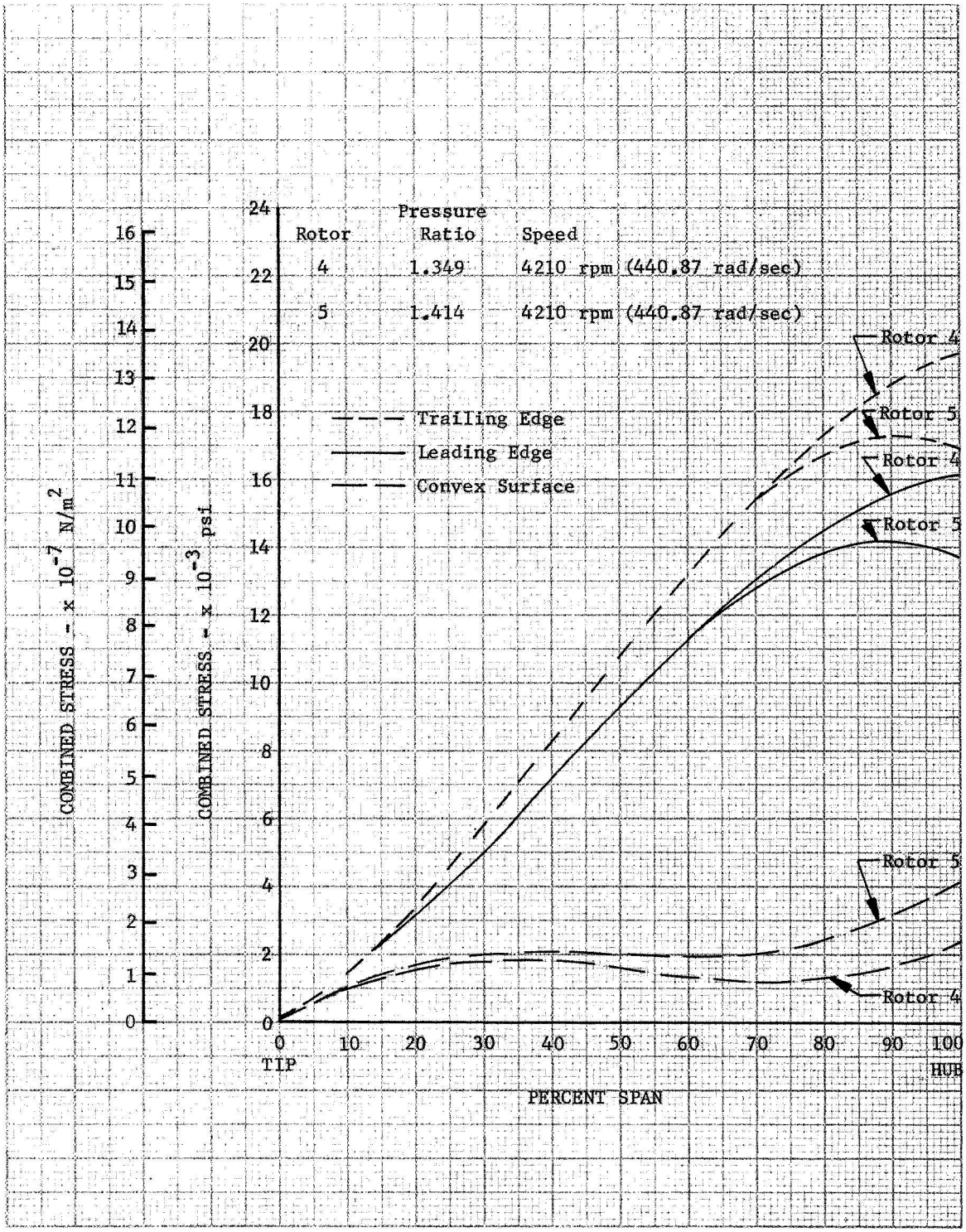

Figure 28. Calculated Rotor Blade Stresses

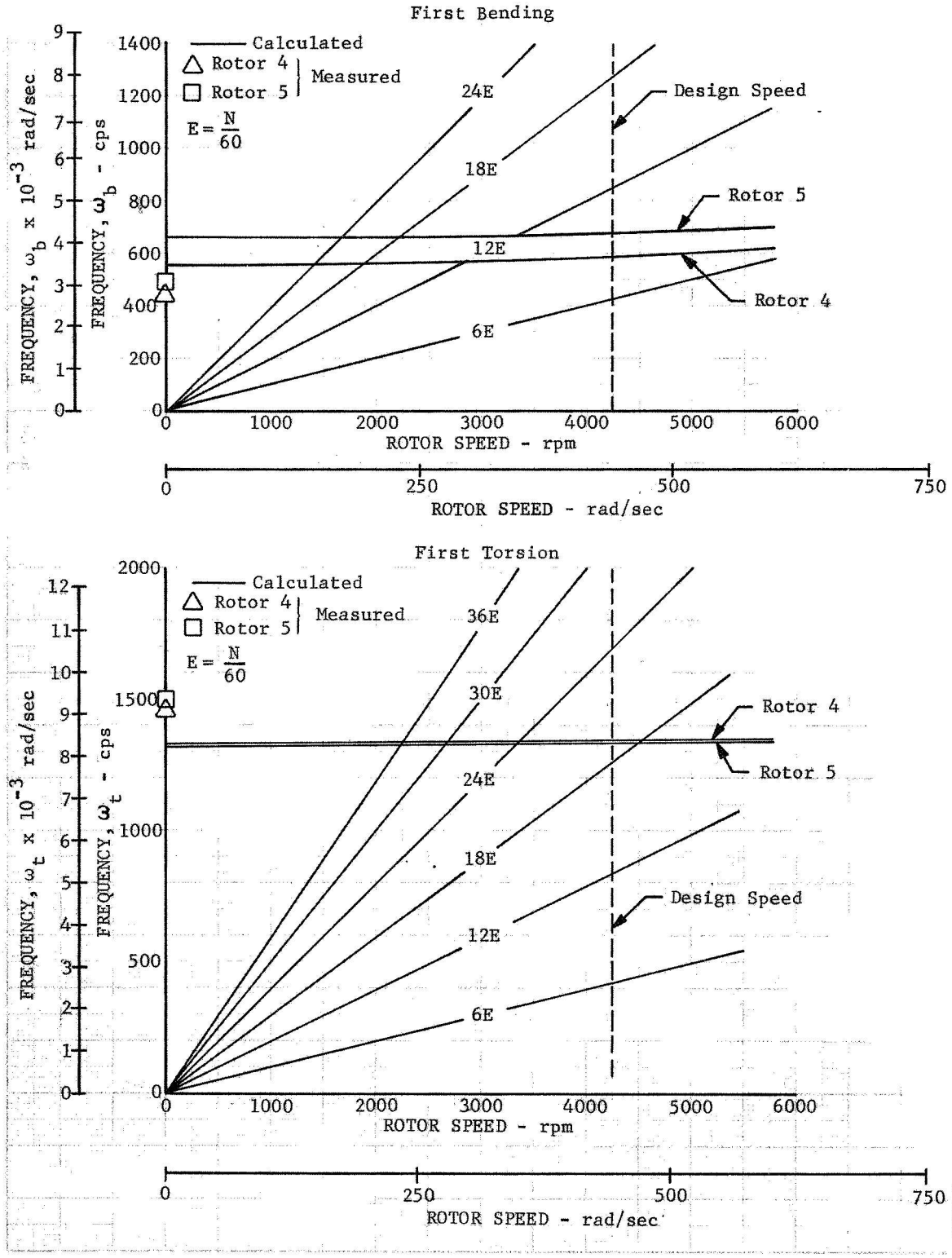

DF 78795

Figure 29. Rotor Resonance Diagram for First Bending and Torsion Mode Vibration

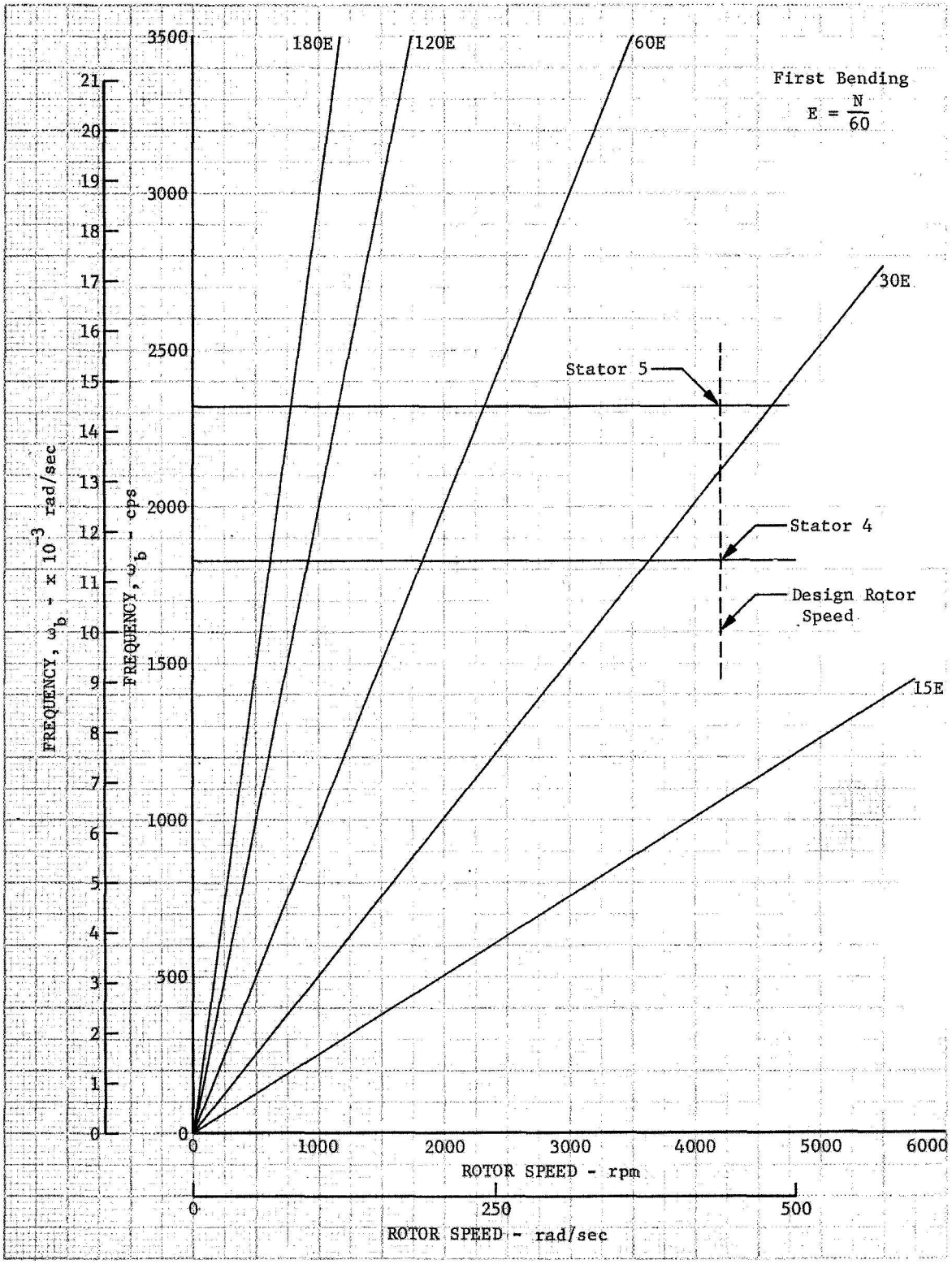

Figure 30. Stator Resonance Diagram for First Bending Mode Vibration

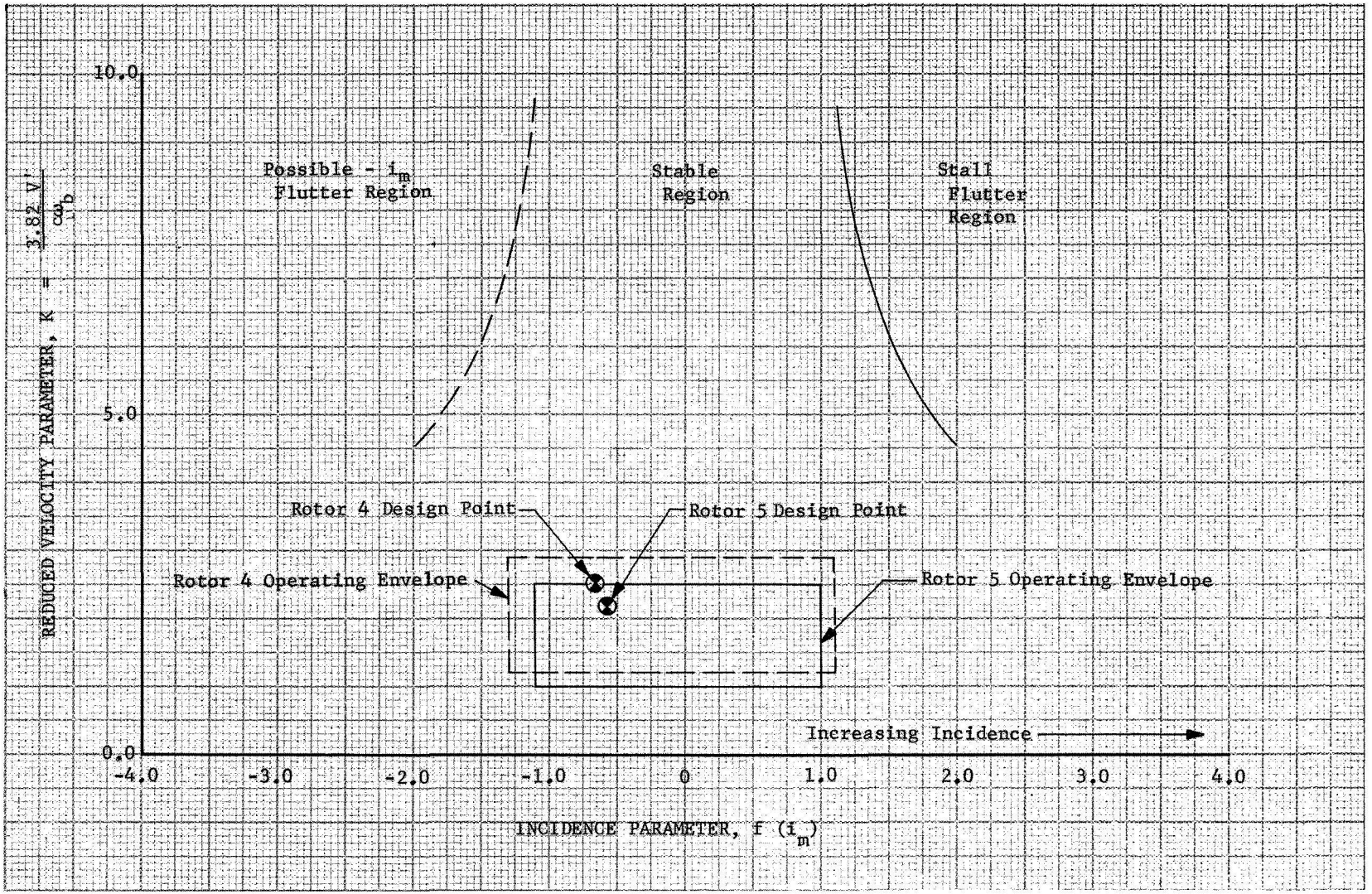

Figure 31. Calculated Rotor Blade Bending Flutter Characteristics

DF 78797

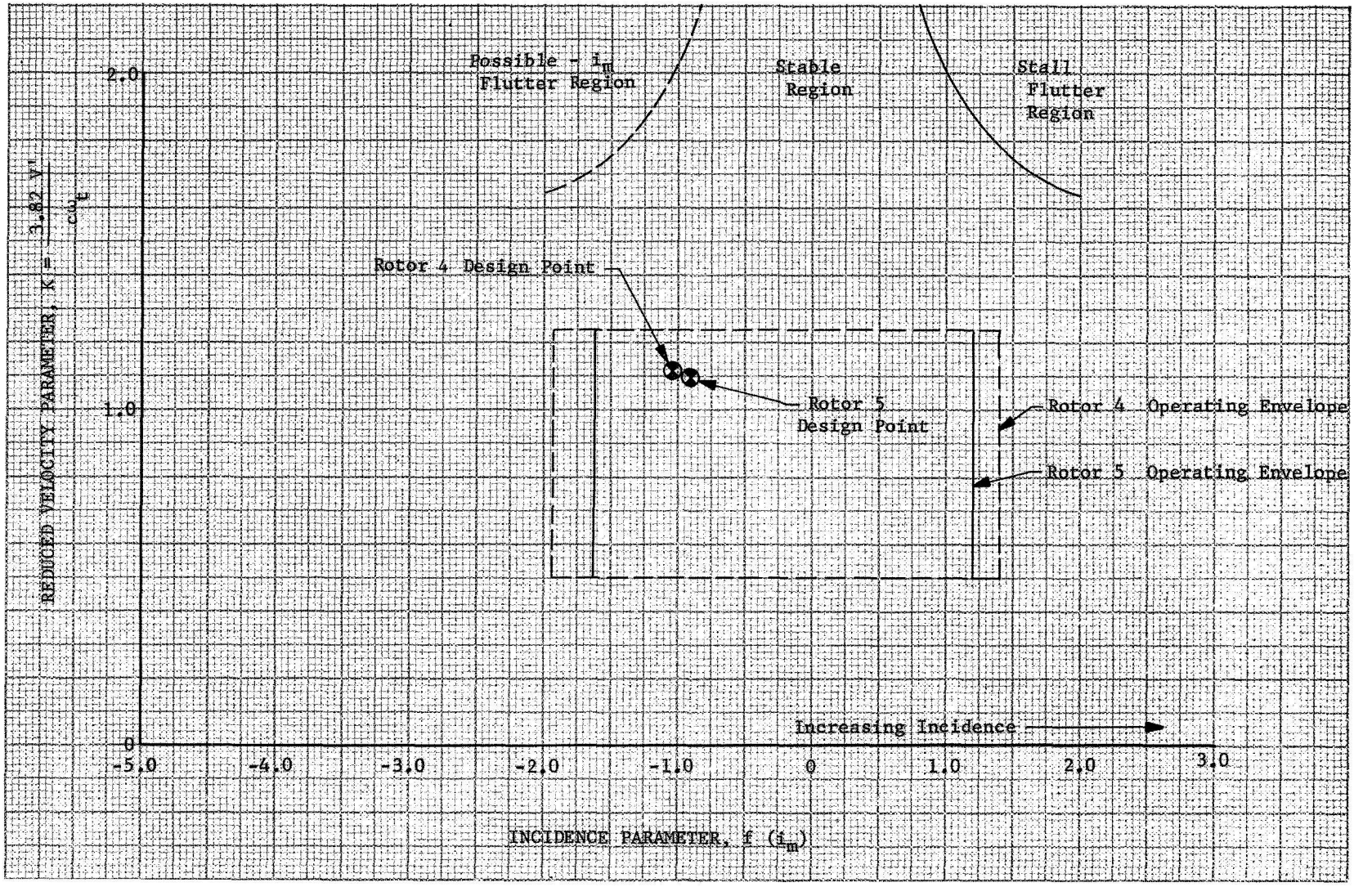

Figure 32. Calculated Rotor Blade Torsional Flutter Characteristics

DF 78798

APPENDIX A
DEFINITION OF SYMBOLS AND DESIGN VARIABLES

Definition of Symbols

A_A	Flowpath annular area, ft^2
a'_0	Inlet relative stagnation velocity of sound, ft/sec
c	Chord length, in.
C_p	Static pressure coefficient
d	Diameter
D_F	Diffusion factor
i_m	Incidence angle, degrees (based on equivalent circular arc meanline)
M	Absolute Mach number
N	Rotor speed, rpm
O	Minimum blade passage gap, in.
O*	Critical blade passage gap, in.
P	Total pressure, psia
PR	Pressure ratio
p	Static pressure, psia
S	Blade spacing, in.
t	Blade maximum thickness, in.
T	Total temperature, °R
U	Rotor speed, ft/sec
V	Velocity, ft/sec
W	Actual flowrate, lb_m/sec
β	Air angle, degrees from axial direction
$\Delta\beta$	Flow turning angle
γ	Ratio of specific heats
$\gamma°$	Blade-chord angle, degrees from axial direction
δ	Ratio of total pressure to NASA standard sea level pressure of 14.694 psia (101,312.2 N/m^2)
$\delta°$	Deviation angle, degrees (radians)
θ	Ratio of total temperature to NASA standard sea level temperature of 518.7°R (288.138°K)
κ	Blade metal angle, degrees from axial direction (based on equivalent circular arc meanline)
ρ	Density, lb_f-sec^2/ft^4

σ	Solidity, c/S
ϕ	Blade camber angle, $\kappa_1 - \kappa_2$, degrees
ω	Frequency, radians/sec
$\overline{\omega}$	Loss coefficient
$\frac{\overline{\omega} \cos \beta_{te}}{2\sigma}$	Loss parameter

Subscripts:

b	Bending
fs	Free stream value
id	Isentropic condition
le	Leading edge
L	Local
te	Trailing edge
t	Torsional
z	Axial component
θ	Tangential component

Superscripts:

'	Related to rotor blade
-	Mass average value
ref	Minimum loss

Definition of Design Variables

Incidence Angle:

Rotor: $i_m = \beta'_{1e} - \kappa_{1e}$ Stator: $i_m = \beta_{1e} - \kappa_{1e}$

Diffusion Factor:

$$\text{Rotor: } D_F = 1 - \frac{V'_{te}}{V'_{1e}} + \frac{d_{te}V\theta_{te} - d_{1e}V\theta_{te}}{(d_{1e} + d_{te})\sigma V'_{1e}}$$

$$\text{Stator: } D_F = 1 - \frac{V_{te}}{V_{1e}} + \frac{d_{te}V\theta_{te} - d_{1e}V\theta_{1e}}{(d_{1e} + d_{te})\sigma V_{1e}}$$

Deviation Angle:

Rotor: $= \beta'_{te} - \kappa_{te}$ Stator: $= \beta_{te} - \kappa_{te}$

Loss Coefficient:

$$\text{Rotor: } \bar{\omega}' = \frac{P'_{teid} - P'_{te}}{\bar{P}'_{1e} - p_{1e}}$$

where:

$$P'_{teid} = P'_{1e}\left\{1 + \frac{\gamma - 1}{2}\left(\frac{U^2_{te}}{a'^2_{O1e}}\right)\left[1 - \left(\frac{d_{1e}}{d_{te}}\right)^2\right]\right\}^{\frac{\gamma}{\gamma - 1}}$$

P' is found from $p/P' = \left[1 + \frac{\gamma - 1}{2} M'^2\right]^{\frac{\gamma}{\gamma - 1}}$

and M' is calculated using trigonometric functions and the measurements of U, β, P, and p.

$$\text{Stator: } \bar{\omega} = \frac{P_{fs} - P_{te}}{P_{fs} - p_{1e}}$$

Static Pressure Coefficient:

$$C_p = \frac{P_L - P_{fs}}{1/2 \rho_{fs} V_{fs}^2}$$

Pressure Ratio:

Rotor: $\frac{\bar{P}_{rotor\ te}}{P_{rotor\ le}}$ Stage: $\frac{\bar{P}_{stator\ te}}{P_{rotor\ le}}$

Corrected Flow:

$$\frac{W\sqrt{\theta}}{\delta}$$

Corrected Rotor Speed:

$$N\sqrt{\theta}$$

Adiabatic Efficiency:

Rotor: $\frac{(PR)^{\frac{\gamma-1}{\gamma}} - 1}{\bar{T}_{te}/518.7 - 1}$ Stage: $\frac{(PR)^{\frac{\gamma-1}{\gamma}} - 1}{\bar{T}_{te}/518.7 - 1}$

Where $\bar{T}_{te}$ refers to the mass averaged total temperature at stator trailing edge.

DISTRIBUTION LIST

Contract NAS3-10481

		Copies
1. NASA-Lewis Research Center 21000 Brookpark Road Cleveland, Ohio 44135 Attention:		
Report Control Officer	MS 5-5	1
Technical Utilization Office	MS 3-19	1
Library	MS 60-3	2
Fluid System Components Division	MS 5-3	1
Pump and Compressor Branch	MS 5-9	6
Dr. B. Lubarsky	MS 3-3	1
A. Ginsburg	MS 5-3	1
M. J. Hartmann	MS 5-9	1
W. A. Benser	MS 5-9	1
D. M. Sandercock	MS 5-9	1
L. J. Herrig	MS 7-1	1
T. F. Gelder	MS 5-9	1
C. L. Ball	MS 5-9	1
L. Reid	MS 5-9	1
L. W. Schopen	MS 77-3	1
S. Lieblein	MS 100-1	1
C. L. Meyer	MS 60-4	1
J. H. Povolny	MS 60-4	1
A. W. Goldstein	MS 7-1	1
J. J. Kramer	MS 7-1	1
W. L. Beede	MS 5-3	1
C. H. Voit	MS 5-3	1
E. E. Bailey	MS 5-9	1
2. NASA Scientific and Technical Information Facility P. O. Box 33 College Park, Maryland 20740 Attention: NASA Representative		6
3. FAA Headquarters 800 Independence Ave., S. W. Washington, D. C. 20553 Attention: Brig. General J. C. Maxwell		1
4. NASA Headquarters Washington, D. C. 20546 Attention: N. F. Rekos (RAP)		1
5. U.S. Army Aviation Material Laboratory Fort Eustes, Virginia Attention: John White		1

		Copies
6.	Headquarters Wright Patterson AFB, Ohio 45433	
	Attention: J. L. Wilkins, SESOS	1
	S. Kobelak, APTP	1
	R. P. Carmichael, SESSP	1
7.	Department of Navy Bureau of Weapons WAshington, D. C. 20525	
	Attention: Robert Brown, RAPP14	1
8.	Department of Navy Bureau of Ships Washington, D. C. 20360	
	Attention: G. L. Graves	1
9.	NASA-Langley Research Center Technical Library Hampton, Virginia 23365	
	Attention: Mark R. Nichols	1
	John V. Becker	1
10.	Boeing Company Commercial Airplane Division P. O. Box 3991 Seattle, Washington 98124	
	Attention: C. J. Schott NS80-66	1
11.	Douglas Aircraft Company 3855 Lakewood Boulevard Long Beach, California 90801	
	Attention: J. E. Merriman	1
	Technical Information Center C1-250	
12.	Pratt & Whitney Aircraft Florida Research & Development Center P. O. Box 2691 West Palm Beach, Florida 33402	
	Attention: R. A. Schmidtke	1
	H. D. Stetson	1
	J. M. Silk	1
	W. R. Alley	1
	R. W. Rockenbach	1
	B. A. Jones	1
	B. S. Savin	1
	J. A. Fligg	1

		Copies
13.	Pratt & Whitney Aircraft 400 Main Street East Hartford, Connecticut	
	Attention: R. E. Palatine	1
	T. G. Slaiby	1
	P. Tramm	1
	M. J. Keenan	1
	B. B. Smyth	1
	A. A. Mikolajczak	1
	Library (UARL)	1
14.	Allison Division, GMC Deparment 8894, Plant 8 P. O. Box 894 Indianapolis, Indiana 46206	
	Attention: J. N. Barney	1
	G. E. Holbrook	1
	B. A. Hopkins	1
	R. J. Loughery	1
	Library	1
	J. L. Dillard	1
15.	Northern Research and Engineering 219 Vassar Street Cambridge 39, Massachusetts	
	Attention: K. Ginwala	1
16.	General Electric Company Flight Propulsion Division Cincinnati 15, Ohio	
	Attention: J. W. Blanton J-19	1
	W. G. Cornell K-49	1
	J. Ringrose H-79	1
	E. E. Hood/J. C. Pirtle J-165	1
	J. F. Klapproth H-42	1
	J. W. McBride H-44	1
	L. H. Smith H-50	1
	S. N. Suciu H-32	1
	J. B. Taylor J-168	1
	Technical Information Center N-32	1
	Marlen Miller H-50	1
17.	General Electric Company 1000 Western Avenue West Lynn, Massachusetts	
	Attention: D. P. Edkins - Bldg. 2-40	1
	F. F. Ehrich - Bldg. 2-40	1
	L. H. King - Bldg. 2-40	1
	R. E. Neitzel - Bldg. 2-40	1
	Dr. C. W. Smith Library Bldg. 2-40M	1

		Copies
18.	Curtiss-Wright Corporation Wright Aeronautical Woodridge, New Jersey	
	Attention: S. Lombardo	1
	G. Provenzale	1
	J. Wiggins	1
19.	Air Research Manufacturing Company 402 South 36th Street Phoenix, Arizona 85034	
	Attention: Robert O. Bullock	1
	John H. Deman	1
20.	Air Research Manufacturing Company 8951 Sepulveda Boulevard Los Angeles, California 90009	
	Attention: Linwood C. Wright	1
21.	Union Carbide Corporation Nuclear Division Oak Ridge Gaseous Diffusion Plant P. O. Box "P" Oak Ridge, Tennessee 37830	
	Attention: R. G. Jordan	1
	D. W. Burton, K-1001, K-25	1
22.	Avco Corporation Lycoming Division 550 South Main Street Stratford, Connecticut	
	Attention: Clause W. Bolton	1
23.	Continental Aviation & Engineering Corp. 12700 Kercheval Detroit, Michigan 48215	
	Attention: Eli H. Benstein	1
	Howard C. Walch	1
24.	Solar San Diego, California 92112	
	Attention: P. A. Pitt	1
	Mrs. L. Walper	1
25.	Goodyear Atomic Corporation Box 628 Piketon, Ohio	
	Attention: C. O. Langebrake	2
26.	Iowa State University of Science and Technology Ames, Iowa 50010	
	Attention: Professor George K. Serovy	
	Dept. of Mechanical Engineering	1

Copies

27. Hamilton Standard Division of
United Aircraft Corporation
Windsor Locks, Connecticut
Attention: Mr. Carl Rohrbach
Head of Aerodynamics and Hydrodynamics 1

28. Westinghouse Electric Corporation
Small Steam and Gas Turbine Engineering B-4
Lester Branch
P. O. Box 9175
Philadelphia, Pennsylvania 19113
Attention: Mr. S. M. DeCorso 1

29. J. Richard Joy
Supervisor, Analytical Section
Williams Research Corporation
P. O. Box 95
Walled Lake, Michigan 1

30. Raymond S. Poppe
Building 541, Dept. 80-91
Lockheed Missile and Space Company
P. O. Box 879
Mountain View, California 94040 1

31. James D. Raisbeck
The Boeing Company
224 N. Wilkinson
Dayton, Ohio 45402 1

32. James Furlong
Chrysler Corporation
Research Office
Dept. 9000
P. O. Box 1118
Detroit, Michigan 48231 1

33. Elliott Company
Jeannette, Pennsylvania 15644
Attention: J. Rodger Schields 1
Director-Engineering

34. R. H. Carmody
Dresser Industries Inc.
Clark Gas Turbine Division
16530 Peninsula Boulevard
P. O. Box 9989
Houston, Texas 77015 1

		Copies
35.	California Institute of Technology Pasadena, California 91109 Attention: Professor Duncan Rannie	1
36.	Massachusetts Institute of Technology Cambridge, Massachusetts 02139 Attention: Dr. J. L. Kerrebrock	1